Zeitschrift: Helvetica Physica Acta
Band: 59 (1986)
Heft: 3

Artikel: On the unusual physical properties of europium-based molybdenum chalcogenides and related Chevrel compounds

Autor: Meul, Hans Willi

DOI: https://doi.org/10.5169/seals-115705

Helvetica Physica Acta, Vol. 59 (1986) 417–489

0018–0238/86/030417–73$1.50 + 0.20/0

On the unusual physical properties of europium-based molybdenum chalcogenides and related Chevrel compounds

By Hans Willi Meul

Département de Physique de la Matière Condensée, Université de Genève, Ch-1211 Genève 4, Switzerland

(15. VIII. 1985; rev. 23. XII. 1985)

Abstract. The unusual superconducting and transport properties of ternary molybdenum chalcogenides MMo_6X_8 with divalent cations (M = Eu, Sr, Ba; X = S, Se) have been studied. These compounds, undergoing a rhombohedral to triclinic structural transformation near 100 K, reveal an anomalous temperature dependence of the resistivity and the Hall coefficient well above that transition. The possible existence of an "intermediate" region with properties different from the ones of the "pure" rhombohedral phase is discussed. Particular emphasis is laid on the investigation of the nature of the low-temperature triclinic phase of these materials. A two-band model is developed which describes well the various transport properties. It is shown that superconductivity can be induced in $EuMo_6S_8$ by suppression of the structural transformation. One way of doing this is partial substitution of Eu by Sn. Very interesting effects are found in the superconducting state of the series $Eu_xSn_{1-x}Mo_6S_8$ due to the presence of the magnetic Eu sublattice. A novel superconducting state induced by an externally applied magnetic field is observed. This phenomenon is interpreted in terms of the Jaccarino–Peter effect. The nature of this field-induced superconducting state and its properties are discussed in detail.

1. Introduction

Ternary molybdenum chalcogenides ("Chevrel phases") have been studied intensively because of their many striking and unusual properties [1]. The variety of interesting physical effects is intimately connected with the complex crystal structure of these materials, which does not simply bring complications, but may rather lead to the discovery of novel phenomena. Today it is widely belived that on the whole the physics of Chevrel phases is relatively well understood, but there are certain experimental facts which are still far from a complete understanding, thus representing a challenge for solid state physicists.

One of the most intriguing and least understood systems are the europium-based molybdenum chalcogenides. At first the surprising absence of superconductivity in $EuMo_6S_8$ [2] had attracted a great deal of attention. From theoretical considerations $EuMo_6S_8$ was expected to be a high-T_c superconductor similar to the isostructural compounds with Pb^{2+} and Sn^{2+}. Furthermore, unusual behaviour of the superconducting transition temperature in the pseudo-ternary series $Eu_xSn_{1-x}Mo_6S_8$ has been reported in [2]: T_c is nearly independent on the

Eu concentration up to $x = 0.6$, but drops abruptly to zero at about $x = 0.8$. Application of hydrostatic pressure greater than 14 kbar has been found to induce superconductivity in $EuMo_6S_8$ with $T_c = 12$ K [3, 4].

This long standing problem of nonsuperconductivity at ambient pressure has been solved by the recent observation of a structural phase transformation occurring in the compounds $M^{2+}Mo_6S_8$ with divalent cations M = Eu, Ba, Sr, Ca at temperatures of about 100 K, where the crystalline lattice is distorted into a low-temperature modification with a low density of states at the Fermi energy [5, 6]. However, this observation has also raised several new questions about the driving mechanism which is responsible for the phase transformation, and the exact nature of the low-temperature phase. A Jahn–Teller-type instability in the electronic system [5] as well as the formation of charge density waves [7] have been proposed. In Fig. 1.1, another remarkable feature of Eu-based Chevrel compounds is shown, namely the very anomalous behaviour of the upper critical field H_{c2} as a function of temperature in the series $Eu_xSn_{1-x}Mo_6S_8$, observed first by Fischer et al. [8] in 1975. The anomalous upturn of H_{c2} at $x = 0.8$ has been interpreted [8] in terms of the Jaccarino–Peter compensation effect [9]. This effect was originally proposed as a mechanism that would allow superconductivity to be induced in a weak ferromagnet by a high external magnetic field. However, this field-induced superconductivity may equally well occur in the paramagnetic state [10], so that the series $Eu_xSn_{1-x}Mo_6S_8$ might be a promising candidate for the first observation of this phenomenon.

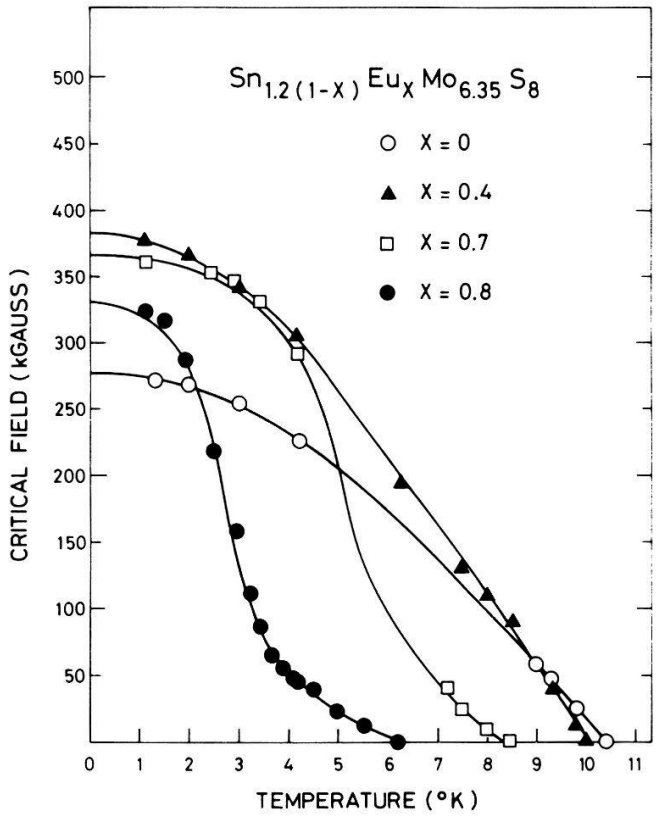

Figure 1.1
Critical field vs temperature for various samples of the series $Sn_{1.2(1-x)}Eu_xMo_6S_8$ (after [8]).

There are other interesting features of Eu-based Chevrel compounds that could not be correctly explained until now, such as the magnetic ordering of $EuMo_6S_8$ below 0.5 K, the anomalously large EPR-line broadening as the temperature decreases, the absence of superconductivity in $EuMo_6Se_8$ even under hydrostatic pressure etc. Some of these exciting problems will be addressed in the present work. Essentially the following questions will be investigated:

(1) Is the high-temperature behaviour of $M^{2+}Mo_6X_8$ compounds which undergo a structural transformation at low temperature, in accord with our present understanding of the rhombohedral phase of Chevrel compounds?
(2) Can we learn something about the origin of the phase transformation and what is the exact nature of the low-temperature phase?
(3) How are superconductivity and the structural phase transition related to each other?
(4) Does the phenomenon of magnetic-field-induced superconductivity exist in the series $Eu_xSn_{1-x}Mo_6S_8$?

These questions will be studied experimentally by means of transport measurements on well characterized samples. Special care has been taken of the preparation of dense and homogeneous samples without any impurity phase. After a detailed description of the sample preparation and the measuring technique in Section 2, the points mentioned above will be treated in Sections 3 to 6.

2. Experimental

2.1. *Sample preparation and characterization*

Sintered samples, produced by standard metallurgical powder techniques, are not very suitable for quantitative transport measurements. The electrical resistance of such samples is often dominated by the characteristics of the grain barriers. Contact problems also cause current fluctuations making the Hall signal very unstable. Furthermore, sintered samples are usually not very homogeneous and have relatively wide superconducting transitions which may mask some interesting effects. Thus it appears that the successful treatment of the problems posed in the introduction is intimately linked with improved preparation methods.

An improvement of the preparation technique has been achieved by two different ways:

(1) by means of a melting technique under high argon pressure developed by R. Baillif [11]
(2) by means of a hot pressing technique developed by M. Decroux [12].

High quality samples have been obtained with the melting technique; the grain

size of these samples was as large as 1 mm and the transport data indicate a high degree of homogeneity, so that good confidence can be placed in the experimental values. Unfortunately, this preparation technique could only be applied to the compounds $EuMo_6S_8$ and $EuMo_6Se_8$ without any problems. Melted samples are characterized by (m) in the present work.

In the case of $SrMo_6S_8$ and $BaMo_6S_8$, a non-negligible amount of the binary phase Mo_2S_3 was formed by the melting process. This impurity phase causes a clear falsification of the transport results of transforming compounds at low temperature because of its metallic behaviour. The melting technique was likewise inapplicable to the series $Eu_xSn_{1-x}Mo_6S_8$: two-phase samples were always obtained with small $SnMo_6S_8$ precipitations in the $EuMo_6S_8$ matrix or vice versa. In those cases a hot-pressing technique has been applied allowing the preparation of pure and compact samples with a typical grain size of some μm.

The starting material for both preparation techniques described above was the correctly formed Chevrel phase in powdered form. This prereacted powder was obtained in two steps. First a homogeneous mixture of appropriate amounts of MX, Mo, and X (M = Eu, Sr, Ba, Sn; X = S, Se) was pressed into pellets and heated up to 700°C for 24 h in sealed quartz tubes in an argon atmosphere (90 Torr at 300 K). The reaction product was not yet the ternary phase; a vehement reaction essentially between Mo and X had taken place. Then the products of the first reaction were crushed, carefully mixed, pressed into pellets and annealed at 1200°C for 48 h under argon atmospherae (90 Torr at 300 K) in sealed quartz tubes. Special care was taken that the losses in weight were not greater than 0.2% before the second reaction. During this reaction any contact of the sample with the quartz tube was avoided by using thin molybdenum foils. Such a protection was necessary because europium may react with the quartz wall at that temperature. X-ray studies revealed that after the second reaction the pure Chevrel phase was obtained. In some cases small amounts of bromine (about 0.5 at −%) were added to the ingots in order to promote the homogenization. Such samples are characterized by (Br) in the present work.

After this pretreatment the materials were then melted in an autoclave at 1800°C and 2 kbar or hot pressed at 1500°C and 1.7 kbar for 2 h with the use of a graphite matrix. For the resistance and magnetoresistance measurements the samples were cut by means of a diamond saw in the shape of small bars of about 10 mm length and $0.6 \times 0.6\ mm^2$ cross section. For the Hall-effect measurements a sample thickness of about 0.3 mm and a length-to-width ratio of about 4 was chosen to prevent the "shorting out" effect of the current electrodes [13].

The samples were fixed on the sample holder by an adhesive strip ("scotch"). The contacts between the leads and the sample were made with silver paint; for the Hall-effect measurement the current contacts were soldered with indium in order to minimize current fluctuations.

2.2. *Measuring probe*

All transport measurements presented here have been carried out with the same measuring probe, originally developed by R. Noer. During the present

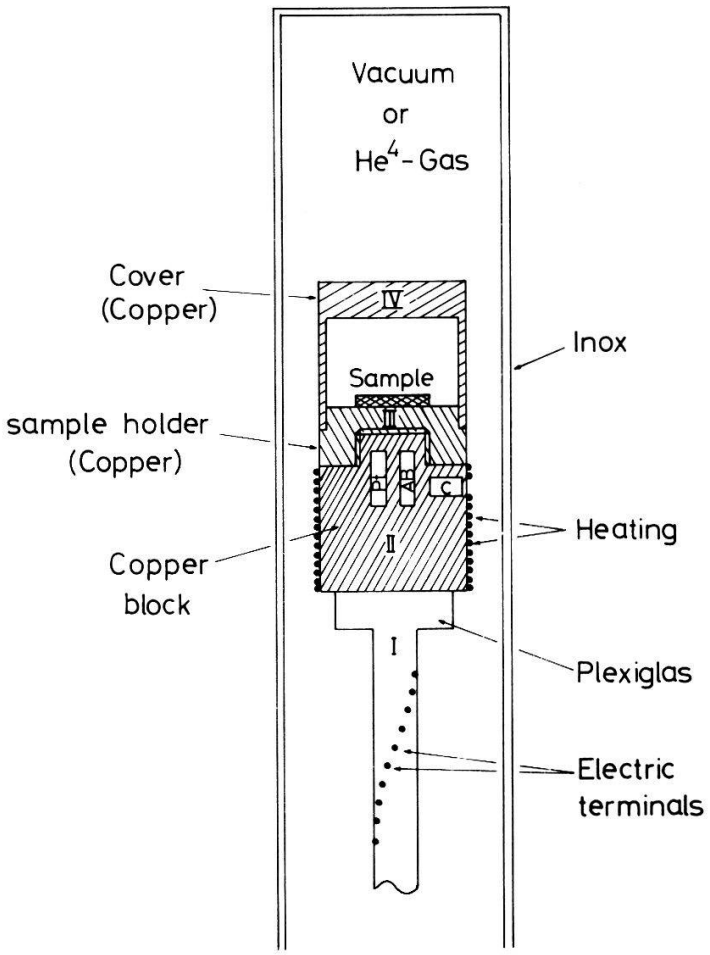

Figure 2.1
Lower part of the measuring probe.

work this probe has been slightly modified in order to reduce the signal noise and to allow measurements in a longitudinal magnetic field, too. The lower part of the measuring probe is shown in Fig. 2.1. It consists essentially of a massive copper cylinder with detachable sample holder and cover. It has been taken care that the sample was in good thermal contact with the copper block containing all the thermometry: a platinum resistor (Pt), an Allen–Bradley resistor (AB), and a capacitance temperature sensor (C). For the galvanomagnetic measurements (magnetoresistance and Hall effect) the temperature has been stabilized by the capacitance sensor which is not sensitive to the magnetic field, and an electronic temperature regulator (Model BT 300, l'Air liquide). The temperature has been determined in zero field by the aid of the resistors Pt and AB. By applying this regulation technique the stability of the temperature has been found to be better than the precision of the temperature measurement which was 1 K at high temperature and 0.05 K at low temperature. For the critical field measurements down to 1.6 K, performed by sweeping the temperature at constant magnetic fields, the capacitance sensor has been used as thermometer calibrated by comparison with the Allen–Bradley resistor in zero field.

The measurements in the presence of a magnetic field have been done by inserting the measuring probe into a superconducting magnet of 7 tesla. A vacuum better than 10^{-3} Torr, measured at the warm part of the measuring

probe, was needed for the high temperature measurements since the distance between the copper block and the liquid helium was smaller than 10 mm.

The critical field measurements at very low temperature and high magnetic fields have been carried out at the Max Planck Institute in Grenoble and the low temperature institute (C.R.T.B.T.) of the Centre National de la Recherche Scientifique in Grenoble. A ^{3}He–^{4}He dilution refrigerator combined with a superconducting coil (12 tesla) or a ^{3}He cryostat inserted into a resistive polyhelix magnet of 25 tesla have been used.

2.3. *Measuring technique*

Figure 2.2 shows the block diagram of the equipment used in the present work. An ac method (222 Hz) has been applied to perform the transport, T_c, and H_{c2} measurements. The sinewave output at the reference oscillator frequency of a lock-in amplifier (Model PAR 124A) has been used to excite an ac current in the sample current circuit, which was decoupled from the lock-in by a transformer T to avoid grounding problems and to increase the maximum sample current. Thus the sample current was shifted by 180° with respect to the reference signal. The sample current has been determined by measuring the voltage drop at the 1 ohm resistor. The current was about 500 μA when measuring resistivity or magnetoresistance, whereas the Hall-effect measurements required at least in the high-temperature region a somewhat higher current up to 40 mA.

The voltage signal V_R due to the sample resistance as well as the Hall voltage V_H have been measured by making use of the differential preamplifier (Model 116) of the lock-in. Particular attention has been paid to the fact that only one well defined ground, namely the chassis of the lock-in, exists in the detecting

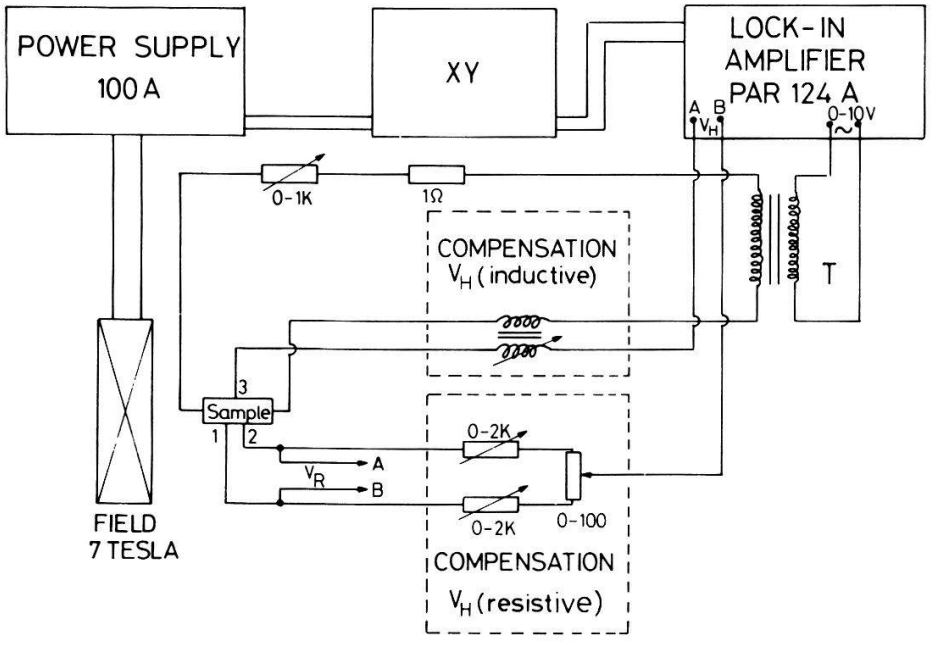

Figure 2.2
Block diagram of the equipment.

circuit. Only shielded voltage leads have been used. The Signal Channel of the lock-in has been operated in the Bandpass mode ($Q = 50$) for providing optimum low-noise performance. Both signals V_R and V_H were in phase with the sample current which could be checked by a phase measurement with the lock-in. The dc output signal of the lock-in has been applied either to the Y-channel of a XY recorder or to a computer for data acquisition (CAMAC system).

2.4. *Hall-effect measuring technique*

Whereas the technique of resistance- and magnetoresistance measurements is straightforward, the Hall-effect measurements need some more consideration. In Fig. 2.3 the typical experimental arrangement of such a measurement is shown. The direction of the Hall field E_H which is perpendicular both to the current and to the magnetic field direction, depends on the charge carrier type. An electron current has been assumed in the figure. To measure the pure Hall voltage V_H, any misalignment of the two voltage contacts must be avoided which is, of course, impossible in practice. A misalignment produces an error voltage which may depend on the magnetic field due to the magnetoresistance of the sample. Using a 3-terminal method the misalignment voltage can be balanced out in zero field with the aid of precision potentiometers. However, the Hall signal V_H may be still non-zero due to inductive and capacitive signal contributions. To achieve a complete annulation of the signal at the entry of the lock-in, a second compensation arrangement was necessary (Fig. 2.2) which consists of a small coil ($N = 19$) in the Hall circuit, inserted into a larger coil ($N = 14$) in the current circuit. By rotating the smaller coil with respect to the larger one, the magnetic flux through the inner coil could be changed and thus the voltage induced in the Hall circuit. The non-resistive part of the signal V_H was usually very small, so that the crossed position of the two coils was the normal operating mode.

The annulation of the misalignment voltage by the potentiometer compensation system may be disturbed in the presence of a magnetic field due to a magnetoresistance of the sample. By reversing the field direction and defining the Hall voltage as

$$V_H = \tfrac{1}{2}(V_H(H) - V_H(-H))$$

any contribution to V_H being an even function of the magnetic field, can be eliminated. Note that normally the magnetoresistance depends on the square of

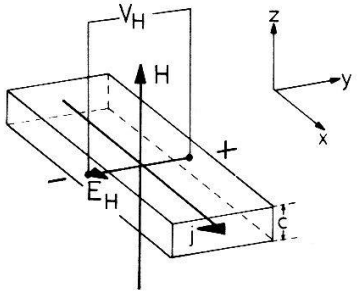

Figure 2.3
Hall effect with negative Hall coefficient R_H.

the magnetic field. In addition, the Hall voltage is only influenced by a magnetoresistance effect, if the position of the voltage contact 3 is very asymmetrical to the positions of the contacts 1 and 2. But even in that case, the difference $V_H(H) - V_H(-H)$ remains unchanged for the compounds studied here. This has been examinated by measuring the Hall effect in a symmetrical and a very asymmetrical contact arrangement.

The ac method has the important advantage that all thermoelectric and thermomagnetic effects which may contribute to the measured voltage V_H, are eliminated by the current oscillation with the exception of the Righi–Leduc effect [14]. This effect can only be suppressed by preventing a longitudinal heat flow through the sample, but it contributes usually less than 1% error to the value of the Hall constant [15] and will be therefore neglected here. A more serious problem may appear due to lead- and sample vibrations in the magnetic field. Such vibrational effects will induce an important error voltage in the Hall circuit and must be prevented by holding rigidly specimen and leads in the field region.

The determination of the sign of the Hall coefficient

$$R_H = \frac{V_H c}{I_x H_z}$$

(c being the sample thickness, I_x the current in x direction, and H_z the magnetic field in z direction) is straightforward when using a lock-in as measureing instrument. If for instance the situation of Fig. 2.3 (negative Hall coefficient) is realized during the positive period of the sample current, the panel meter of the lock-in will indicate a negative Hall voltage, i.e. the right sign, when the voltage contact on the left side of the sample is connected to the input A of the preamplifier, the other voltage contact to the input B, and the difference $A-B$ of the signals is measured. (The phase shift coming from the transformer T can be compensated by setting the Phase selector to 180!) During the negative period of the current, the Synchronous Detector of the lock-in inverts the polarity of the input signal and a well defined sign is obtained.

2.5. *H_{c2}- and T_c-measuring technique*

The superconducting transition temperature T_c as well as the upper critical field $H_{c2}(T)$ have been determined by taking the midpoint of the resistive transitions. The transition width has been defined as the temperature interval between 10% and 90% of the transition.

Above 1.5 K and in fields up to 7 tesla the resistive transitions have been measured by sweeping the temperature at constant magnetic fields. At very low temperature, however, it was easier to stabilize the temperature and vary the field. For the measurements carried out at Grenoble, another measuring probe has been used, but the measuring technique was identical with the one described above (lock-in). To avoid self-heating effects of the sample in the mK region, a very low current density of the order of 0.01 A/cm^2 has been applied. For the H_{c2} measurements, the magnetic field has been applied parallel to the current.

3. On the nature of the rhombohedral phase of $M^{2+}Mo_6X_8$ compounds

3.1. *Introduction*

The recent observation of a low-temperature structural phase transformation in Chevrel compounds with M = Eu, Ba, Sr, Ca [5], explaining well the absence of superconductivity in these materials, has raised the question about the physical reason for the structural instability. In contrast to the compounds with "small" atoms M = Cu, Ni, Co, Zn, ... , which show a pronounced tendency to undero structural transformations due to the delocalization of the M atoms over 12 possible positions around the centre of the unit cell of the rhombohedral phase, the transformations in the case of "large" M atoms rather seem to be correlated with an electronic instability of the Mo_6X_8 clusters, since the position of the M atom remains unchanged by the phase transition. Thus the question arises, whether the rhombohedral phase of Chevrel compounds is generally unstable. Indeed, just recently a tiny structural distortion from the rhombohedral space group has been observed in $PbMo_6S_8$ and $SnMo_6S_8$ below 100 K by high-resolution powder neutron diffraction [16]. However, this distortion is not identical with the rhombohedral to triclinic lattice deformation observed in $EuMo_6S_8$, $BaMo_6S_8$, . . . ; the neutron diffraction data rather suggest a supercell ordering.

We will now attempt to find out whether we really understand the physical properties of $M^{2+}Mo_6S_8$ compounds in their rhombohedral crystal structure and whether there is any difference between the rhombohedral phase of $EuMo_6S_8$ or related compounds and the one of $PbMo_6S_8$. For this purpose, mainly the transport properties resistivity, magnetoresistance, and Hall effect will be investigated, since they are very informative about the electronic structure and the interactions between the charge carriers. For a correct interpretation of the transport measurements, a realistic model of the situation at the Fermi energy is needed. To establish such a model, it is useful to take full band-structure calculations as a basis. Such calculations have been carried out for Chevrel phases by several authors. Here, we essentially follow the work by Nohl, Klose, and Andersen [17], who used a LMTO–ASA formalism for their computations.

In the beginning of Section 3.2, a brief recapitulation of the main results obtained by Nohl et al. is given, allowing us to establish subsequently a simplified band model near the Fermi energy, appropriate for analysing our transport data. In particular, it will be tried to calculate the concentration of charge carriers participating in the transport processes.

It is important to realize that such a band model and also the underlying full band-structure calculations do not contain dynamical electron–electron correlations which may be responsible for the observed structural instability of Chevrel phases. Band-structure calculations are therefore expected to describe correctly the one-electron behaviour of Chevrel phases. Discrepancies appearing between experiment and theory may be attributed to some collective phenomenon in the electronic system.

3.2. *Electronic band structure and Fermi surface*

The starting point for all band structure calculations is an inspection of the exact crystalline structure of the solid. The room-temperature rhombohedral structure of Chevrel phases with large M atoms is shown in Fig. 3.1. It is basically a cubic CsCl-type structure in which the Cs atoms are replaced by M while the Cl atoms are replaced by a slightly distorted Mo_6X_8 cluster. The main deviation from cubic symmetry is a rotation of the cluster of about 25° about the threefold axis [111] with respect to the lattice, whereas the rhombohedral distortion of the lattice only plays a minor role. The rhombohedral angle is very nearly 90°. The lattice constant a_R which corresponds to the M-atom distances, is about 6.55 Å. Figure 3.1 demonstrates that the building elements of the crystal are the Mo_6X_8 clusters which are fairly well separated from each other. It is therefore reasonable to describe the band structure of Chevrel phases in terms of the molecular-orbital (MO) states of a single cluster. The bands will then be formed by appropriate superpositions of these MO states.

In Fig. 3.2 the energy levels of a regular, i.e. undistorted (cubic) Mo_6S_8 cluster is shown [17]. The highest occupied and the lowest empty levels have mainly molybdenum 4*d* character, since they are essentially linear combinations of atomic Mo 4*d* wave functions such that the octahedral symmetry of the cluster is respected. This level scheme and the symmetry character of the wave functions can qualitatively be understood in terms of a simple MO model [18]. Inspection of the valence electron shells of the Mo and X atoms suggests that the 4*d*, 5*s*, and 5*p* states of the Mo atoms and the 3*s* and 3*p* states of the X atoms are involved in the various metal–metal and metal–chalcogen bonds. First of all, we note that

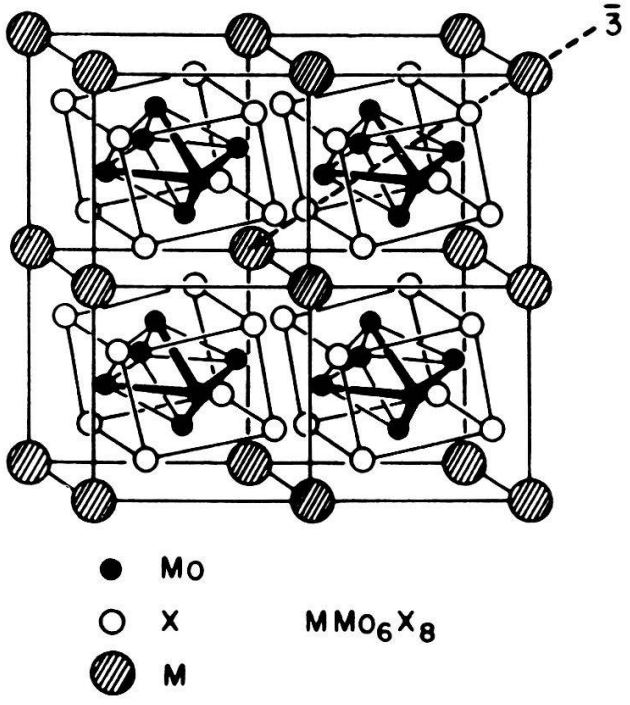

Figure 3.1
Crystal structure of $M^{2+}Mo_6X_8$-compounds.

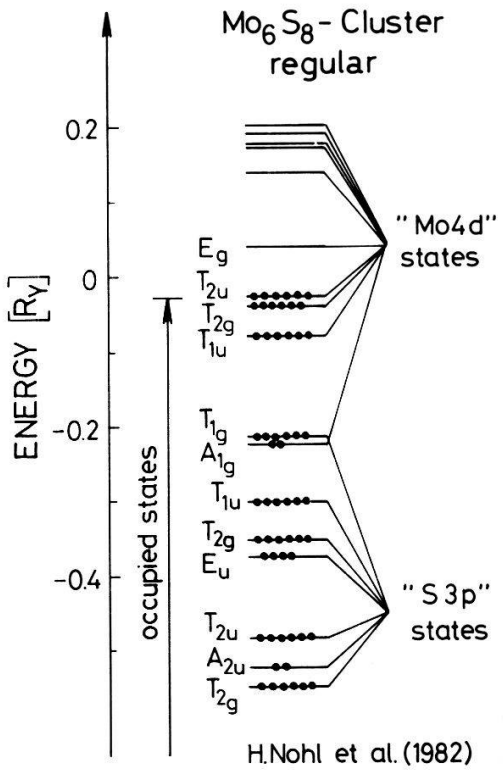

Figure 3.2
Electronic energy levels of a regular Mo_6S_8 cluster [17].

each Mo atom is surrounded by four X atoms sitting at the corners of a square and thus forming a MoX_4 unit with covalent Mo–X bonds. For these bonds the 5*s* orbital, the $5p_x$ and $5p_y$ orbitals, and the $4d_{xy}$ orbital of the Mo atom are assumed to be used. This leaves the $5p_z$ orbital and the remaining 4*d* orbitals for bonding to the other metal atoms of the cluster and for binding an additional X atom from the neighboring cluster. The p_z orbital is suitable for this latter bond. Then, using the remaining $6 \times 4 = 24$ Mo 4*d* orbitals, LCAO–MO wave functions with the appropriate transformation properties are constructed resulting in 12 binding (low lying) and 12 antibinding MO orbitals. The 12 binding states are the following:

A_{1g} (singlet)
T_{1u} (triplet)
T_{2g} (triplet)
E_g (douplet)
T_{2u} (triplet).

For a correct determination of the single-cluster-level scheme, hybridization between the Mo and X states must be taken into account. It appears that the highest bonding state of the Mo_6X_8 cluster is the doubly degenerate E_g level followed by an energy gap of 1 eV. One of these E_g states with nearly pure $x^2 - y^2$ character is shown schematically in Fig. 3.3: it is composed of the molybdenum $d_{x^2-y^2}$ atomic orbitals located at the centers of the Mo_6X_8 cube. The level scheme of Fig. 3.2 suggests that the conduction band in the real $M^{2+}Mo_6X_8$ crystal will be the band which is formed by appropriate superpositions of E_g molecular orbitals. Full band-structure calculations show in fact, that this is true for all $M^{2+}Mo_6X_8$

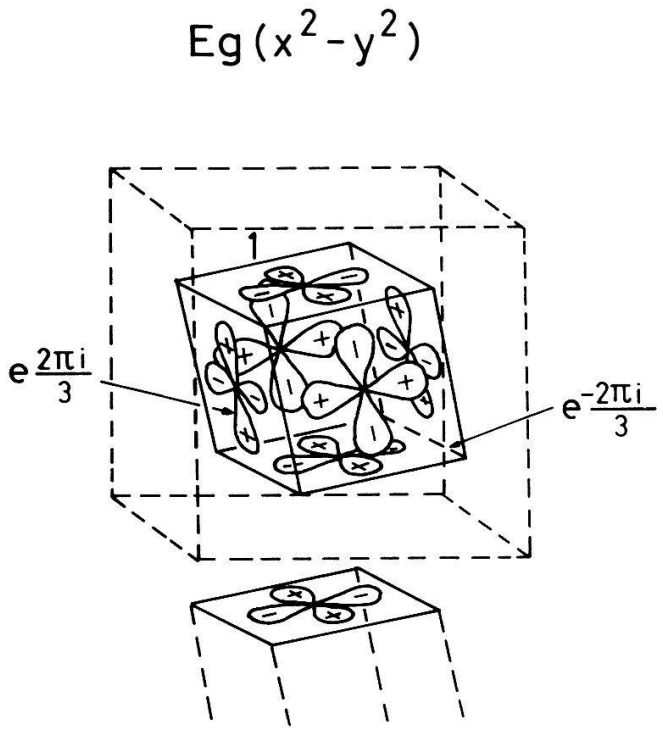

Figure 3.3
One of the $E_g(x^2-y^2)$-molecular orbital states (after [17]). The relative phase factors are also indicated.

compounds [17]. This E_g band is extremely narrow (40 mRy) and has a high density of states at the Fermi energy due to the large intercluster distances and the x^2-y^2 symmetry character of the wave functions. The E_g band will be half filled in a perfect crystal with divalent M atoms since the role of the third element is to transfer 2 electrons onto the cluster. Due to hybridization effects with lower lying bands, the E_g band has not a pure x^2-y^2 character, but contains small admixtures of essentially two other bands T_{1u} and T_{2g} at certain points of the Brillouin zone.

A first approximation to the conduction band in Chevrel phases can be obtained by neglecting all interactions with lower lying bands and calculating in tight binding approximation the matrix elements

$$H_{ij} = \sum_{R\neq 0} \exp(i\mathbf{kR}) \langle \Phi_i(\mathbf{r}-\mathbf{R}) \,|H|\, \Phi_j(\mathbf{r}) \rangle \tag{3.1}$$

where Φ_i represents the state shown in Fig. 3.3 and Φ_j the state being degenerate with Φ_i. $\mathbf{R}$ is one translation vector of the rhombohedral lattice. It is easy to show by diagonalizing the 2×2 matrix H_{ij}, that the energy dispersion of the pure E_g band is given by

$$E(k) = \tfrac{1}{2}\Delta[I+J+K \pm \tfrac{1}{3}(I^2+J^2+K^2-JK-IK-IJ)^{1/2}] \tag{3.2}$$

with $I = \cos(\mathbf{kR}_i)$ and analogously for J and K. Thus in first approximation the conduction band of Chevrel phases consists of two E_g subbands which are degenerate along the ternary axis [111], but different from each other at general points of the Brillouin zone. The density of states of this model E_g band, first

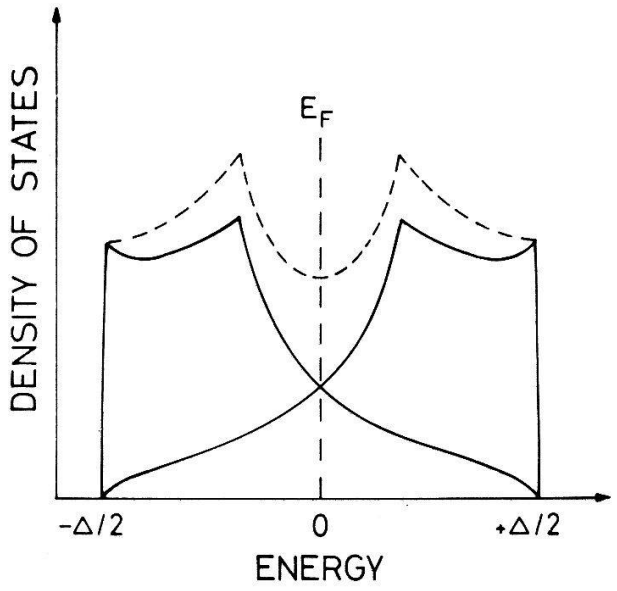

Figure 3.4
Density of states of the model E_g-band.

derived by Andersen et al. [19], is shown in Fig. 3.4. Assuming 40 mRy as band width we find a density of 0.5 states eV^{-1} $spin^{-1}$ Mo^{-1} at the Fermi energy from both subbands together.

From these simple considerations we expect that both electrons and holes will contribute to the transport in Chevrel compounds MMo_6X_8 and a two-band model is needed for the interpretation of the transport measurements. Such a two band model contains adjustable parameters whose number is usually such that almost any set of data can ultimately be fitted using seemingly "reasonable" values of these parameters. Therefore, it is very useful to have an idea about the theoretically expected density of charge carriers in Chevrel phases.

The expected number of electrons and holes participating in the transport processes can be approximately determined by calculating the Fermi surface in the ideal case of a pure E_g-conduction band. It is clear that the actual shape of the Fermi surface depends very sensitively on small details of the band structure, but the enclosed volume can be considered to stay roughly constant.

The model Fermi surface for $M^{2+}Mo_6X_8$ compounds consists of an electron "polyhedron" (cube with bulges in [100] and equivalent directions) centered at the R point of the Brillouin zone (Fig. 3.5), and an equally shaped hole surface at the zone center touching the electron surface on the ternary axis. Since the conduction band of a perfect $M^{2+}Mo_6X_8$ crystal is half filled, the volumes of the two pieces of the Fermi surface must be equal. We find that the volume of either part of the Fermi surface corresponds to 19.2% of the total volume of the Brillouin zone related to one subband. Taking 280 $Å^3$ for the volume of the rhombohedral unit cell, we get 3.6×10^{21} states per cm^3 and spin in either subband. This means that the expected densities of electrons and holes in the case of a pure E_g-conduction band are

$$n_e = n_h = 1.4 \times 10^{21}\ \mathrm{cm}^{-3}$$

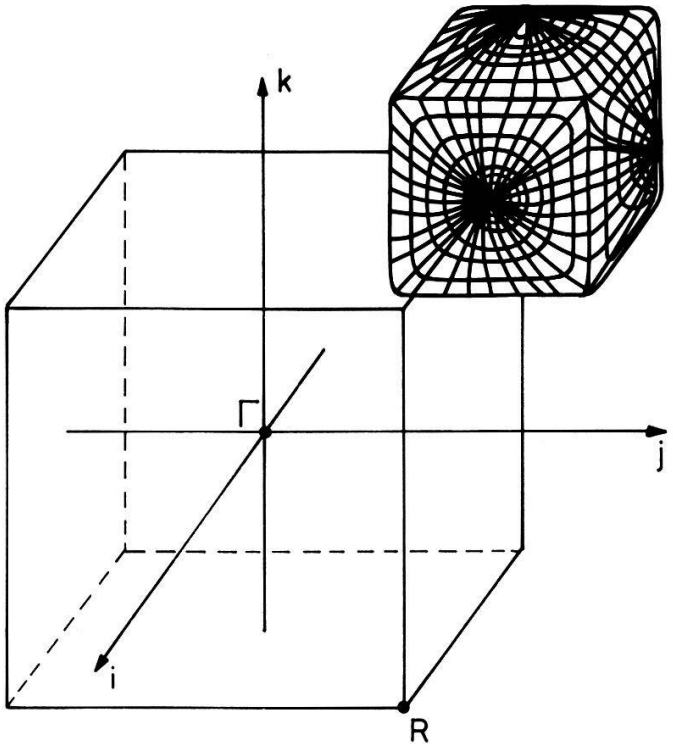

Figure 3.5
Electronic part of the model Fermi surface of $M^{2+}Mo_6X_8$ compounds.

Such a low carrier density is not surprising for Chevrel phases and does not point to any anomalous behaviour. The total number of states per spin in a non-degenerate band is given by the number of unit cells in the crystal. Since the unit cell of ternary compounds is relatively large, the total number of electrons which can be put into one band, is much smaller for Chevrel phases than for simple metals. The bands derived from the molybdenum molecular orbitals are usually rather narrow and often separated from each other by small energy gaps due to hybridization effects. Thus the majority of the 22 cluster electrons is "condensed" in completely filled bands and cannot participate in the conduction process.

The results obtained above will be modified when interactions between the various bands of the valence band complex are taken into account. In Fig. 3.6 the model conduction band is compared with the "real" energy bands of $PbMo_6S_8$ and $BaMo_6S_8$ near the Fermi energy, as obtained by Nohl et al. [17] in their LMTO–ASA calculations. The most important effect occurs near the centre of the Brillouin zone: Due to hybridization with the relatively broad T_{1u} band, the E_g band maximum is shifted away from the zone center to a point midway between Γ and R along the ternary axis. This gives rise to anisotropy and cuts the hole surface into two pockets separated by a small electron sphere at Γ. There is a second, but weaker effect occurring near R and M, where the E_g band hybridizes with the top of the T_{2g} band. The electron polyhedron, however, seems to be more or less conserved.

Thus, hybridization does not change very much the estimated density of charge carriers, but it has an important influence on the shape of the Fermi surface and the density of states.

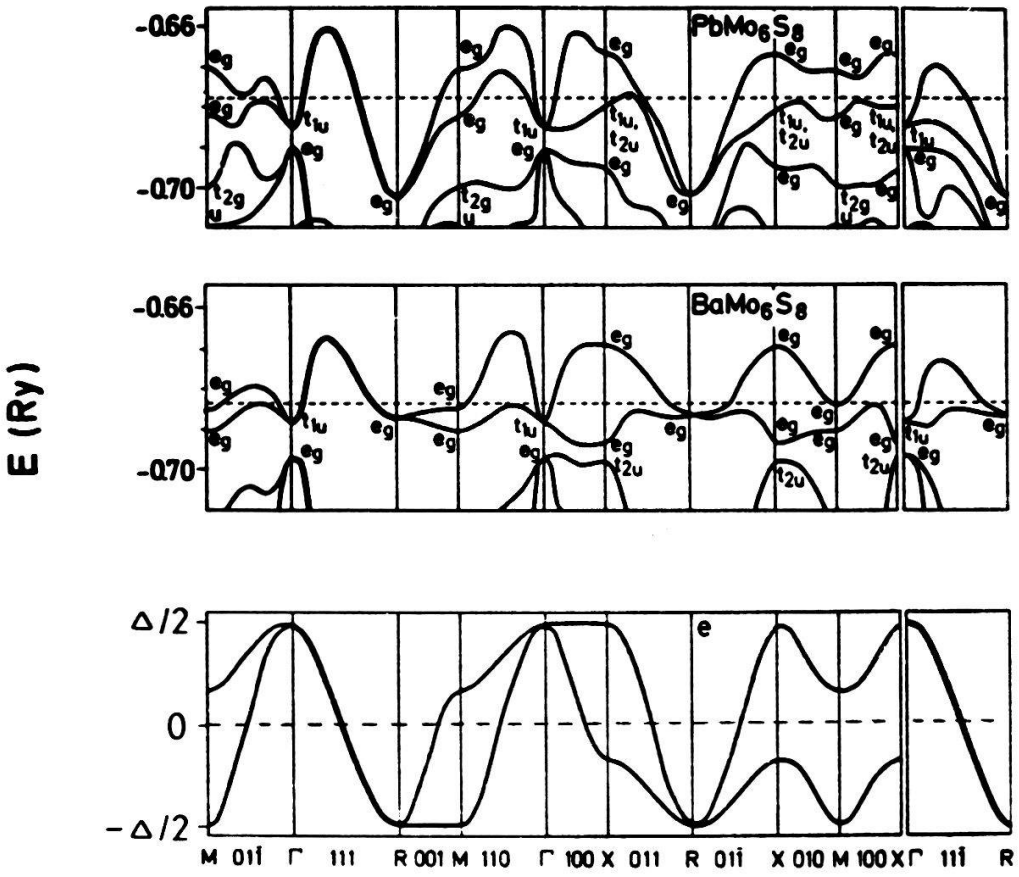

Figure 3.6
Conduction bands of $PbMo_6S_8$ and $BaMo_6S_8$, compared with the two E_g subbands (after [17]).

Figure 3.7 shows schematically that the density of states becomes asymmetric with a flattened-out high energy side. As a consequence the Fermi energy in "real" $M^{2+}Mo_6X_8$ compounds may be located more near the peak appearing in the density of states in good accord with the high T_c values observed. Finally it should be emphasized that according to the full band-structure calculations solely the two E_g subbands cross the Fermi energy confirming the validity of the proposed two-band model.

3.3. *Resistivity of* $M^{2+}Mo_6X_8$ *compounds*

After these introductory remarks about our present understanding of the rhombohedral phase of Chevrel compounds with large divalent M atoms, we will investigate in detail their transport properties. Let us start with the discussion of the electrical resistivity. Figure 3.8 shows the resistivity of a single crystal of $PbMo_6S_8$ as a function of temperature [20]. At room tempeature one finds a resistivity value of about 0.5 mΩcm, which can easily be understood by taking a typically metallic mobility of about 10 cm^2/Vs and a charge carrier concentration as estimated in the previous section. The resistivity shows a pronounced tendency towards saturation at high temperature which may be interpreted by the electron mean free path l becoming comparable to the lattice spacing $a_R = 6.5$ Å. In a

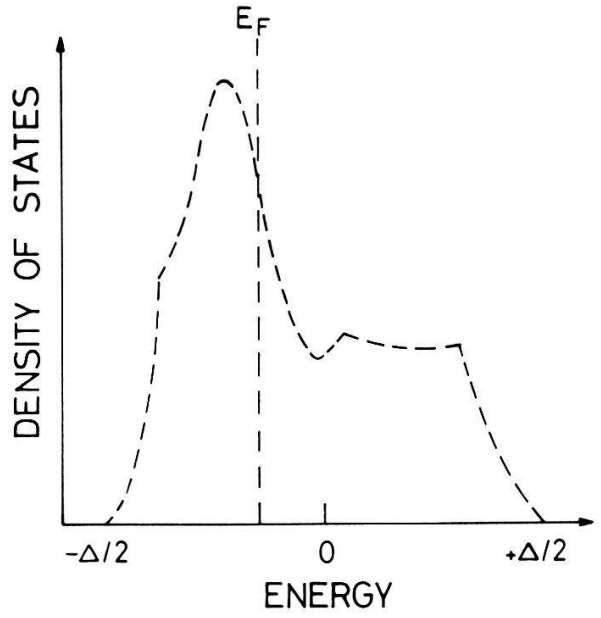

Figure 3.7
Density of states of the conduction band of $M^{2+}Mo_6X_8$ compounds (schematically after [17]).

nearly free electron model the mobility is given by

$$\mu = \frac{e\tau}{m^*} = \frac{el}{m^* v_F} = \frac{el}{\hbar k_F} \tag{3.3}$$

with the usual meaning of the symbols used. When taking $k_F = 2.2/a_R$ as mean radius of the electron Fermi surface at R (see Fig. 3.5 and Fig. 3.6), we get as lower limit of the electronic mobility

$$\lim_{l \to a_R} \mu_e = 2.9\ \mathrm{cm^2/Vs}.$$

With $n_e = n_h = 1 \times 10^{21}/\mathrm{cm^3}$ and taking $2.9\ \mathrm{cm^2/Vs}$ for both mobilities, we find a theoretical saturation value of about 1 mΩcm for the resistivity of $M^{2+}Mo_6X_8$ compounds. By extrapolating the resistivity curve of Fig. 3.8 to higher temperature, one finds as a first confirmation of our estimation that indeed the resistivity of $PbMo_6S_8$ seems to saturate at that value.

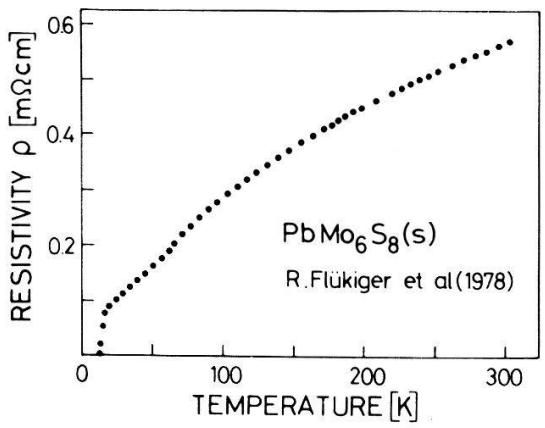

Figure 3.8
Resistivity of a single crystal of $PbMo_6S_8$ [20].

The decrease of the resistivity with decreasing temperature is believed to result from the temperature dependence of the mobilities. There appears a slight anomaly in the resistivity at about 60 K (discontinuity in dR/dT); below, the resistivity depends linearly on temperature and lies slightly above the curve one would expect by extrapolating the high-temperature part of the resistivity to lower temperature. This anomaly is probably related to the lattice distortion recently discovered in $PbMo_6S_8$ below 100 K [16]. Thus, the behaviour of $PbMo_6S_8$ agrees completely with our theoretical expectations above 100 K, but at lower temperature, there is a tiny anomaly which may result from some instability.

Table 3.1 [21]
Rhombohedral lattice parameters and T_c values of the $M^{2+}Mo_6S_8$ compounds studied in the present work.

	a_R	α_R	V_R	T_c
$PbMo_6S_8$	6.54	89.47	279.3	15.2
$SnMo_6S_8$	6.52	89.73	276.5	14.2
$EuMo_6S_8$	6.53	89.30	278.5	—
$SrMo_6S_8$	6.56	89.44	282.1	—
$BaMo_6S_8$	6.64	89.00	292.7	—

So far, we have talked about $PbMo_6S_8$ and the (fairly) stable $M^{2+}Mo_6X_8$ compounds. Now we will see how the compounds undergoing a rhombohedral to triclinic lattice transformation behave in their rhombohedral phase. Table 3.1 gives the rhombohedral lattice parameters of the compounds studied in the present work. The lattice constants of $M^{2+}Mo_6S_8$ with M = Pb, Sn, Eu, Sr are very similar, so that the electronic structure as well as the density of states should be nearly identical in these compounds. However, whereas $PbMo_6S_8$ and $SnMo_6S_8$ are high-T_c superconductors, $EuMo_6S_8$ and $SrMo_6S_8$ reveal semiconductor-like resistivities at low temperature, as can be seen in Fig. 3.9 and Fig. 3.10. Because of the striking similarity of $EuMo_6S_8$ and $SrMo_6S_8$, the magnetic moment of the Eu ions or valence fluctuations must be ruled out as explanation for the resistance anomaly at low temperature. In the following, $SrMo_6S_8$ will be considered as a non-magnetic reference compound for $EuMo_6S_8$.

In Fig. 3.11 and Fig. 3.12 the resistivities of $BaMo_6S_8$ and $EuMo_6Se_8$ are presented. Both compounds have been found to show the triclinic lattice distortion [5, 22]. However, the phase transition is here accompanied by a sudden drop of the resistance which points to a metallic ground state in the triclinic phase. The low-temperature behaviour of $M^{2+}Mo_6X_8$ compounds will be discussed in Section 4. Here we will concentrate on the rhombohedral phase.

There is strong evidence for resistivity saturation at high temperature in all cases presented. For an accurate determination of the saturation value, single crystals or at least melted specimens are needed. In the melted samples of $EuMo_6S_8$ and $EuMo_6Se_8$ we find room-temperature resistivities of 1.0 mΩcm and

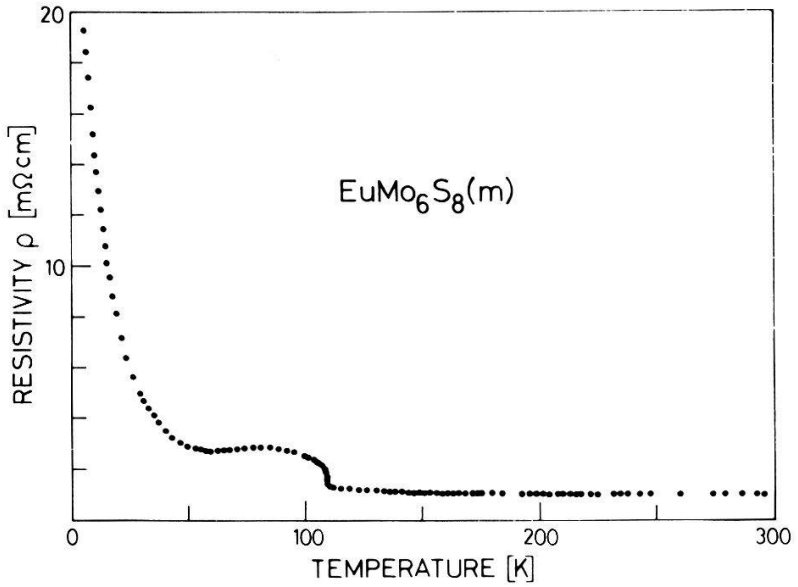

Figure 3.9
Resistivity of $EuMo_6S_8$ versus temperature.

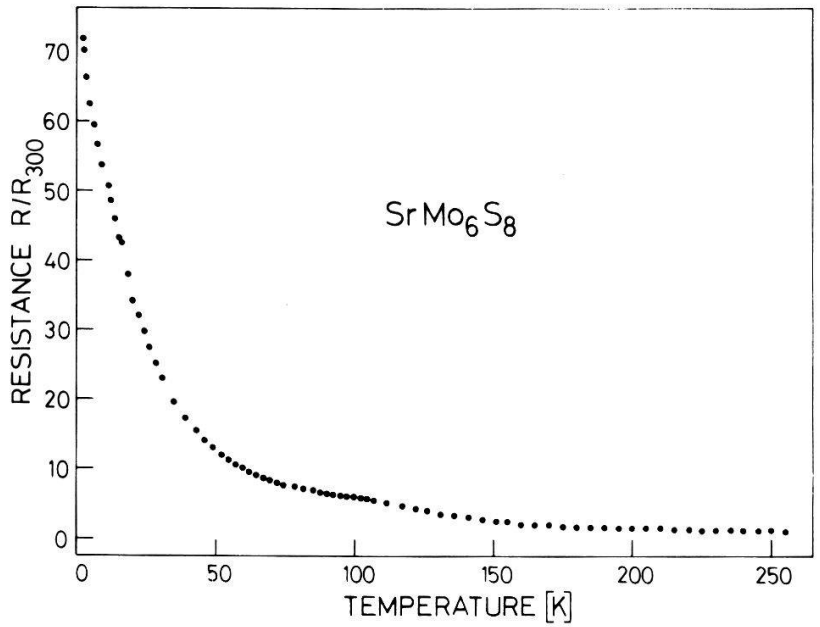

Figure 3.10
Resistivity of $SrMo_6S_8$ versus temperature.

1.2 mΩcm, respectively, in good agreement with the theoretical expectations. In cases where only hot pressed samples were available ($SrMo_6S_8$ and $BaMo_6S_8$), the saturation values were somewhat higher than 1 mΩcm (by a factor of 2 or 3). We believe that contact problems at the grain boundaries are responsible for these higher values. However, this hypothesis has still to be proved.

The variation of the resistivity of $EuMo_6S_8$, $SrMo_6S_8$, $BaMo_6S_8$, and $EuMo_6Se_8$ with temperature in the rhombohedral phase differs from the

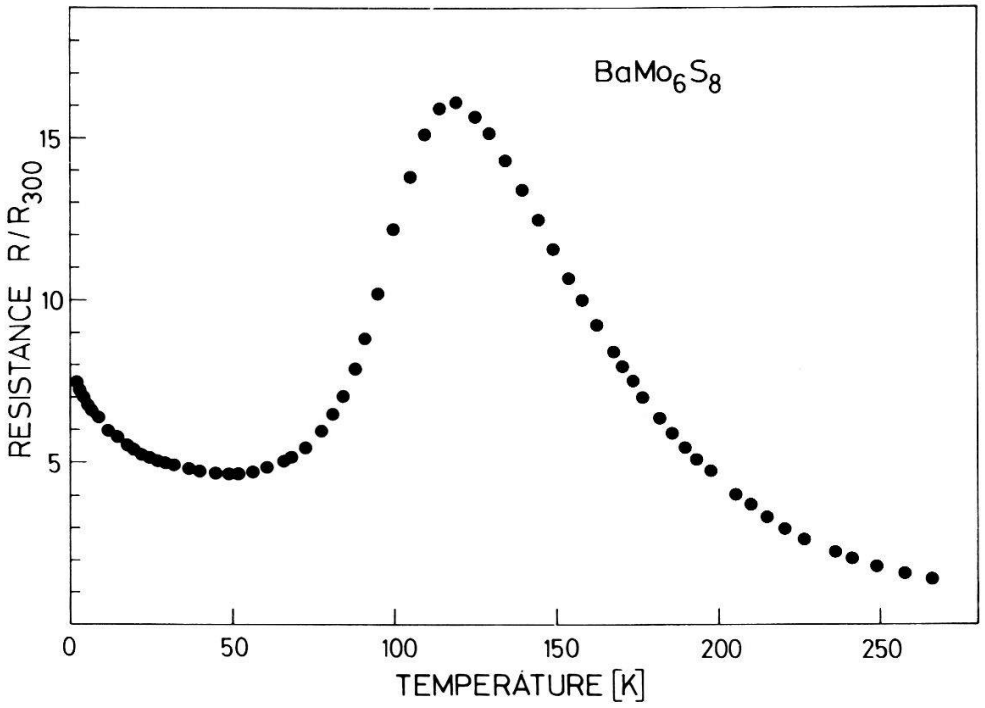

Figure 3.11
Resistivity of $BaMo_6S_8$ versus temperature.

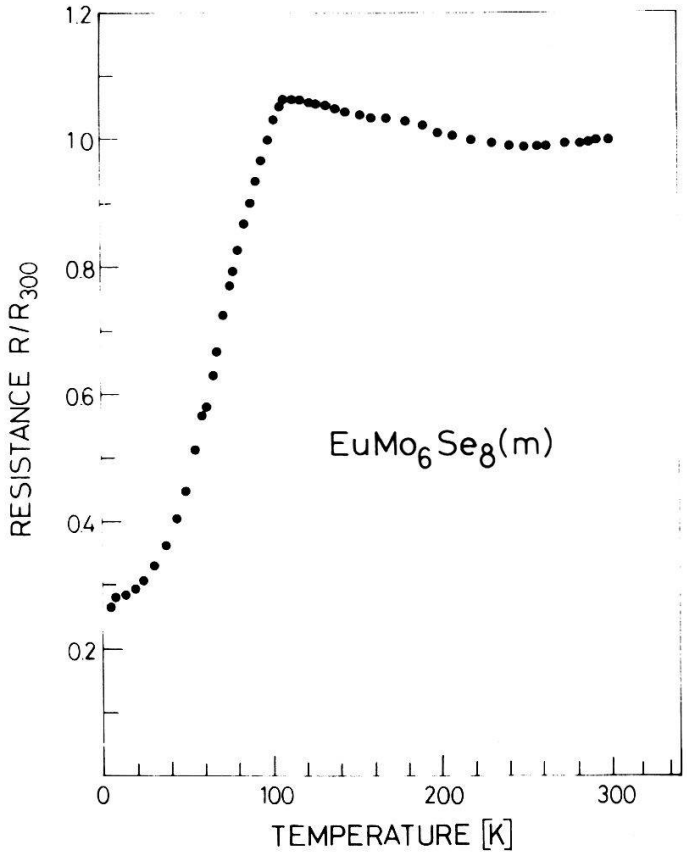

Figure 3.12
Resistivity of $EuMo_6Se_8$ versus temperature.

"standard behaviour" of $PbMo_6S_8$. The resistivity of $EuMo_6S_8$ slowly decreases, as the temperature decreases below 300 K, and passes through a minimum at 220 K. Below, a small continuous rise over a temperature interval of more than 100 K is observed which precedes the sharp increase at 109 K, where the structural phase transformation takes place. Figure 1 of Ref. [23] exhibits this behaviour in a more clear-cut way. The same behaviour of the resistance above the phase transformation is found in $EuMo_6Se_8$ with a resistance minimum at 260 K.

In $SrMo_6S_8$, there is also a clear rise of the resistivity, as the temperature drops below 250 K. The existence of a resistance minimum at 250 K is brought out in Fig. 2 of Ref. [6]. This increase of the resistance appearing already in the rhombohedral phase of $M^{2+}Mo_6X_8$ compounds, can be observed in $BaMo_6S_8$ in a much more pronounced way. Since the triclinic structure transformation seems to be of first order because of the sharp peak occurring in the specific heat at the transition temperature [6], it is very unlikely that the resistance rise in the rhombohedral phase comes about by fluctuation effects above the transformation. A large transformation interval of the order of 100 K due to sample inhomogeneities must equally well be excluded because of the high sample quality.

In summary, as a first indication for an anomalous behaviour of $M^{2+}Mo_6X_8$ compounds in their rhombohedral crystal structure, we have found a resistance minimum at temperatures above 200 K, followed by an unexpected increase of the resistance, as the temperature decreases. This resistance increase is usually very small, but in the case of $BaMo_6S_8$ it is very pronounced. This may indicate the existence of partial gaps at the Fermi energy due to some collective phenomenon. This effect should be distinguished from the triclinic transformation which takes place at much lower temperature.

In the following we will call the temperature interval between the resistance minimum and the triclinic phase transition the "intermediate region". Before trying an interpretation of the resistance anomaly correlated with that temperature interval, let us investigate the Hall effect in the rhombohedral phase.

3.4. *Hall coefficient of* $M^{2+}Mo_6X_8$ *compounds at ambient temperature*

In this section, we would like to come to a more quantitative study of the properties of Chevrel compounds with divalent cations in the high-temperature phase by investigating the Hall effect at ambient temperature. A good starting point for the discussion of the Hall coefficient R_H is the following expression which can be derived from the Boltzmann equation in the case of cubic metals [24]

$$R_H = \frac{12\pi^3}{e} \int \left(\frac{1}{\rho_k}\right) \tau_k^2 v_k^2 \, dS \Big/ \left(\int \tau_k v_k \, dS\right)^2 \tag{3.4}$$

Here, $1/\rho_k$ is the mean curvature at point k on the Fermi surface, v_k is the electron velocity, τ_k the relaxation time, and dS the element of area. Clearly, if

the Fermi surface is nonspherical then $1/\rho_k$, v_k, and τ_k will differ from point to point and the computation of R_H becomes very complex. To overcome such complications one can choose two distinct groups of electrons from geometrically distinct regions of the Fermi surface and express equation (3.4) as a summation. This is the two band approach. Using

$$\sigma = \frac{e^2}{12\pi^3\hbar} \int \tau_k v_k \, dS \tag{3.5}$$

we get for the Hall coefficient

$$R_H = \frac{\sigma_1^2 R_{H1} + \sigma_2^2 R_{H2}}{(\sigma_1 + \sigma_2)^2} \tag{3.6}$$

where R_{Hi} is defined equivalently to R_H in equation (3.4). Interactions between electrons coming from different pieces of the Fermi surface, are neglected in this approach. When approximating the two distinct parts of the Fermi surface by appropriate spheres, then the mean curvature of the Fermi surface is given by the Fermi vector k_F and the electron velocity v_k will be constant. We then find

$$R_{Hi} = \frac{\langle \tau_k^2 \rangle_{S_{Fi}}}{e n_i \langle \tau_k \rangle_{S_{Fi}}^2} \tag{3.7}$$

where $\langle \tau_k \rangle_{S_{Fi}}$ is the average value of τ_k over the Fermi surface part S_{Fi} and n_i the corresponding density of electrons. At high temperature, phonon scattering will be the dominant scattering process. When the temperature is higher than the Debye temperature, all states are available to any scattered electron because of the long q vector, and therefore the relaxation time should be isotropic. Assuming that one part of the Fermi surface will be a hole surface, Equation (3.6) reduces to

$$R_H = \frac{\mu_h^2 n_h - \mu_e^2 n_e}{e(\mu_h n_h - \mu_e n_e)^2} \tag{3.8}$$

where $\mu = e\tau/m^*$ and $\sigma = en\mu$ have been used.

Since in a compensated metal like $M^{2+}Mo_6X_8$, electron-hole scattering has no effect on the Hall coefficient [25], it is expected that equation (3.8) will be quite a good approximation for describing the Hall effect in Chevrel compounds with divalent cations at ambient temperature in sufficiently low magnetic fields. Equation (3.8) only holds in the low-field limit which is characterized by $\mu \ll (\mu_0 H)^{-1}$. Here, the lifetime of an electron between collisions remains short enough that the topological features of the Fermi surface are not manifested in the electron motion. In higher fields the Hall coefficient R_H generally depends on the magnetic field.

Figure 3.13 shows schematically how the Hall coefficient varies when going from the low-field to the high-field limit [26]. Unfortunately, no theory exists for

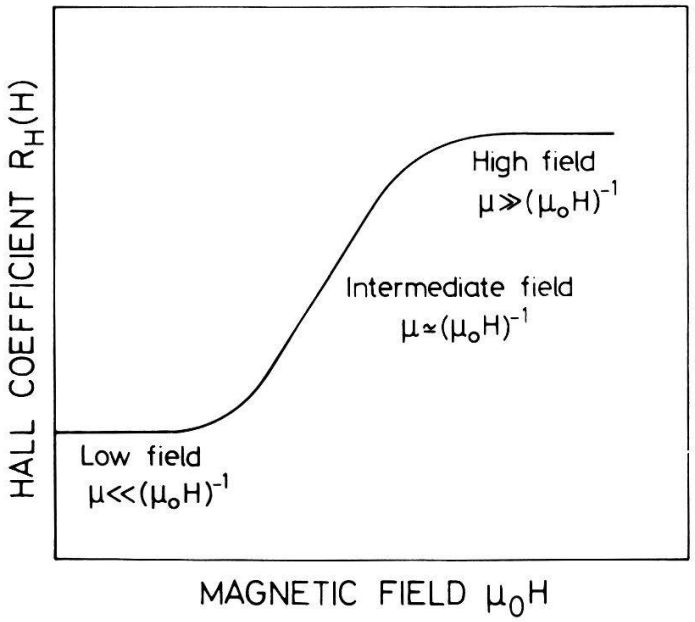

Figure 3.13
Magnetic-field dependence of the Hall coefficient for $R_H(0) < R_H(\infty)$. Schematically after [26].

the intermediate region, and the high-field conditions are hard to achieve experimentally. Chevrel phases at ambient temperature and fields up to 7 tesla are situated in the low-field region well below the transition regime of R_H, since the charge carrier mobilities are very small. The measured Hall voltage was in all cases a linear function of the applied field in agreement with the low-field condition. At low temperature, however, this condition was clearly violated in certain compounds.

Figure 3.14 presents the Hall coefficient $R_H(0)$ of $M^{2+}Mo_6X_8$ compounds as well as the pseudoternary series $Eu_xSn_{1-x}Mo_6S_8$ at ambient temperature. $R_H(0)$ is found to be always positive. For theoretical reasons, compounds with an even number of electrons per cluster should have equal electron and hole concentrations. Real samples always contain a certain amount of lattice defects and

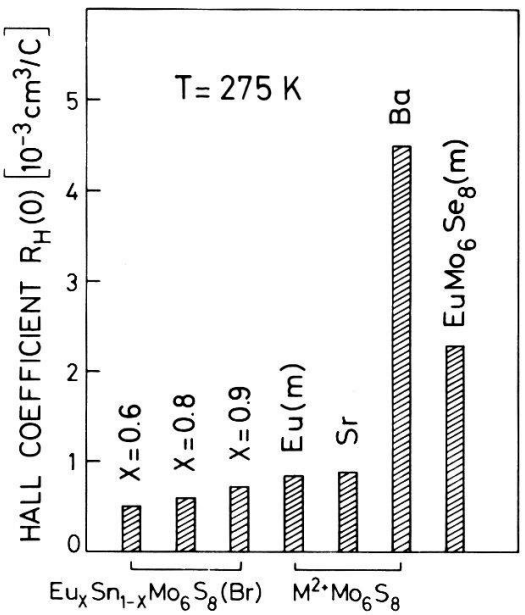

Figure 3.14
Hall coefficient of some MMo_6X_8 compounds and the series $Eu_xSn_{1-x}Mo_6S_8(Br)$ at ambient temperature.

impurities which may lead to a change of the compensation state in favour of one carrier type. However, a negative Hall effect at ambient temperature has never been observed, suggesting that the positive sign may be an intrinsic, characteristic feature of the rhombohedral phase. In terms of the two-band model, this would mean that the hole mobility is always somewhat higher than the electron mobility. Next, the values of the Hall constant will be analysed. Let us start with $EuMo_6S_8$ having a Hall coefficient $R_H(0) = 0.84 \times 10^{-3}\,cm^3/C$ at 276 K. Thus the effective number of carriers is $n_{eff} = 7.4 \times 10^{21}/cm^3$. This number can only mean an upper limit of the real charge density. Assuming $n_h = n_e = n$, we have

$$R_H(0) = \frac{1}{ne}\frac{\mu_h - \mu_e}{\mu_h + \mu_e} \tag{3.9}$$

Therefore, the ratio R_H/ρ, usually called Hall mobility, just gives the difference of the two mobilities

$$\frac{R_H}{\rho} = \mu_H = \mu_h - \mu_e \tag{3.10}$$

At this point we would like to stress that the Hall constant is usually much less influenced by the sample quality than is the resistivity [13]. Thus for a correct quantitative interpretation of the quantity R_H/ρ, one needs very compact and pure samples. Fortunately, the melted sample $EuMo_6S_8$ fulfills this stringent condition. We find $R_H/\rho = 0.8\,cm^2/Vs$. Taking as concentration for both carrier types $n = 1 \times 10^{21}\,cm^{-3}$, we finally find the following transport parameters:

$EuMo_6S_8$ $T = 276\,K$	$\mu_h = 3.5\,cm^2/Vs$ $\mu_e = 2.7\,cm^2/Vs$ $n_e = n_h = 1 \times 10^{21}\,cm^{-3}$

Although these parameters are not the result of a direct measurement, their values are quite reasonable. The resistivity of $EuMo_6S_8$ at high temperature is nearly temperature-independent, i.e. "saturated". Therefore, one should expect mobilities which are very close to the estimated lower limit of $2.9\,cm^2/Vs$ in Chevrel compounds. This is indeed the case indicating that the carrier densities are correctly determined.

It should be mentioned that resistivity saturation has also been reported for other materials, such as A15 compounds [27], intermediate valence compounds [28], concentrated transition-metal alloys [29], and has been interpreted in terms of the Ioffe–Regel resistivity limitation [30] due to an electron mean free path of the order of the interatomic spacing. The saturation resistivity in those cases is typically $150\,\mu\Omega cm$ and thus one order of magnitude smaller than in Chevrel phases. This is, however, not surprising since the conduction electron density in ternary molybdenum chalcogenides seems to be much lower than in the binaries due to the cluster structure of the former compounds.

In all cases, there should be an extraordinary scattering mechanism making the mean free path very short. In A15 and Chevrel-phase compounds, lattice instabilities might be the main reason for such a strong scattering. In $EuMo_6S_8$, $SrMo_6S_8$, etc. the saturation of the resistivity already appears at ambient temperature, whereas in Nb_3Sn or $PbMo_6S_8$ temperatures of about 1000 K are needed for saturation, in good agreement with the relative strength of the lattice instabilities.

Coming back to the discussion of Fig. 3.14, we find that $SrMo_6S_8$ may in fact be considered as non-magnetic reference compound for $EuMo_6S_8$, since also the Hall coefficients of both compounds are nearly equal. Figure 3.15 shows that the Hall constant slightly decreases when substituting Eu by Sn. Such a substitution has the effect of progressively suppressing the structural phase transformation [32] and thus weakening the lattice instability. But at 250 K, i.e. in the "pure" rhombohedral phase of $EuMo_6S_8$, the number of charge carriers should be unaltered by this substitution in first approximation, so that the decrease of the Hall constant with increasing Sn concentration is mainly a mobility effect. The sample $Eu_{0.6}Sn_{0.4}Mo_6S_8(Br)$ becoming superconducting at $T_c = 8$ K, exhibits a Hall coefficient which is, at ambient temperature, about 40% smaller than the one of pure $EuMo_6S_8$. Hall-effect measurements on thin films of $PbMo_6S_8$ [33] have yielded a Hall constant $R_H(0) = 0.1 \times 10^{-3}\,cm^3/C$ at room temperature, which is 8 times smaller than the Eu value; however, it is not clear whether a sputtered film exhibits properties which are representative for the bulk behaviour of $PbMo_6S_8$.

Figure 3.14 further indicates that $BaMo_6S_8$ and $EuMo_6Se_8$ behave somewhat differently. Particularly $BaMo_6S_8$ exhibits at 275 K a Hall coefficient which is larger by a factor of 5 than the value found in $EuMo_6S_8$. Since also the resistivity

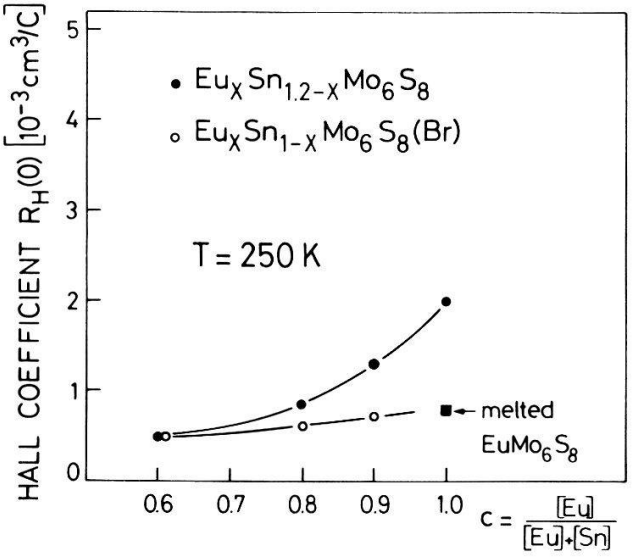

Figure 3.15
Hall coefficient of the pseudo-ternary series $Eu_xSn_{1.2-x}Mo_6S_8$ [31] and $Eu_xSn_{1-x}Mo_6S_8$(Br) at 250 K.

of $BaMo_6S_8$ at ambient temperature is significantly larger than the estimated maximum resistivity of 1 mΩcm in the rhombohedral phase, one may conclude that pseudo-gaps have been opened at the Fermi energy, leading to a reduction of the density of states and the conduction electrons.

3.5. *Temperature dependence of the Hall coefficient in the rhombohedral phase*

The temperature dependence of the Hall constant can be quite a complicated problem even in simple metals, since Fermi-surface anisotropy as well as scattering effects play an important role. We will therefore begin with the most simple case which Chevrel phases are able to offer. Figure 3.16 shows the Hall coefficient of $Eu_{0.6}Sn_{0.4}Mo_6S_8(Br)$ as a function of temperature. R_H very slowly decreases, as the temperature is reduced, but below 80 K, one finds a continuous increase of the Hall constant down to the temperature at which the sample becomes superconducting. A similar behaviour is found in $Eu_{0.75}Sn_{0.25}Mo_6S_8(Br)$ and $Eu_{0.5}Sn_{0.5}Mo_6S_8$ (Fig. 3.17) as well as in thin films of $PbMo_6S_8$ [33]. This suggests that the increase of the Hall constant at low temperature is a general feature of superconducting Chevrel compounds $M^{2+}Mo_6X_8$. One possible reason for such a behaviour may be anisotropy. Equation 3.7 shows that even for spherical Fermi surfaces anisotropic scattering may influence the Hall constant. The Cauchy–Schwarz inequality tells us that $\langle \tau_k^2 \rangle \geq \langle \tau_k \rangle^2$ and equality holds only when $\tau_k = \tau_{k'}$ for all k and k', i.e., when the relaxation time is isotropic (high temperature). However, since two different types of charge carriers contribute to the transport properties in the present case, only the relative change between R_{H1} and R_{H2} is manifested in the measured Hall constant. Therefore, a unique determination of the anisotropy factor is impossible.

The striking similarity between the behaviour of the Hall constant, presented in Fig. 3.16, and the one reported for $PbMo_6S_8$ suggests an alternative explanation: the increase of the Hall constant at low temperature may be due to a

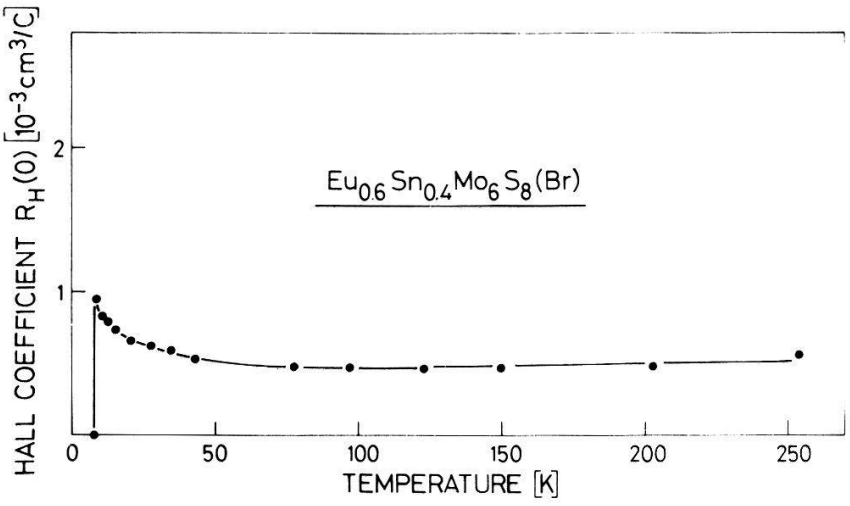

Figure 3.16
Hall coefficient of $Eu_{0.6}Sn_{0.4}Mo_6S_8(Br)$ as a function of temperature.

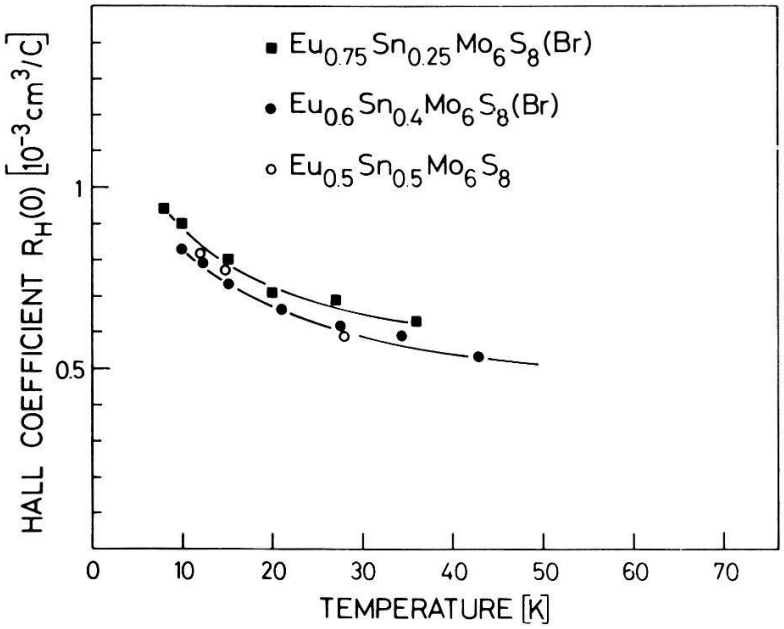

Figure 3.17
Low-temperature behaviour of the Hall constant in the series $Eu_xSn_{1-x}Mo_6S_8$ for various Eu concentrations.

supercell-ordering transition as proposed for $PbMo_6S_8$ in [15]. The increase may indicate a reduction of the carrier concentration and we may then ask, what will be the critical temperature of $PbMo_6S_8$ when the lattice distortion or the corresponding electronic transition can be suppressed.

We now turn to the more complicated case of compounds, which undergo a triclinic phase transformation at low temperature. Particularly the behaviour of the Hall coefficient in the "intermediate" region between triclinic phase and "pure" rhombohedral phase will be envisaged. The existence of such an intermediate region is clearly brought out in Fig. 3.18, which presents the Hall constants of some $M^{2+}Mo_6X_8$ compounds. As the temperature is reduced below room temperature, $EuMo_6S_8$ and $SrMo_6S_8$ first behave similarly: the Hall constants slowly decrease with decreasing temperature. Below 220 K, however, R_H of $SrMo_6S_8$ starts to increase rapidly, whereas $EuMo_6S_8$ is steering for a change of sign. Note that the triclinic structure transformation occurs at 110 K in these two samples. (The transformation temperature of $SrMo_6S_8$ has been determined by the break in the resistivity which accompanies the triclinic lattice transformation according to [34].) The change of sign, observed in the melted sample of $EuMo_6S_8$, does not appear in hot-pressed or sintered samples. This suggests that impurity effects may inhibit the change of sign. Since $EuMo_6S_8$ is a compensated metal according to our previous discussion, it may react very sensitively to any small perturbation. Nevertheless, near 220 K one finds in all samples, independently of the preparation technique, a pronounced tendency towards an increase of the absolute value of the Hall constant. Impurity limited $EuMo_6S_8$ samples [31] exhibit a behaviour similar to the one of $EuMo_6Se_8$(m) in Fig. 3.18.

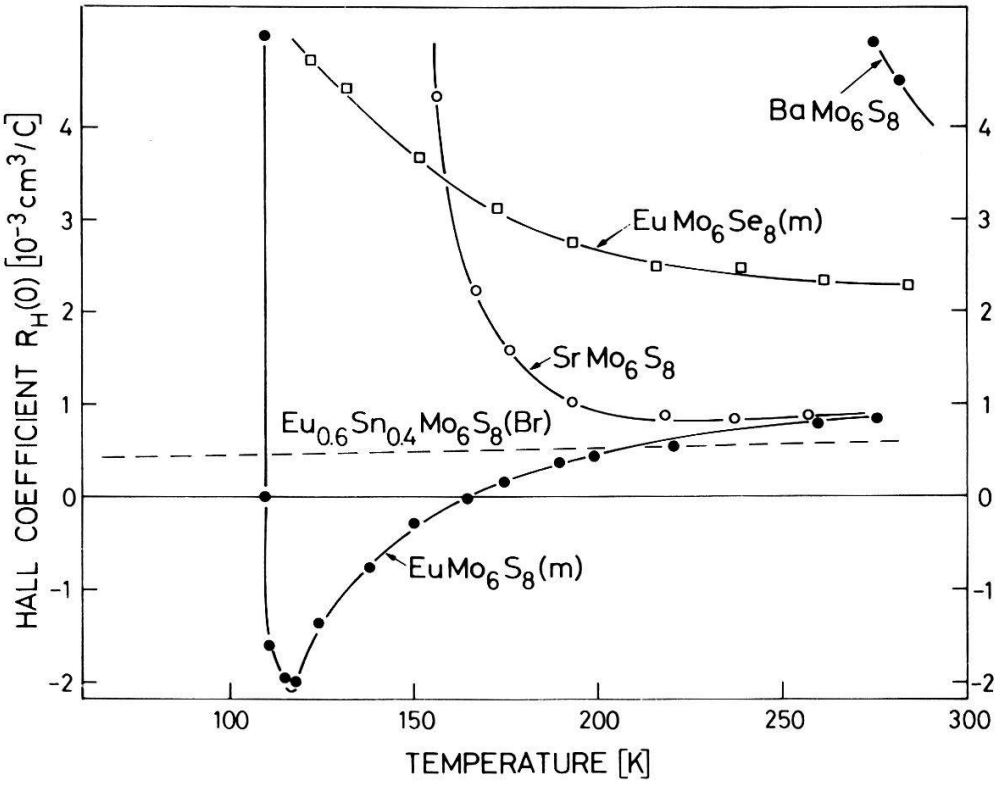

Figure 3.18
Hall coefficient of $M^{2+}Mo_6X_8$ compounds in the "intermediate" regime. The dashed line presents the behaviour of $Eu_{0.60}Sn_{0.40}Mo_6S_8(Br)$ which is considered to be the normal behaviour in the rhombohedral structure.

Figure 3.18 clearly indicates that the anomalous behaviour in the intermediate region becomes increasingly pronounced when going from $EuMo_6S_8$ to $SrMo_6S_8$ and $BaMo_6S_8$. This seems to be correlated with the rhombohedral lattice parameters: the more separated the Mo_6S_8 clusters are, i.e. the more localized the electrons are at the Mo octahedra, the more pronounced the transport anomalies appear in the intermediate region. Note that a larger intercluster distance will result in even narrower bands and higher densities of states. We therefore believe that in the pure rhombohedral phase no qualitative difference exists between Chevrel compounds with divalent cations. Since $BaMo_6S_8$ shows the transport anomalies appearing in the intermediate region in a more clear-cut way than the other compounds, we will use it as a guide to investigate the nature of this region.

Figure 3.19 shows the Hall coefficient of $BaMo_6S_8$ in the high-temperature phase. The strong rise of R_H is correlated with a similar increase of the resistivity. An analysis in terms of the two-band model indicates that neither the number of carriers nor their mobilities stay constant in the "intermediate" regime of $BaMo_6S_8$. The number of carriers is reduced, probably due to the destruction of certain portions of the Fermi surface by gapping.

The pseudogap created by the instability is believed to be very small, of the order of several meV. The thermal energy near 200 K is much larger than the gap, so that the effect is expected to be smeared out resulting in a very weak

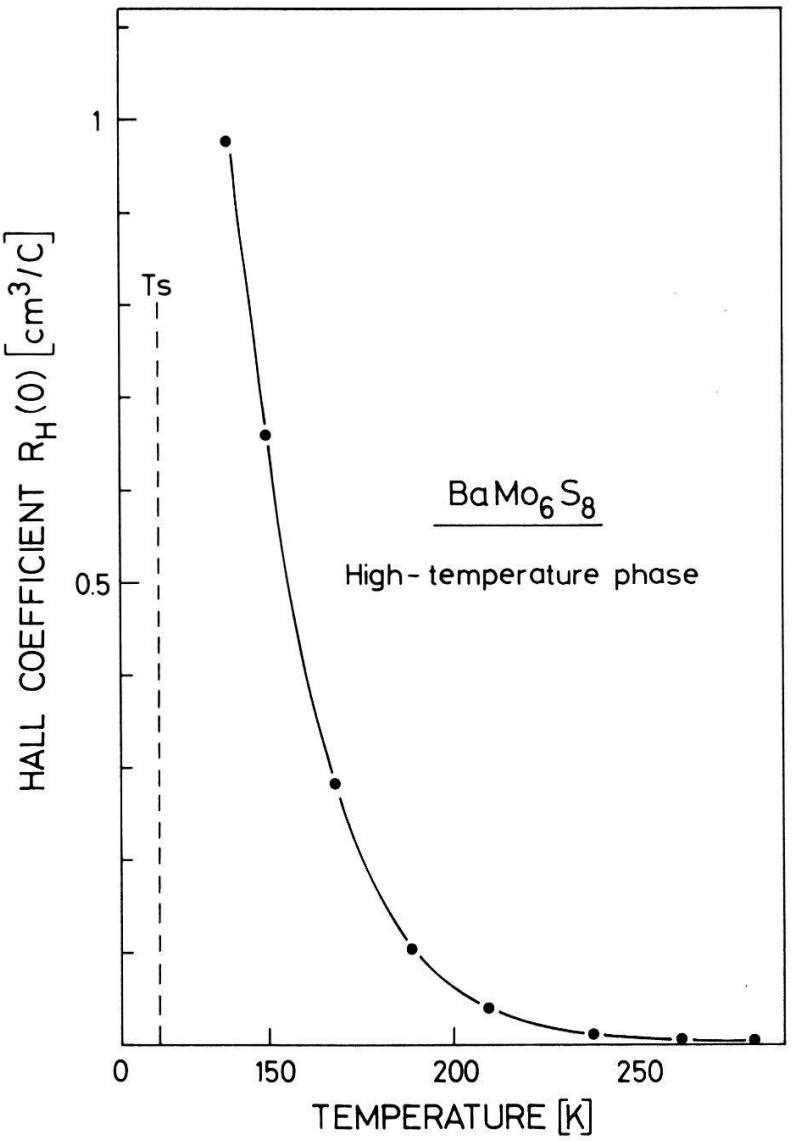

Figure 3.19
Hall coefficient of $BaMo_6S_8$ in the "intermediate region".

temperature dependence of the observed anomalies. Only in $BaMo_6S_8$, the gap should be of the order of the thermal energy.

The physical reason for such a partial gapping might be a slight distortion of the rhombohedral lattice that is similar to the lattice anomaly recently discovered in $PbMo_6S_8$ [16]. This assumption is confirmed by the similar behaviour of the Hall coefficient in $PbMo_6S_8$ below that lattice transformation and in $M^{2+}Mo_6X_8$ compounds in the "intermediate region".

We therefore propose that two distinct electronic transitions may appear in the compounds considered here, a very small one near ambient temperature and a more pronounced one at about 100 K. Such multiple transitions are a well-known phenomenon in lower-dimensional systems such as linear chain metals (see Section 4.4). In the superconducting compounds $PbMo_6S_8$ and $SnMo_6S_8$, only the first transition takes place at low temperature.

Up to now, no evidence for an anomaly of the lattice parameters in the

rhombohedral phase of $BaMo_6S_8$, $EuMo_6S_8$, etc. could be found. Since the effects are small even in the transport properties, a slight lattice distortion or a periodic lattice modulation could easily remain undetected. High-resolution neutron diffraction may be the most appropriate technique for searching such effects. The main results of this section are summarized in Table 3.2.

Table 3.2
Transport properties of $M^{2+}Mo_6X_8$ compounds in the intermediate regime. T_I is the temperature at which the anomalous behaviour of resistance $R(T)$ and Hall constant $R_H(T)$ starts to appear thus defining the beginning of the intermediate regime. T_s is the temperature of the triclinic lattice transformation.

	T_I[K]	T_s[K]	$R(T_s)/R(T_I)$	$R_H(T_s)/R_H(T_i)$
$EuMo_6S_8$(m)	220	109	1.4	3.7
$SrMo_6S_8$	220	110*	5	150
$BaMo_6S_8$	>300	120*	>16†	>300†
$EuMo_6Se_8$(m)	260	103	1.1	2.7

*) The triclinic transformation temperature is somewhat higher in melted samples (139 K for $SrMo_6S_8$ and 171 K for $BaMo_6S_8$ [6]).
†) Indicated is the ratio $R(T_s)/R(300\,K)$ and $R_H(T_S)/R_H(300\,K)$

4. On the nature of the low-temperature phase of $M^{2+}Mo_6X_8$ compounds

4.1. *Introductory remarks*

The question about the nature of the triclinic structure transformation is not completely answered. From a crystallographic point of view, the symmetry is lowered due to a slight deformation of the Mo_6X_8 clusters without changing the unit-cell volume. As a consequence the doubly degenerate E_g-band may split off leading to a low density of states at the Fermi surface. Specific heat measurements [6] and band-structure calculations [17] have confirmed this supposition. This suggests that the low-temperature properties of $M^{2+}Mo_6X_8$ compounds are the direct consequence of the rhombohedral to triclinic phase transformation. In compounds with strong E_g-band splitting a semiconductor-like behaviour should be observed at low temperature due to the freezing in of conduction electrons. When the modification of the band structure is less pronounced, we may expect a metallic or semimetallic ground state. On the other hand, it is not excluded that other physical mechanisms are responsible for the low-temperature behaviour, whose appearance is only favoured by the electronic structure of the triclinic phase. We will therefore investigate the transport properties of $M^{2+}Mo_6X_8$ compounds in the transformed triclinic phase.

4.2. *Hall effect in the low-temperature phase*

We have already seen in Figs. 3.9 to 3.12 that the electrical resistivity of $EuMo_6S_8$ and $SrMo_6S_8$ increases at low temperature, whereas $EuMo_6Se_8$ seems to

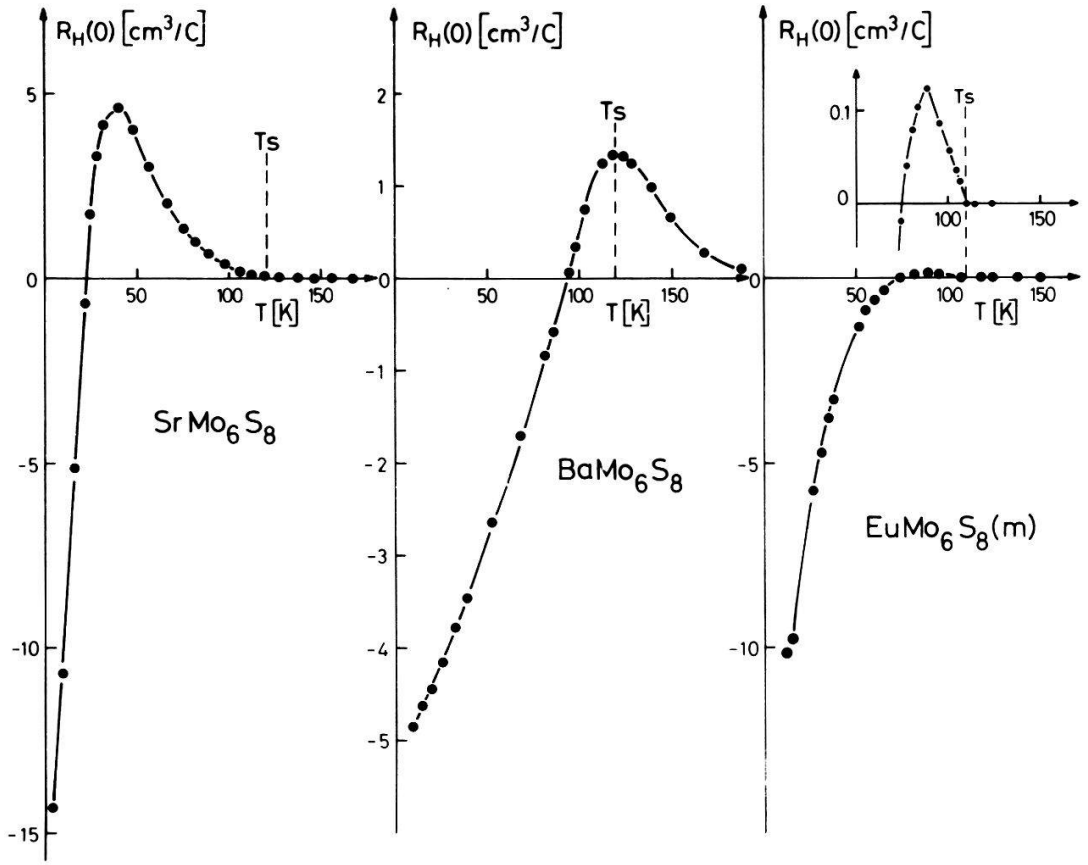

Figure 4.1
Hall coefficient in Chevrel compounds with M = Sr, Ba, Eu near and below the phase transition. The insert in the Eu-diagram presents details of the Hall constant at T_S.

have metallic properties in the triclinic phase. The behaviour of $BaMo_6S_8$ is more complicated, but at 4 K its resistance is more than 7 times higher than at room temperature. An interpretation of these results is not meaningful before having more information about the low-temperature properties of these materials. In Fig. 4.1 we present the Hall constant of $SrMo_6S_8$, $BaMo_6S_8$, and $EuMo_6S_8$ in the temperature region below 200 K. The relatively large values of R_H at 4 K in all three compounds indicate a charge carrier concentration of about $10^{17}/cm^3$, which is 4 orders of magnitude smaller than the value determined at ambient temperature. Such a conduction electron concentration does not point to a real band gap, but rather to a semimetallic situation at the Fermi energy. This hypothesis is confirmed by the behaviour of the resistivity at low temperature, which does not really diverge. The similarity in the behaviour of the Hall effect near and below the phase transition region for all three compounds is striking. In $SrMo_6S_8$ and $EuMo_6S_8$, the maximum of the Hall constant appears well below the phase transition temperature T_s, whereas it coincides with T_s in $BaMo_6S_8$.

If the structural phase transformation causes a splitting of the E_g-band, then one should expect that the compounds behave as compensated semimetals or gapless semiconductors at low temperature. In such a case, the sign of the Hall effect is dominated by mobility effects. In Fig. 4.2 the Hall mobilities μ_H, defined as the ratio of Hall coefficient to resistivity, are presented for the three

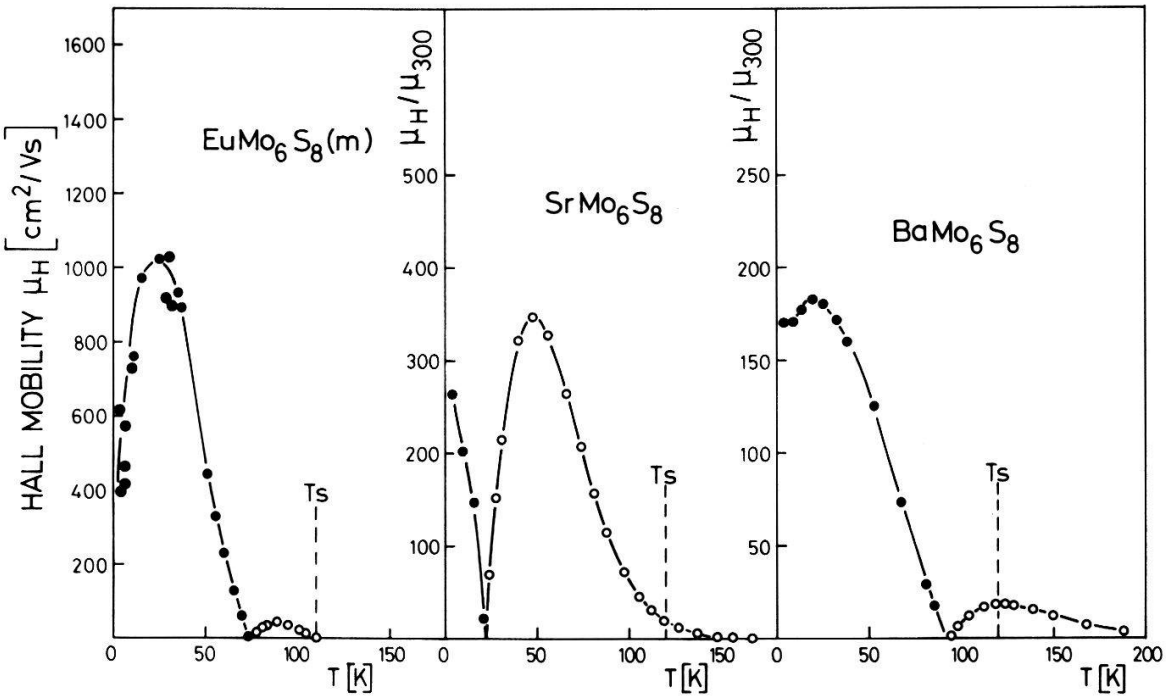

Figure 4.2
Hall mobilities of Chevrel compounds with M = Eu, Sr, Ba near and below the phase transition. Open circles indicate positive sign, full circles negative sign.

compounds. Only relative Hall mobilities $\mu_H(T)/\mu_H(300\,\mathrm{K})$ are given when the samples were prepared by hot pressing. But the Hall mobility at 300 K is expected to be not very different from $1\,\mathrm{cm}^2/\mathrm{Vs}$ for $SrMo_6S_8$ and $BaMo_6S_8$. The temperature dependence of the Hall mobilities is very reminiscent of the behaviour of R_H shown in Fig. 4.1, in good agreement with our assumption of a compensated system (cp. equations (3.5) and (3.6)). Below the phase transition a strong increase of the mobilities is observed. High mobilities are a well known phenomenon in semiconductor physics. Due to the relative complex structure of semiconductor valence bands, the hole effective mass in a given semiconductor is generally larger than the electron effective mass. Therefore, it is usually true that the electron mobility is larger than the hole mobility. As a result, the Hall constant of an intrinsic semiconductor at low temperature is generally of negative sign.

This argument may also hold in the present case but in a less pronounced way. The ratio of electron to hole mobility must not necessarily be very different from unity. Furthermore, impurities may easily prevent the electrons from becoming more mobile than the holes, resulting in a positive Hall effect at low temperature. A positive Hall effect has been observed for both $Sr_xMo_6S_8$ and $Eu_xMo_6S_8$, when the nominal M-atom concentration was $x = 1.0$. It turned out, that with a nominal concentration $x = 1.1$ stoichiometric crystals could be fabricated. M-atom vacancies may act as electron scattering centers, but may also influence the position of the Fermi energy towards a p-type semiconducting behaviour with positive Hall constant.

Figure 4.3 shows that below the triclinic phase transformation, a deviation of

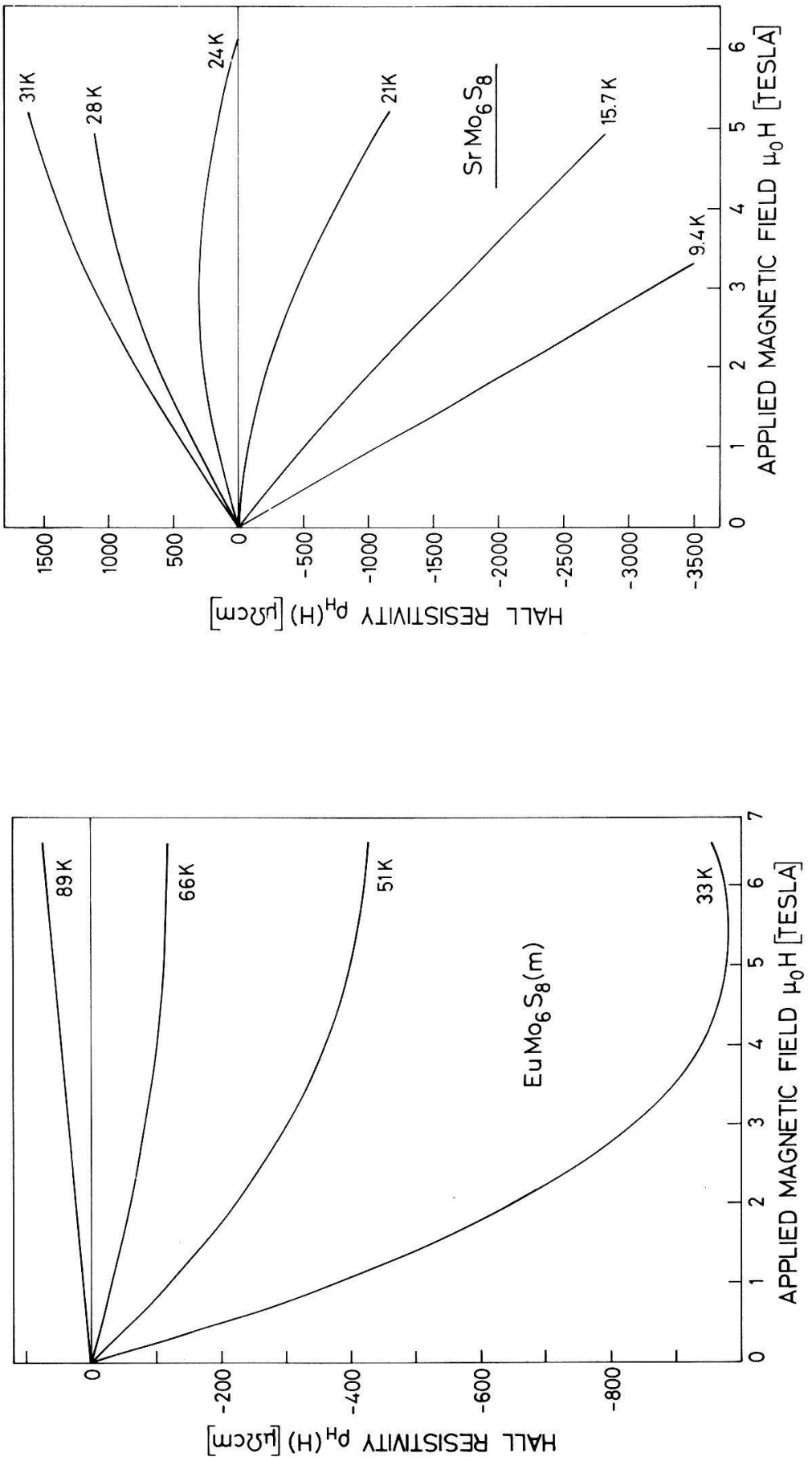

Figure 4.3
Hall resistivity of $EuMo_6S_8$ and $SrMo_6S_8$ in the low-temperature phase. Further information about the Hall resistivity of $EuMo_6S_8$ below 33 K can be found in Fig. 4.15.

the Hall resistivity $\rho_H = R_H H$ from a linear field dependence is observed. This may be explained by a transition from the low-field region to the intermediate-field region (Fig. 3.13). The observed Hall mobilities are not in disagreement with such a transition at about 2 tesla. On the other hand, the deviation from linearity in the Hall resistivity is found to be most pronounced near the compensation point of the Hall coefficient ($\mu_h^2 n_h - \mu_e^2 n_e = 0$) at 22 K in $SrMo_6S_8$. This suggests that the non-linear Hall resistivity may result from a slight change in the collision times for spin-up and spin-down electrons (or holes) and/or from a small modification of the number of charge carriers as a function of field due to band-shift effects, disturbing the initial compensation state in zero field. This variation of the Hall coefficient with magnetic field should become increasingly unimportant the further away one is from the compensation point. This is indeed observed in $SrMo_6S_8$ at 9.4 K (Fig. 4.3), where the Hall resistivity is nearly a linear function of the applied field up to 6 tesla. The longitudinal magnetoresistance of $SrMo_6S_8$ at 4 K was found to be smaller than our detection limit which was mainly given by the precision concerning the longitudinal orientation of the sample in the field (±5°). Thus, if there is any longitudinal magnetoresistance, it must be smaller than 10^{-2} in fields up to 7 tesla. The transverse magnetoresistance of $SrMo_6S_8$ at low temperature exhibits a normal, positive behaviour with quadratic field dependence.

The situation is somewhat different in $EuMo_6S_8$ because of the existing exchange interaction between conduction electrons and Eu ions which may significantly amplify the action of the external field on the conduction electron spins. Since the exchange field, describing the mean polarization of the conduction electron spins due to their interaction with the localized Eu moments, is determined by the magnetization, its strength increases with decreasing temperature at fixed external fields. Therefore, even well below the compensation point of the Hall coefficient at 75 K in $EuMo_6S_8$, the term $\mu_h^2 n_h - \mu_e^2 n_e$ may be strongly influenced by the action of the exchange field. The anomalous behaviour of the Hall resistivity of $EuMo_6S_8$ at 33 K (Fig. 4.3) may be interpreted in that sense. The low-temperature properties of $EuMo_6S_8$ will be discussed in more detail in Section 4.3.

In $EuMo_6Se_8$, we find transport properties in the low-temperature phase which differ from the ones of the sulfides and which are reminiscent of a metallic ground state. The Hall constant of $EuMo_6Se_8$ as a function of temperature is shown in Fig. 4.4. Note that the scale of R_H is enlarged by a factor of 1000 compared with Fig. 4.1 to make visible the small variation of the Hall constant near the phase transition. Specific-heat measurements and temperature-dependent X-ray investigations [22, 34] also demonstrate that the change of the physical properties due to the phase transformation is much smaller than in the sulfides. Again, the mobilities increase with decreasing temperature, as already seen in the sulfides; however, the variation is smaller. The spectacular resistance drop at T_s is not in disagreement with such small variations: A small increase of the mobilities is sufficient to explain completely the resistivity curve, if the charge carrier concentration remains nearly unchanged at the phase transition.

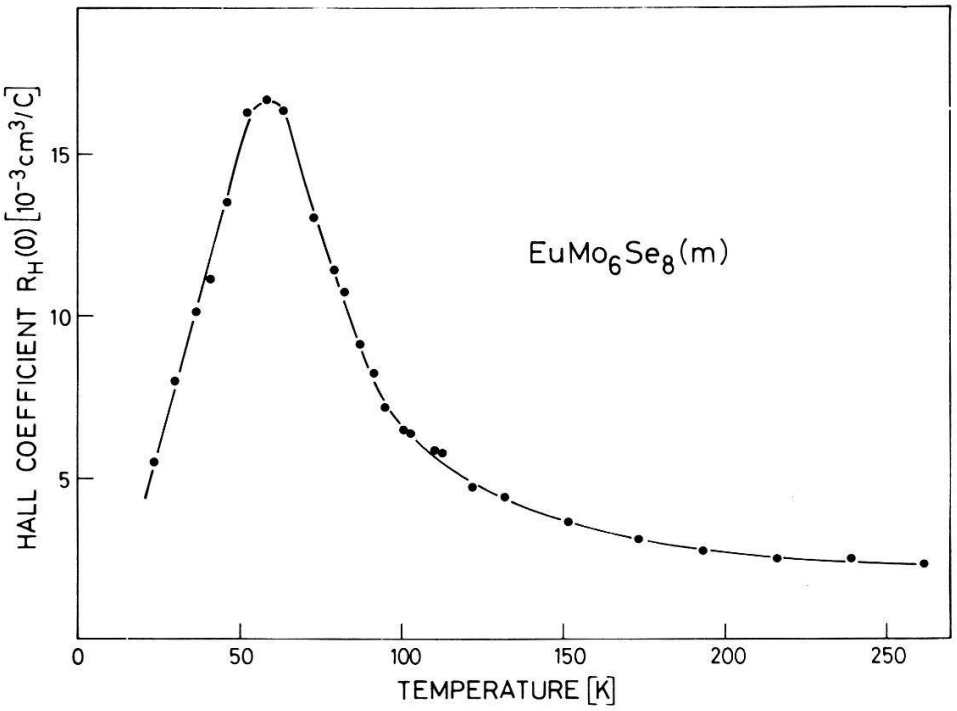

Figure 4.4
Hall coefficient of $EuMo_6Se_8$ versus temperature.

In Fig. 4.5 the Hall mobility of $EuMo_6Se_8$ is shown as a function of temperature. At low temperature, we again observe a tendency towards a change of sign, but the electron mobility does not really catch up to the Hall mobility.

Hall-effect measurements are usually performed with the aim of determining the conduction electron concentration. The interpretation of the Hall data, however, is extremely model-dependent. Unfortunately in the low-temperature phase we cannot proceed as for the rhombohedral phase, where the charge carrier concentration could be determined by relying on existing band-structure calculations. For the triclinic phase the atomic positions in the cluster have been accurately measured only for $BaMo_6S_8$ [5]. Therefore, it is only in this case where

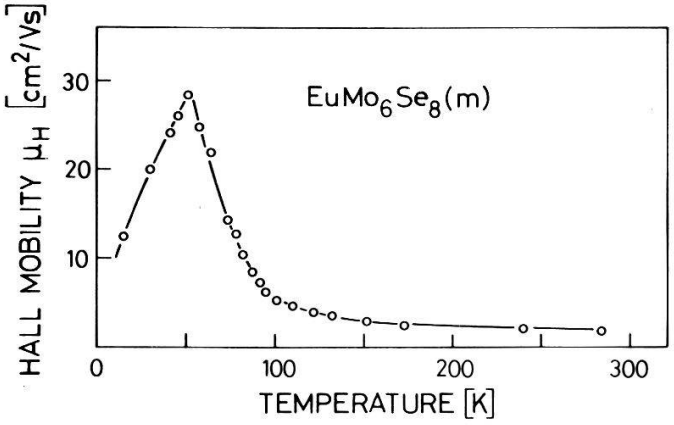

Figure 4.5
Hall mobility of $EuMo_6Se_8$ versus temperature.

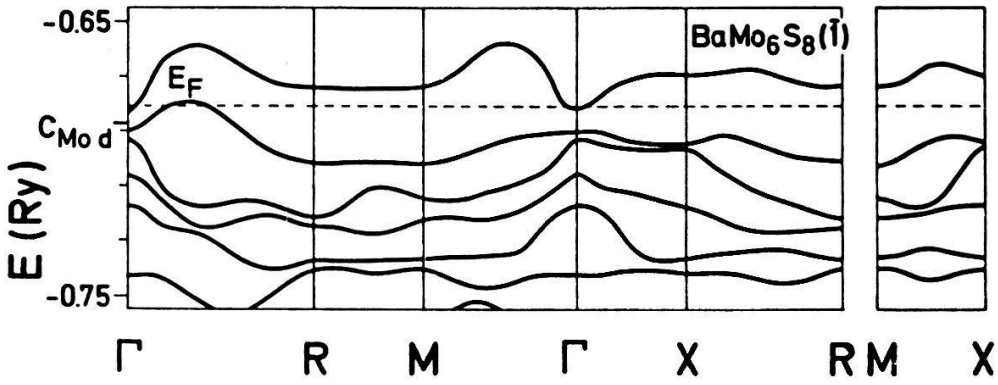

Figure 4.6
Band structure of $BaMo_6S_8$ in the low-temperature phase (after [17]).

band-structure calculations may lead to a reliable result. Nevertheless, we will roughly estimate the current carrier concentrations and mobilities at low temperature for the various compounds.

The band structure of $BaMo_6S_8$ at low temperature is shown in Fig. 4.6 (after [17]). This result may suggest that also the other compounds are essentially compensated semimetals, for which a two-band approach is not a bad approximation. This means that according to equation (3.5) we only need information about one mobility in order to find the charge carrier concentration, since the Hall constant R_H and the mobility difference (Hall mobility) are determined experimentally. An idea about the value of the hole mobility at low temperature can be obtained in the following way: In a compensated system, the observed temperature dependence of the Hall mobility mainly results from the competition between electrons and holes. For some unknown reason the electron mobility seems to increase just below the phase transition much less rapidly than the hole mobility (with the exception of $BaMo_6S_8$). We therefore assume that just below the transition temperature the hole mobility dominates the Hall mobility μ_H. By extrapolating this part of the Hall mobility to lower temperatures, we estimate the following hole mobilities at 4 K:

$EuMo_6Se_8$: $10^2\ cm^2/Vs$
$SrMo_6S_8$: $10^3\ cm^2/Vs$
$BaMo_6S_8$: $10^2\ cm^2/Vs$

For $BaMo_6S_8$, the electronic mobility rise below T_s has been extrapolated. These values should be considered as an order-of-magnitude result. Using these numbers we find the following electron and hole concentrations $n_e = n_h = n$ at helium temperature:

$EuMo_6Se_8$: $n = 1 \times 10^{20}\ cm^{-3}$
$SrMo_6S_8$: $n = 6 \times 10^{16}\ cm^{-3}$
$BaMo_6S_8$: $n = 6 \times 10^{17}\ cm^{-3}$

The conduction electron concentration of $EuMo_6Se_8$ is found to be only ten times smaller than the one of the high-T_c superconductor $PbMo_6S_8$. Whether this small

reduction of the electron concentration in $EuMo_6Se_8$ is sufficient to inhibit the occurrence of superconductivity or whether the triclinic phase is incompatible with superconductivity at all, cannot be decided here. Note that not the electron density, but the density of states at the Fermi energy is the appropriate quantity which determines the superconducting properties. The situation in $EuMo_6S_8$ at low temperature will be discussed in the following section.

4.3. *The anomalous transport properties of* $EuMo_6S_8$ *at low temperature*

The similarity of the transport properties of molybdenum sulfides with divalent cations leads us to the conclusion that the structural phase transformation and its direct consequences are not affected when a nonmagnetic M atom is replaced by a magnetic one. However, at low temperature the Eu-based Chevrel compounds exhibit many unusual physical properties which may result from their magnetic character.

We have found that $SrMo_6S_8$ may be considered as nonmagnetic counterpart of $EuMo_6S_8$. We shall call the behaviour of $EuMo_6S_8$ anomalous only when $SrMo_6S_8$ does not reveal the same feature. The lack of superconductivity and the resistance rise at low temperature are therefore not anomalous in the above sense. What is unusual, however, is the large, negative magnetoresistance that has been found in $EuMo_6S_8$ at low temperature [35, 36, 37]. In Fig. 4.7 the longitudinal magnetoresistance of $EuMo_6S_8$ is shown at various temperatures. It can be saturated when $\mu_B H > k_B T$. The saturation value of the magnetoresistance is strongly sample-dependent and can be as large as 92% in very pure samples. This value is, however, only obtained when the sample is cooled down very

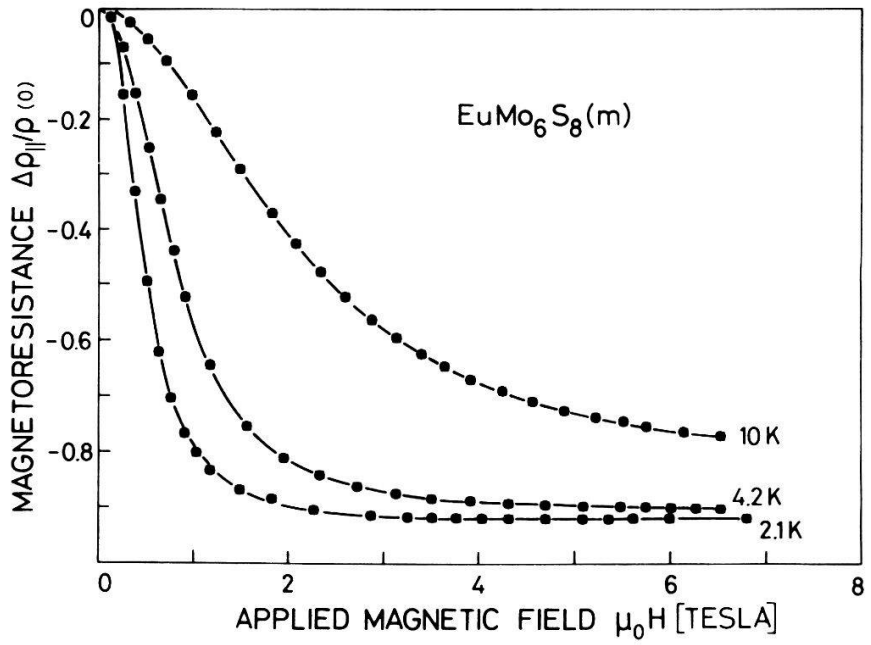

Figure 4.7
Longitudinal magnetoresistance of $EuMo_6S_8$ at low temperature. The longitudinal magnetoresistance of $SrMo_6S_8$ at 4 K does not differ from the zero line in this figure.

slowly through the structural phase transition. A too rapid cooling can reduce the saturation value of the magnetoresistance in melted samples by 50% [38]. This may explain why sintered samples usually reach a magnetoresistance of only 40%, because of the inevitable strains between the grains. Furthermore, there is a clear correlation between the saturation value of the magnetoresistance and the resistance ratio $R(2\,\mathrm{K})/R(300\,\mathrm{K})$, as can be seen in Fig. 4.8 for differently prepared samples.

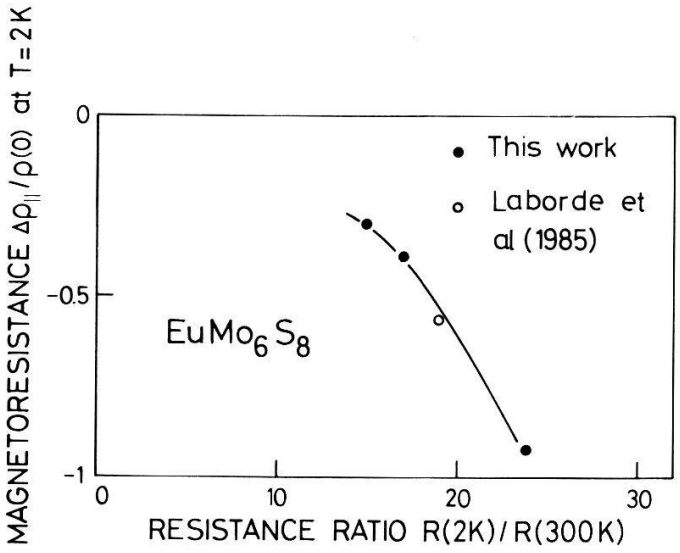

Figure 4.8
Relation between the saturation value of the magnetoresistance and the resistance ratio in $EuMo_6S_8$.

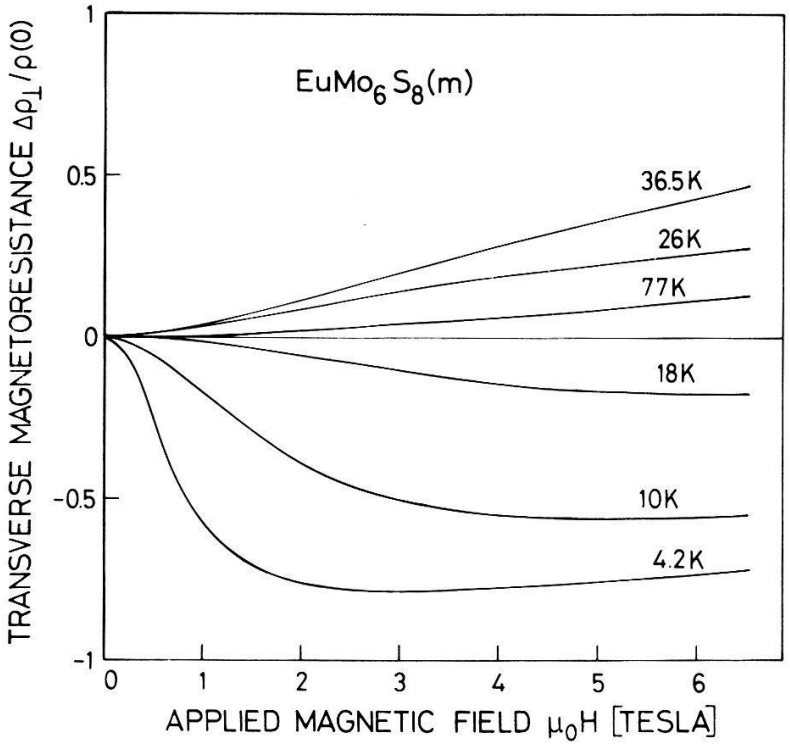

Figure 4.9
Transverse magnetoresistance of $EuMo_6S_8$ at various temperatures.

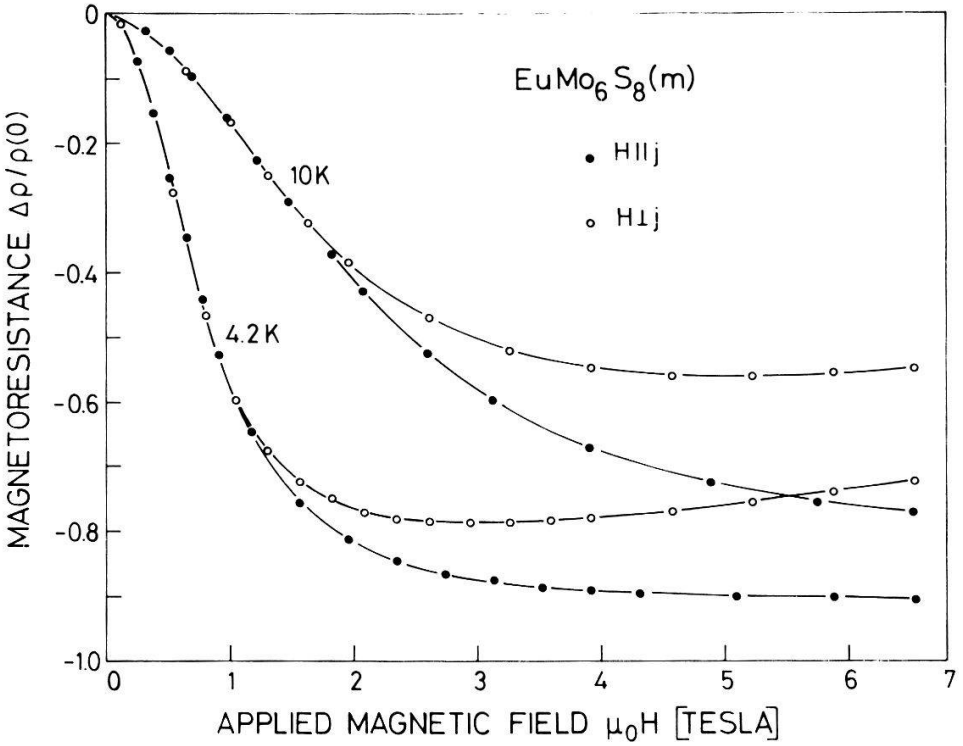

Figure 4.10
Magnetoresistance of $EuMo_6S_8$ for parallel and perpendicular current-field arrangement.

This anomalous effect appears equally well in the transverse magnetoresistance, which is also strongly negative at low temperature (see Fig. 4.9). There is, however, in addition the normal, positive contribution which becomes increasingly important as the temperature increases. As a result, above 20 K the transverse magnetoresistance reveals a positive sign. Since the anomalous, negative contribution is isotropic in first approximation (Fig. 4.10), it can be subtracted from the transverse magnetoresistance. We then obtain the pure transverse magnetoresistance which is found to depend quadratically on the applied field in the low-field region (Fig. 4.11), allowing us to define the magnetoresistance mobility μ_M by

$$\Delta\rho/\rho(0) = \mu_M^2(\mu_0 H)^2 \tag{4.1}$$

The magnetoresistance mobility of $EuMo_6S_8$ is shown in Fig. 4.12 as a function of temperature. One finds good agreement with the Hall mobility shown in Fig. 4.2. However, the magnetoresistance mobility is larger by a factor of 2. The large error at low temperature results from the subtraction of the anomalous part which dominates at low fields. Nevertheless, it turns out that the pure transverse magnetoresistance mobility at 10 K is about 1000 cm^2/Vs (cp. Fig. 4.11). This means that the magnetoresistance mobility decreases below 30 K. Such a decrease is consistent with the observed decrease of the absolute value of the Hall mobility below 30 K (Fig. 4.2), since in the two-band approach for a compensated semimetal both the Hall mobility and the magnetoresistnce mobility depend on the difference of electon and hole mobility [39].

A possible explanation for the observed decrease of Hall and magnetoresistance mobility might be an additional scattering mechanism which appears below

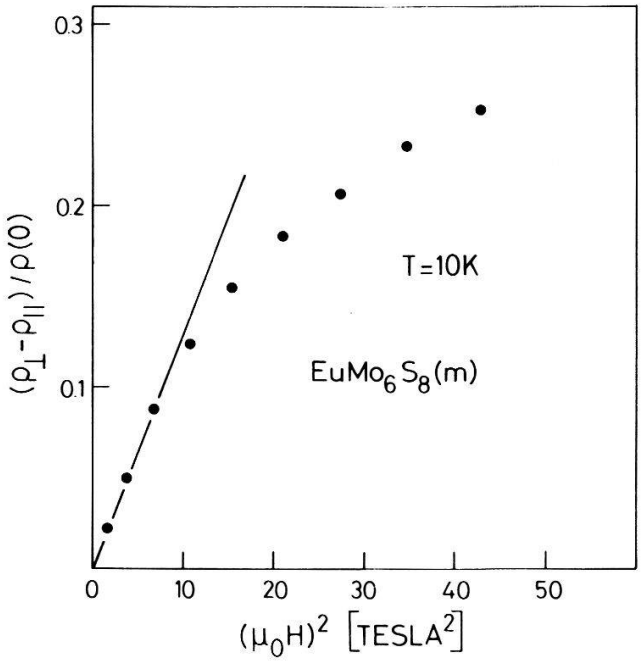

Figure 4.11
Pure transverse magneto-resistance of $EuMo_6S_8$ vs square of the applied field at 10 K.

30 K and which leads to a reduction of the electron mobility without having an equal effect on the holes. Temperature dependence and order of magnitude may point to a magnetic scattering (Kondo effect). At this point, we would like to point out that it seems to be a general feature of $M^{2+}Mo_6X_8$ compounds that electrons are more sensitive to impurity or magnetic scattering than holes. This may be explained by the fact that the wave functions in the two bands at the Fermi energy are somewhat different from each other, even in the rhombohedral phase.

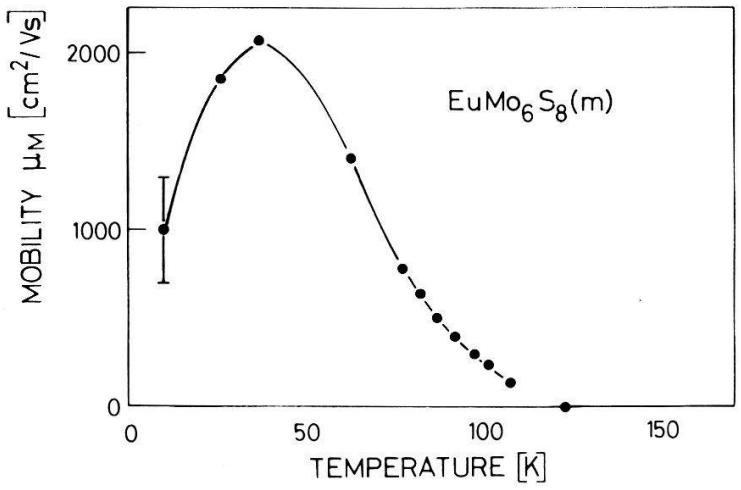

Figure 4.12
Magnetoresistance mobility of $EuMo_6S_8$ as a function of temperature.

As a consequence of our supposition of a magnetic scattering process appearing below 30 K, we are forced to attribute a certain part of the low-temperature resistance rise in $EuMo_6S_8$ to this effect. However, we find that the sum of electron and hole mobility is reduced by only 15% due to this scattering effect. Thus, the major part of the resistance rise must result from a diminution of the current carrier concentration.

In the following, we will concentrate on the large, negative magnetoresistance, since it is certainly one of the clues to understanding the unusual behaviour of $EuMo_6S_8$. The observed negative magnetoresistance has been interpreted [35] as a result of spin-flip-scattering suppression in the magnetic field. A dilute-Kondo-alloy theory [40] has been used to describe the field dependence of the magnetoresistance. According to that theory, the magnetoresistance should depend on the square of the magnetization at low magnetic fields. Dc- and ac-susceptibility measurements have shown that $EuMo_6S_8$ obeys a Curie–Weiss law above 0.5 K with a very small paramagnetic Curie temperature [41, 42, 43], indicating a very weak magnetic interaction between the Eu spins. Recently a Curie temperature smaller than 0.1 K has been reported [43]. Below 0.5 K, $EuMo_6S_8$ orders magnetically, but the exact ordering type is still unclear [42, 43].

The magnetization of $EuMo_6S_8$ above 1 K can therefore be described by a Brillouin function for free Eu moments. In Fig. 4.13, the magnetoresistance of $EuMo_6S_8$ at 2.1 K is compared with the Kondo-alloy theory. There is a clear disagreement with respect to the magnetic-field dependence when using the free

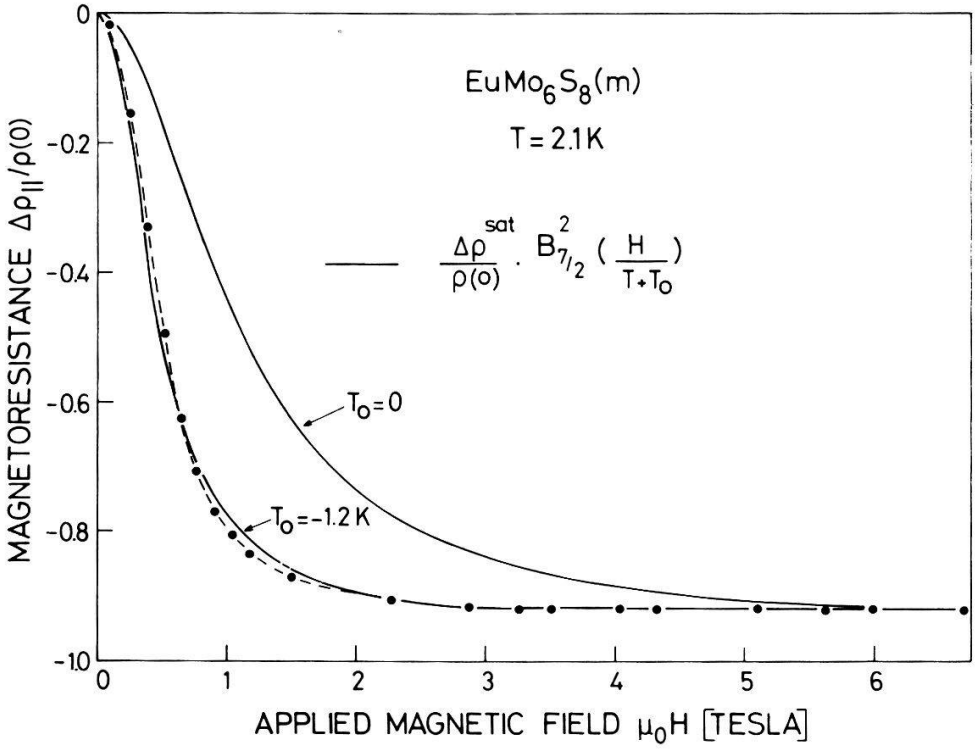

Figure 4.13
Comparison between magnetoresistance measurement and Kondo-alloy theory at 2.1 K for $EuMo_6S_8$.

Brillouin function. One has to introduce a ferromagnetic interaction temperature $T_0 = -1.2\,\mathrm{K}$ in order to obtain a better accord. However, such an interaction between the Eu moments in the paramagnetic state is not consistent with the existing magnetic data.

Moreover, if one tends to explain the negative magnetoresistance in terms of the spin-flip-scattering theory, then one also has to attribute the major part of the resistance rise in zero field at low temperature to spin-flip scattering. The exchange coupling between the Eu spins and the conduction electron spins, however, is much too weak for such a strong scattering effect. It should be mentioned that all measurements of the exchange interaction in $EuMo_6S_8$ [8, 44, 45, 46] have been done on samples which do not undergo the structural phase transformation. Thus the exchange constant J is only known for the rhombohedral phase of $EuMo_6S_8$: $J = -28\,\mathrm{meV}$ after [45]. However, since the modification of the atomic positions in the unit cell due to the phase transition is small and since the exchange interaction does not depend on the density of states in first approximation, we expect that the exchange coupling does not change significantly when entering the triclinic phase. Therefore, the applicability of the spin-scattering-suppression argument to the magnetoresistance of $EuMo_6S_8$ must seriously be questioned.

The band structure at the Fermi energy in the triclinic phase rather suggests comparing $EuMo_6S_8$ at low temperature with narrow gap or gapless magnetic semiconductors which frequently exhibit anomalously large, negative magnetoresistivities [47]. When the field is applied, the conduction and valence bands are split into Landau levels and each Laudau level is split into Zeeman levels corresponding to the two spin orientations of the electrons. Due to the exchange interaction, the spin splitting is much larger than the Landau splitting with the result, that the top Landau levels of the valence band are raised above the bottom of the conduction band, thus inducing an overlap between the conduction and valence bands. When neglecting the splitting into Landau levels, the spin splitting of the band states is given by

$$\Delta E = \pm g\mu_B\mu_0 H \pm \bar{J} B_{7/2}(H/T) \tag{4.2}$$

where $B_{7/2}(H/T)$ is the Brillouin function for Eu^{2+} ions and $\bar{J}$ the mean exchange constant ($\bar{J} = xSsJ$ with $x = 1/15$ for the Eu concentration per formula unit, $S = 7/2$, and $s = 1/2$). We take $\bar{J} = -10\,\mathrm{meV}$ which seems to be a realistic value for $EuMo_6S_8$ in its triclinic phase.

To obtain a negative magnetoresistance of 92% by exchange splitting of valence and conduction bands, one needs a very particular situation at the Fermi energy [32, 36]. The most important condition is a very weak overlap (a few meV) of the two bands, so that the Fermi energy is located very close to the band edges. The weaker the band overlap is, the larger is the resulting magnetoresistance. A zero-gap condition, however, results in a too large magnetoresistance.

By the action of the applied field and the produced exchange splitting of the bands, the number of charge carriers increases leading to an increase of the

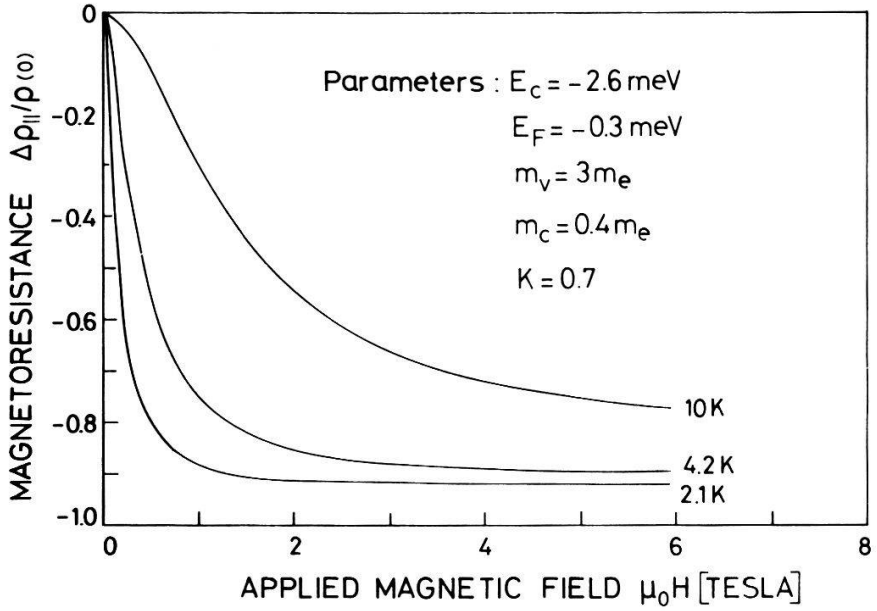

Figure 4.14
Calculated magnetoresistance at various temperatures by assuming a two-band model with weakly overlapping bands. The model parameters chosen are explained in the text. Further information about the calculation can be found in [36].

conductivity. Figure 4.14 shows the calculated magnetoresistance at various temperatures. The model parameters have been chosen such that the measured Hall coefficient $R_H(0)$ is correctly accounted for. The best results have been obtained by assuming a band overlap $E_c = -2.6$ meV and different band masses m_c and m_v. The Fermi energy E_F has been adjusted in such a way that perfect-crystal conditions $n_e = n_h$ are fulfilled. Finally the mobility ratio $K = \mu_h/\mu_e$ has been fixed by means of the resistivity and Hall coefficient at 4 K. In the two-band approach, we thus find the following transport parameters at low temperature:

$EuMo_6S_8$: ($T = 4$ K)
$n_e = n_h = 1.2 \times 10^{17}\ \mathrm{cm}^{-3}$
$\mu_e = 1600\ \mathrm{cm}^2/\mathrm{Vs}$
$\mu_h = 1100\ \mathrm{cm}^2/\mathrm{Vs}$

Such a two-band model is in good agreement with the band structure calculated for $BaMo_6S_8$ (Fig. 4.6). However, it seems to us that there must be a reason for such a unique situation at the Fermi energy. Note that, because of the similar behaviour of all molybdenum sulfides with divalent cations at low temperature, the same weak band overlap should be assumed in all cases. Interaction effects between band electrons might be a possible explanation. In fact, the exchange splitting effects, which have been developed for band electrons, are equally well possible for bound states, such as excitonic levels, impurity states etc. Then the small energy differences, necessary for the large magnetoresistance effect to occur, are provided in a natural way by the binding energy of the bound states.

Recently, it has been proposed to introduce the concept of magnetic polarons into the discussion of the magnetoresistance of $EuMo_6S_8$ [37]. This

means that the triclinic phase of $M^{2+}Mo_6X_8$ compounds is thought to have basically a metallic character, but due to spatial disorder the conduction electrons get weakly localized as the temperature drops, with the result that the resistance increases. Such an interpretation seems to be confirmed by the fact that the low-temperature transport properties of these materials are strongly sample dependent (for $EuMo_6S_8$ see [36]). In magnetic compounds, the localization effects are modified by the exchange interaction. Here, disorder may favour the formation of magnetic polarons, i.e. bound states between conduction electrons and localized magnetic moments [48]. External magnetic fields will destroy that bound state and thus cause a negative magnetoresistance.

Since sintered samples of $EuMo_6S_8$ generally reveal a smaller resistance rise and a smaller amplitude of the negative magnetoresistance than melted ones [36], we are forced to assume when applying the magnetic polaron concept to this material that the degree of disorder is highest in the melted specimens. However, this assumption clearly violates our experience with sample preparation and characterization.

We conclude that, even if the large, negative magnetoresistance in $EuMo_6S_8$ can be fairly well described by exchange splitting effects, the full mechanism is not yet completely understood.

The anomalous behaviour of $EuMo_6S_8$ is also manifested in the Hall resistivity at low temperature, as can be seen in Fig. 4.15. The Hall resistivity completely changes its behaviour at the same magnetic field at which the

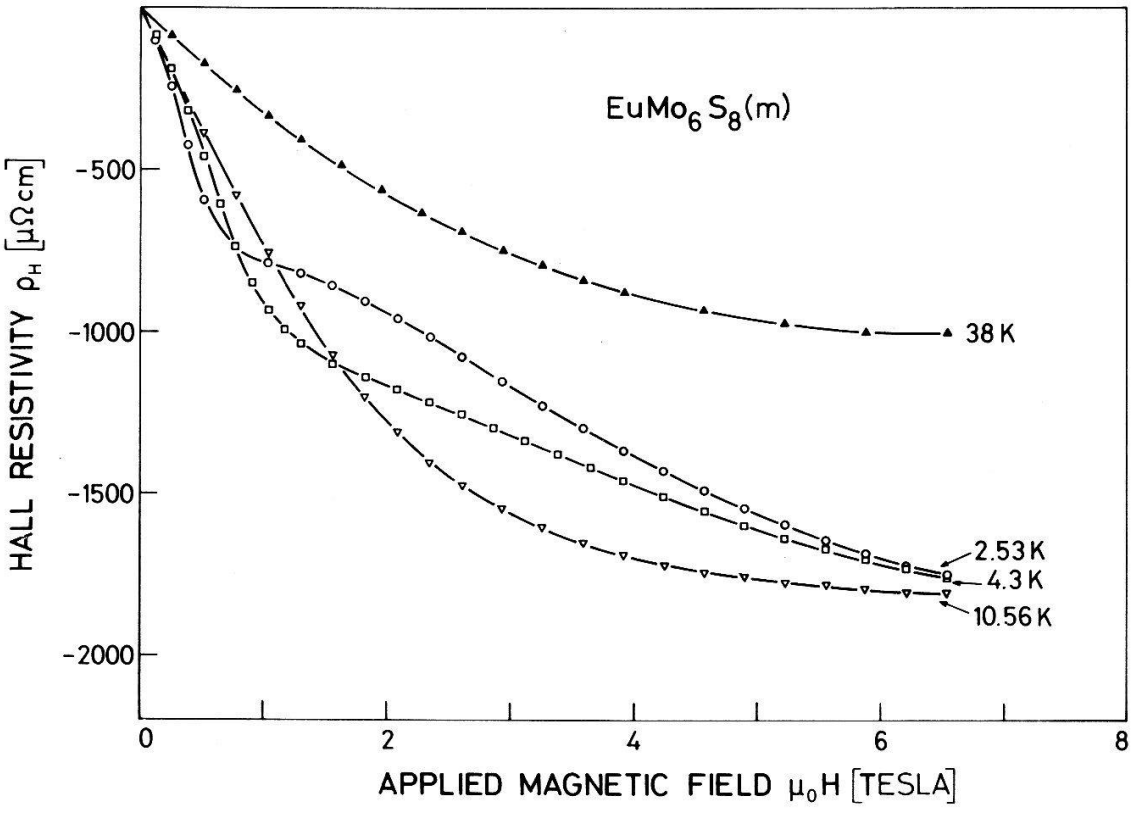

Figure 4.15
Hall resistivity of $EuMo_6S_8$ at low temperature as a function of magnetic field.

magnetoresistance starts to saturate. Consider for example the curve at 4.3 K in the figure: the Hall resistivity first depends nearly linearly on the applied field with an initial slope $R_H(0) = -10\,\mathrm{cm}^3/\mathrm{C}$, but at about 1 tesla there is a "transition" to another linear region between 2 and 5 tesla with a new Hall constant $R_{H^*} = -1.5\,\mathrm{cm}^3/\mathrm{C}$. Assuming that the mobilities are independent of the magnetic field in first approximation, we find that the change of the Hall coefficient by a factor of 6.7 is equivalent to a negative magnetoresistance of 85% as a result of the increase of the conduction electron concentration by this factor 6.7. Thus the spectacular magnetoresistance effect does not change very much the fact that there are only "a few" conduction electrons in $EuMo_6S_8$ at low temperature, with or without magnetic field.

In the above discussion, we have completely neglected a possible field dependence of the mobilities. On the other hand, we proposed a magnetic scattering effect to explain the observed low-temperature decrease of both the magnetoresistance mobility and the absolute value of the Hall mobility. The suppression of this scattering process in the magnetic field contributes to the galvanomagnetic properties of $EuMo_6S_8$ according to the Kondo-alloy theory, as discussed previously. Whereas an increase of the electron mobility as well as an increase of the current carrier concentration in the field will lead to a resistance reduction, these effects will contribute with different signs to the field dependence of the Hall resistivity. In fact, Fig. 4.15 clearly demonstrates that there is a slight deviation from a linear field dependence of the Hall resistivity towards higher absolute values of the Hall coefficient at low temperature and in fields lower than 1 tesla. This may be interpreted by an increasing electron scattering time with increasing field, thus enhancing the absolute value of the difference of electron and hole mobilities. An estimation of the spin-flip contribution to the anomalous low-temperature properties of $EuMo_6S_8$ by means of the Hall-resistivity data is difficult, since two effects are superposed with different signs. However, the 15% scattering contribution estimated from the Hall-mobility and magnetoresistance-mobility data, seems to be consistent with the Hall-resistivity data. We therefore conclude that magnetic scattering only plays a subordinate role in view of the anomalous low-temperature transport properties.

It is evident that the transport properties are very sensitive to crystal defects or doping effects if the band structure near the Fermi energy is similar to the one proposed above. A small change of the position of the Fermi energy may have drastic consequences. In Fig. 4.16, the Hall resistivity of various samples $Eu_xMo_6S_8$ is shown at 4.3 K. Careful sample characterization proves the melted specimen (case (a)) to be a stoichiometric crystal with $n_e = n_h$. Since the role of the cation M^{2+} is mainly to transfer two electrons into the conduction band complex, which contains only 2.5×10^{17} current carriers per cm^3 at liquid helium temperature, a cation deficiency of 0.1%, corresponding to a mean electron deficit of $3.5 \times 10^{18}\,\mathrm{cm}^{-3}$, is sufficient to commute the sign of the Hall effect (case (d) in Fig. 4.16). Losses of this order of magnitude during the sample preparation are not unreasonable when having a nominal Eu concentration $x = 1.0$. They can be compensated by starting with a certain Eu excess. Curve b) in Fig. 4.16 shows

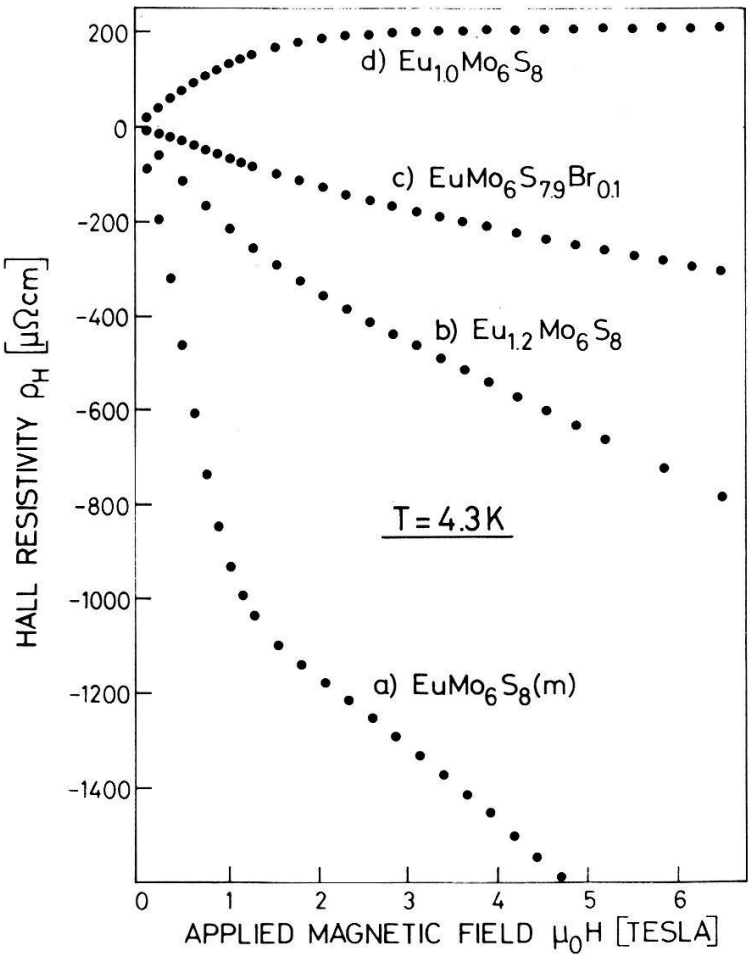

Figure 4.16
Hall resistivity of various samples of the compound $Eu_xMo_6S_8$ at 4.3 K as a function of magnetic field.

that then the Hall effect again becomes negative; a perfect crystal, however, cannot be obtained by this method. The conduction electron deficiency due to Eu vacancies can also be partially compensated by substituting S by Br (case (c)), since bromine enters the Chevrel phase in the simply negative charged state.

It should be pointed out that in the above discussion a rigid-band model has been assumed. It is however well known that changes in the charge transfer are accompanied by a slight contraction or expansion of the Mo_6 octahedra [49], leading to a modification of the band structure.

4.4. *Some comments on the possible nature of the triclinic structure transformation*

We would like to close the present section with some remarks on the modifications occurring in the electronic system as the crystals undergo the triclinic structure transformation. Figure 4.17 summarizes the resistivity behaviour of $M^{2+}Mo_6X_8$ compounds at the phase transition. In all cases, the mobility of the current carriers increases. This increase is manifested in a clear reduction of the resistivity or at least its temperature derivative just below the transition temperature. Only in $EuMo_6S_8$, there is a significant diminution of the

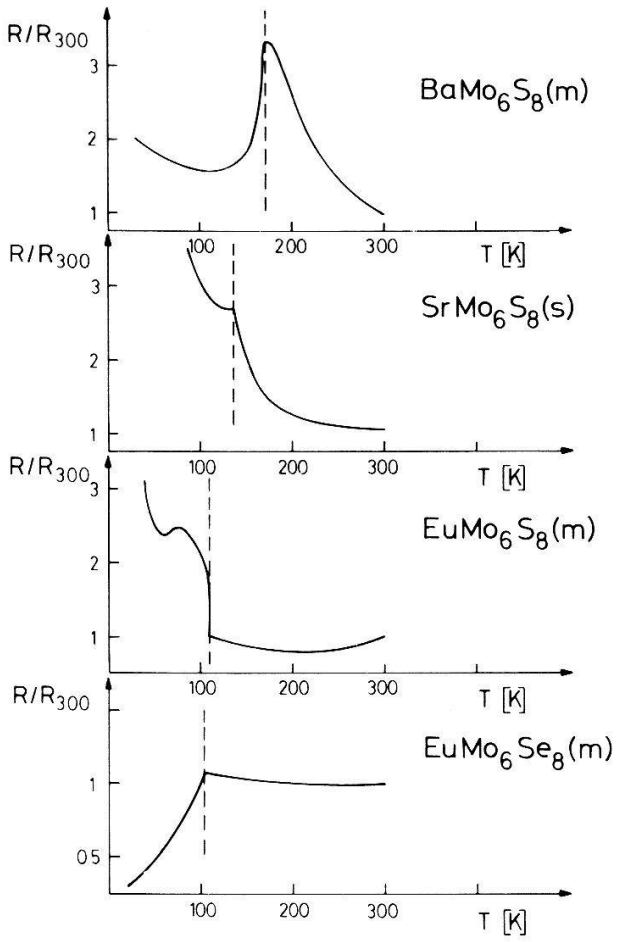

Figure 4.17
Resistivity behaviour of $M^{2+}Mo_6X_8$ compounds at the structural phase transition (schematically).

number of charge carriers such that it exceeds the mobility rise leading to the resistivity jump. In the other cases, the number of charge carriers seems to be much less affected by the transformation. In $BaMo_6S_8$, there is already a significant gap opened in the "rhombohedral" phase, so that the triclinic structure transformation cannot influence very much the electron concentration. On the other hand, the modification of the Fermi surface may affect the density of states and thus the electron scattering time and the effective masses in a more important way. In $EuMo_6Se_8$ the reason for the nearly unchanged carrier concentration is the smallness of the lattice deformation. But again, since the density of states is more sensitive to details of the Fermi surface than the number of conduction electrons, this slight modification may lead to an increase of the mobilities. $SrMo_6S_8$ seems to be an intermediate case between $EuMo_6S_8$ and $BaMo_6S_8$.

The behaviour of the Hall coefficient as a function of temperature as well as a function of magnetic field is very reminiscent of the Hall effect observed in the linear chain metal $NbSe_3$ [50], where two phase transitions due to charge-density-wave formation take place [51]. Below the first transition at $T_1 = 142$ K, the Hall constant slightly increase similarly to the behaviour of R_H in $M^{2+}Mo_6X_8$ compounds in the "intermediate" region. At the second transition $T_2 = 58$ K, R_H starts to increase more rapidly, passes through a maximum which is located well

below the CDW transition, and changes the sign at low temperature. The low-temperature value of the Hall coefficient indicates a charge carrier concentration of about $10^{18}/cm^3$.

Charge-density-wave formation has also been proposed for $EuMo_6S_8$ [7]. However, no direct evidence for such a phenomenon has been found by crystallographic investigations. But even if the exact nature of the phase transformation in $EuMo_6S_8$ is still controversial, we believe that in any case certain portions of the Fermi surface are destroyed by a gap formation. This has general consequences for the transport properties: a reduction of the conduction electron concentration and a simultaneous mobility increase. In compensated systems, this will lead to a competition between the mobilities of the two carrier types resulting in the peak structure of the Hall coefficient below the phase transformation. It is very unlikely that electron and hole mobilities obey exactly the same temperature law. Assuming the following temperature dependence of the mobilities:

$$\mu(T) \sim (T_0/T)^s \tag{4.3}$$

with slightly different powers for electrons and holes, then the carrier type with the lower s value will have a faster increase of its mobility at temperatures above a characteristic temperature T_0. Below T_0, the situation is inverted. Our transport measurements on Chevrel compounds suggest a value of s being slightly higher for electrons than for holes. T_0 determines the compensation point of the Hall coefficient and is about 50 K in $M^{2+}Mo_6X_8$ compounds.

5. Superconductivity and structural phase transformation

5.1. *Introductory remarks*

We now come to the probably most exciting part of the present work, namely the investigation of the unusual superconducting properties of Eu-based Chevrel compounds. In particular, we will study the interplay of superconductivity with the competitive phenomena of magnetism (Section 6) and structural phase transformations. Besides the absence of superconductivity in $EuMo_6S_8$, the anomalous dependence of the superconducting transition temperature T_c on the Eu concentration in the series $Eu_xSn_{1-x}Mo_6S_8$ has attracted a great deal of attention. The recent discovery of structural phase transformation in $EuMo_6S_8$ suggests that both observations are related to that phase transformation. In this chapter, the correlation between superconductivity and the structural transition will be investigated by means of transport measurements. Different approaches to suppress the phase transformation will be discussed.

5.2. *The series* $Eu_xSn_{1-x}Mo_6S_8$

The unusual dependence of the superconducting transition temperature T_c on the Eu concentration in the series $Eu_xSn_{1-x}Mo_6S_8$ is shown in Fig. 5.1. As can be

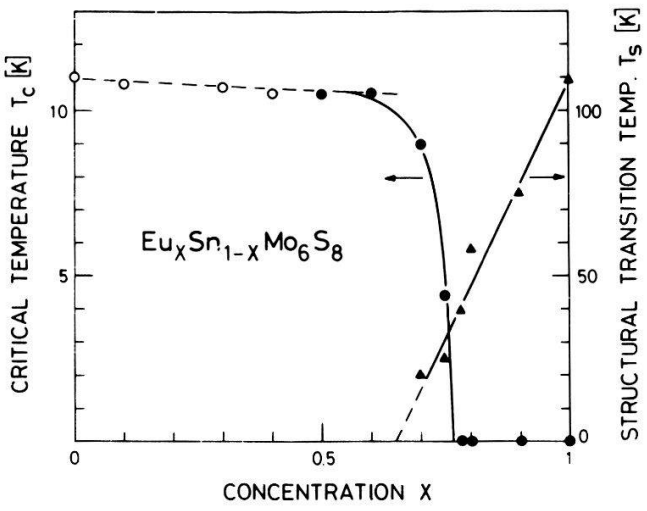

Figure 5.1
Superconducting and structural transition temperatures versus Eu concentration in the series $Eu_xSn_{1-x}Mo_6S_8$.

seen, T_c is nearly independent of the Eu concentration up to $x = 0.6$ indicating that magnetic scattering effects only play a minor role. Because of the particular crystal structure of Chevrel phases with relatively large Eu–Mo interatomic distances, the exchange interaction between conduction electrons and magnetic ions is very weak leading to a negligible exchange scattering pair breaking. At higher Eu concentrations, however, T_c abruptly drops to zero and superconductivity disappears for $x \geq 0.8$. Instead, an anomalous resistance rise appears at low temperature, whose beginning is shifted to higher temperatures with further increasing Eu concentration. This resistance anomaly results from the structural phase transformation and allows the determination of the transformation temperature T_s in the series $Eu_xSn_{1-x}Mo_6S_8$ [32]. An important condition, however, is the availability of sufficiently dense and homogeneous samples. Such samples have been obtained for the series $Eu_xSn_{1-x}Mo_6S_8$ by applying an hot-pressing technique (see Section 2). Figure 5.1 is quite representative of the bulk behaviour of the series, since T_c has been measured inductively and the resistance rise determining T_s must be due to the major part of the samples according to percolation arguments. We find that superconductivity occurs when the structural transition has been suppressed. There is, however, a small concentration interval around $x = 0.75$ where the two phases may coexist. In the following, it will be studied how the anomalous transport properties of $EuMo_6S_8$ change when the Sn concentration increases, and how T_c is correlated to the Hall coefficient, i.e. the conduction electron density.

Figure 5.2 shows the Hall constant of the series $Eu_xSn_{1-x}Mo_6S_8$ in the Eu-rich concentration region at helium temperature. As expected, the value of the Hall constant decreases rapidly when increasing the Sn concentration. The sample with $x = 0.5$ has been measured above the superconducting transition. According to our discussion in Section 4, the observed positive sign of the Hall coefficient seems to result from crystal defects. The scatter of the data points in

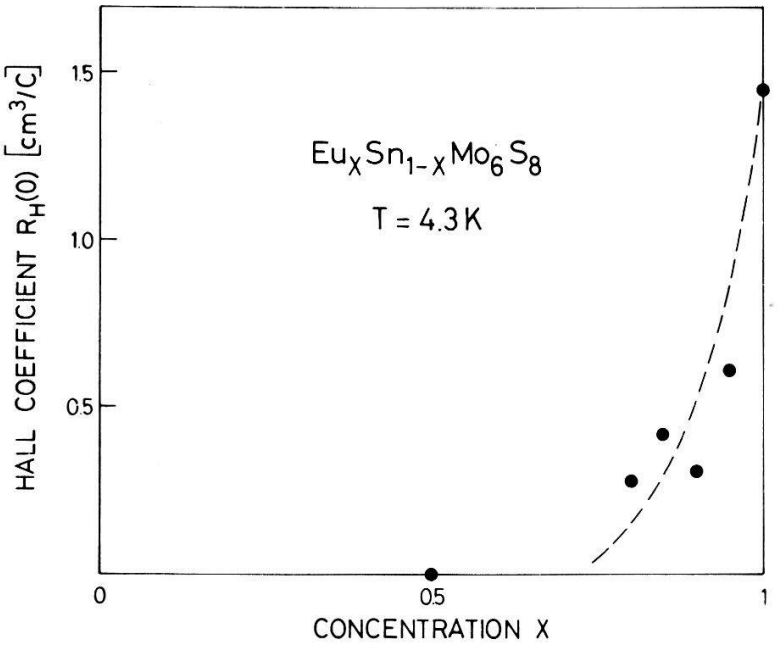

Figure 5.2
Hall coefficient at 4.3 K versus Eu concentration in the series $Eu_xSn_{1-x}Mo_6S_8$.

Fig. 5.2 indicates that the Eu concentration does not exactly correspond to the nominal value, but fluctuates somewhat around it. On the superconducting side of the phase diagram where T_c varies rapidly, we observe wide superconducting transitions of typically 2–3 K. We conclude that those samples are not very suitable for a closer examination of the relation between superconducting properties and structural phase transformation.

The sample preparation has therefore been modified in that a small quantity of bromine (0.5 at-%) was added to the ingots. This has the following consequences:

(1) X-ray studies prove that samples prepared in this way do not contain any detectable impurity phase. The presence of bromine seems to favour the formation of the Chevrel phase and to promote the homogenization of the samples (at least in the Eu-rich concentration region).
(2) As can be seen from Fig. 5.3, adding small quantities of bromine makes the variation of T_c with x close to $x = 0.8$ less steep and thus the superconducting transitions less wide.
(3) As already mentioned in Section 4, the Hall effect of $EuMo_6S_8$ at low temperature has negative sign in samples containing some bromine, similar to the behaviour of melted high-quality samples. Thus, in the critical concentration range where superconductivity and the triclinic phase may coexist, the change of sign of the Hall coefficient is a sensitive indicator for the appearance of the structural phase transformation.

Consequently, the series $Eu_xSn_{1-x}Mo_6S_8$(Br) seems to be more appropriate for the investigation envisaged. In Fig. 5.4 the Hall coefficient $R_H(0)$ of the series $Eu_xSn_{1-x}Mo_6S_8$(Br) for $x = 0.6,\ 0.75,\ 0.8,\ 0.9$ is shown as a function of

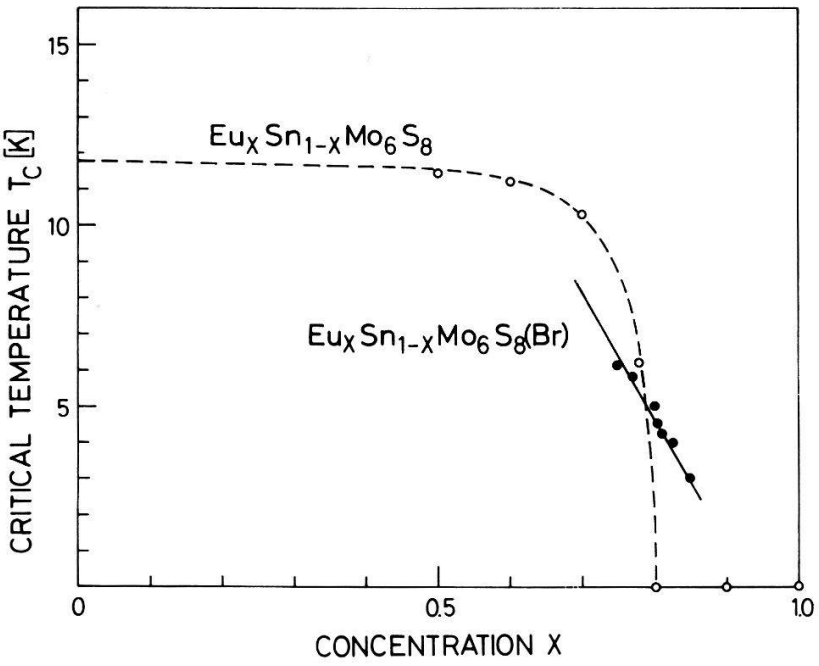

Figure 5.3
Effect of adding small amounts of Br on the critical temperature of the series $Eu_xSn_{1-x}Mo_6S_8$.

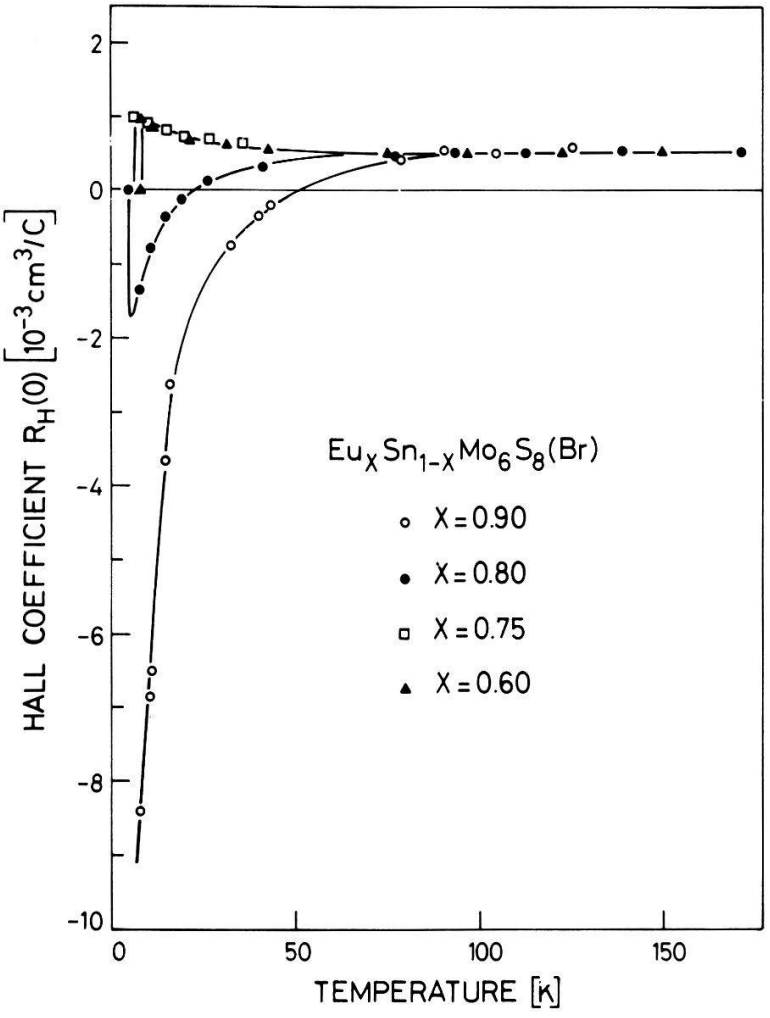

Figure 5.4
Hall coefficient of the series $Eu_xSn_{1-x}Mo_6S_8$(Br) as a function of temperature.

temperature. Above 100 K the same value $R_H(0) = 0.5 \times 10^{-3}$ cm^3/C has been found for all samples studied. The Hall constant reacts to the phase transformation with a change of sign and progressively increasing absolute values as the temperature decreases. The characteristic peak structure always observed in pure $M^{2+}Mo_6X_8$ compounds near T_s, has disappeared. Defining the structural phase-transition temperature T_s as that temperature at which the Hall coefficient starts to deviate from the linear high-temperature behaviour towards the change of sign, then one finds that the phase transformation appears in samples with $x > 0.75$. According to the discussion in Section 3, the slight increase of R_H in samples with Eu concentrations up to $x = 0.75$ seems to be a general feature of superconducting Chevrel compounds at low temperature and should be distinguished from the effect of the transition into the triclinic phase. The relation between the critical temperature T_c (resistively measured) and the Hall coefficient at 8 K, i.e. above T_c, is presented in more detail in Fig. 5.5. On the Eu-rich side of the phase diagram, the triclinic phase characterized by a negative Hall coefficient does not allow superconductivity to occur. For $0.75 \leq x \leq 0.90$, superconductivity appears in the triclinic phase; however, the relatively low critical temperature indicates that the density of states at the Fermi energy is significantly reduced. Below $x = 0.75$, the transport properties such as resistivity, Hall effect, and magnetoresistance do not exhibit any detectable indication for the occurrence of the structural transition. On the other hand, the T_c reduction which is observed when the Eu concentration is higher than $x = 0.5$ still points to a modification of the density of states at the Fermi energy, probably due to the beginning of band-shift effects. The structural transformation has another

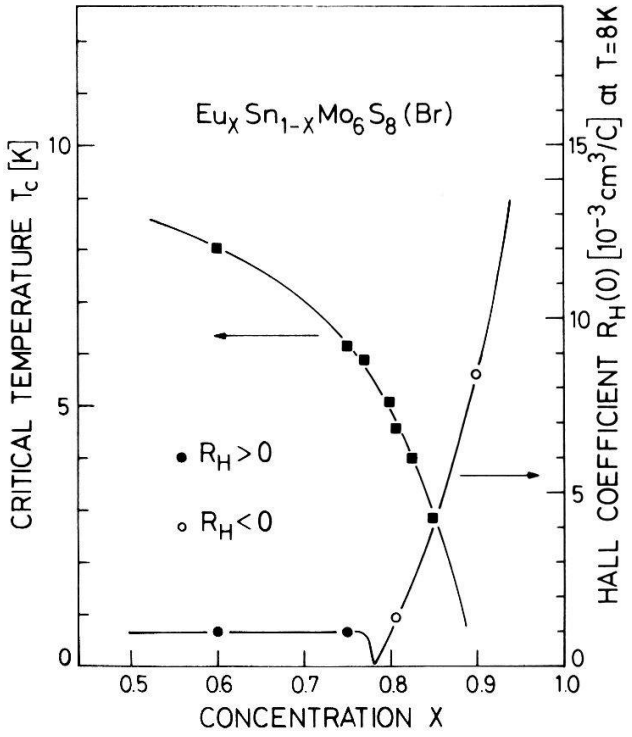

Figure 5.5
Relation between critical temperature and Hall coefficient above T_c in the series $Eu_xSn_{1-x}Mo_6S_8$(Br).

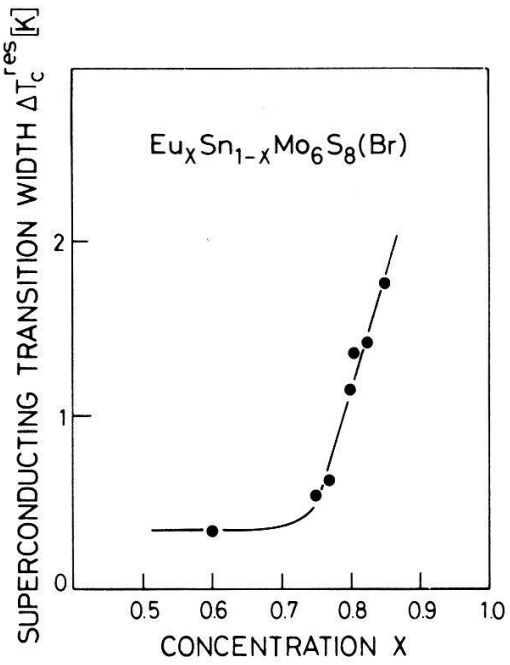

Figure 5.6
Superconducting transition width's versus Eu concentration in the series $Eu_xSn_{1-x}Mo_6S_8(Br)$.

important (indirect) influence on the superconducting properties which is shown in Fig. 5.6: the superconducting transitions are broadened in the coexistence interval. At $x = 0.8$, one typically finds transition widths of 1–2 K.

In conclusion, we have shown that the Eu concentration $x = 0.75$ in the series $Eu_xSn_{1-x}Mo_6S_8(Br)$ is an upper limit above which the structural transformation starts to affect the transport properties. We would like to stress that for $x = 0.75$ no negative magnetoresistance has been found in the normal state in magnetic fields up to 22 tesla, and the resistance ratio $R_N/R(300\,\mathrm{K})$ is smaller than unity (R_N is the resistance above T_c). It is worth noting that the occurrence of superconductivity in the series $Eu_xSn_{1-x}Mo_6S_8(Br)$ is correlated with the sign of the Hall coefficient. Good superconducting properties are connected with a positive Hall effect. In fact, the superconductors with the highest critical temperatures such as Nb_3Sn, V_3Si, $PbMo_6S_8$, Be_{am}, Nb, Pb, etc. have positive Hall coefficients. The connection of this empirical correlation [52] with superconductivity theory is not yet clear.

5.3. *$EuMo_6S_8$ under pressure*

Before the discovery of the structural phase transformation in $EuMo_6S_8$, it was found by two groups independently [3, 4] that high-T_c superconductivity can be induced in this compound by applying hydrostatic pressures greater than 7 kbar. In a recent study [53] it has been unambiguously proved that the pressure-induced superconductivity of $EuMo_6S_8$ is a bulk effect. Furthermore, a clear correlation between the suppression of the rhombohedral to triclinic structural distortion with pressure and the appearance of superconductivity has been established [54]. Figure 5.7 shows the resistivity of $EuMo_6S_8$ under 14 kbar as a function of temperature [55]. At that pressure the structural transformation is completely suppressed and superconductivity occurs at 11.6 K. The similarity with

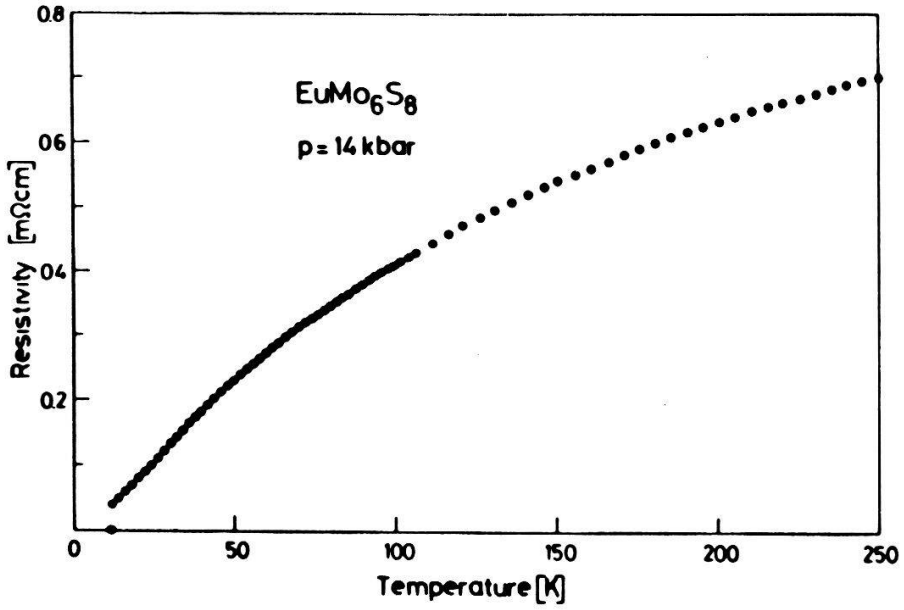

Figure 5.7
Resistivity of $EuMo_6S_8$ at 14 kbar versus temperature [55].

the temperature dependence of the resistivity of $PbMo_6S_8$ (Fig. 3.8) is striking. Thus, application of pressure and substitution of Eu by Sn (chemical pressure) lead to a suppression of the structural transformation. However, the former method has the advantage that melted, high-quality samples can be used.

5.4. *The series* $EuMo_6S_{8-y}Br_y$

One may expect that the structural transformation can also be suppressed by adding one more electron to the 22 cluster electrons in $EuMo_6S_8$, because all $M^{3+}Mo_6X_8$ compounds are known to be structurally stable. Such an additional cluster electron would remove the half-filled band situation which seems to be the reason for the instability. Since the superconducting state of $EuMo_6S_8$ is expected to present anomalous properties in high magnetic fields, it is preferable to increase the number of conduction electrons by a substitution on the *S* sites without touching the Eu sublattice. Br has been chosen, because it is expected to enter the *S* sites on the ternary axis leaving the 3-fold symmetry intact. Figure 5.8 shows the resistivity of the series $EuMo_6S_{8-y}Br_y$ for various Br concentrations as a function of temperature. Obviously, this substitution progressively removes the anomalous resistance rise at low temperature and at $y = 0.7$ there is an indication for the onset of superconductivity below 2 K. Such a critical temperature would be consistent with the T_c value of 1.4 K found in the isoelectronic compound $GdMo_6S_8$. In Fig. 5.9 the transverse magnetoresistance at 4.3 K is presented for various Br concentrations. Again, the anomalous negative magnetoresistance observed in $EuMo_6S_8$ at low temperature, has disappeared for $y = 0.5$. The main problems with this approach are whether the Br atoms really enter the Chevrel phase and what will be the influence on the lattice parameters and the electronic band structure. The variation of the rhombohedral angle and the volume of the

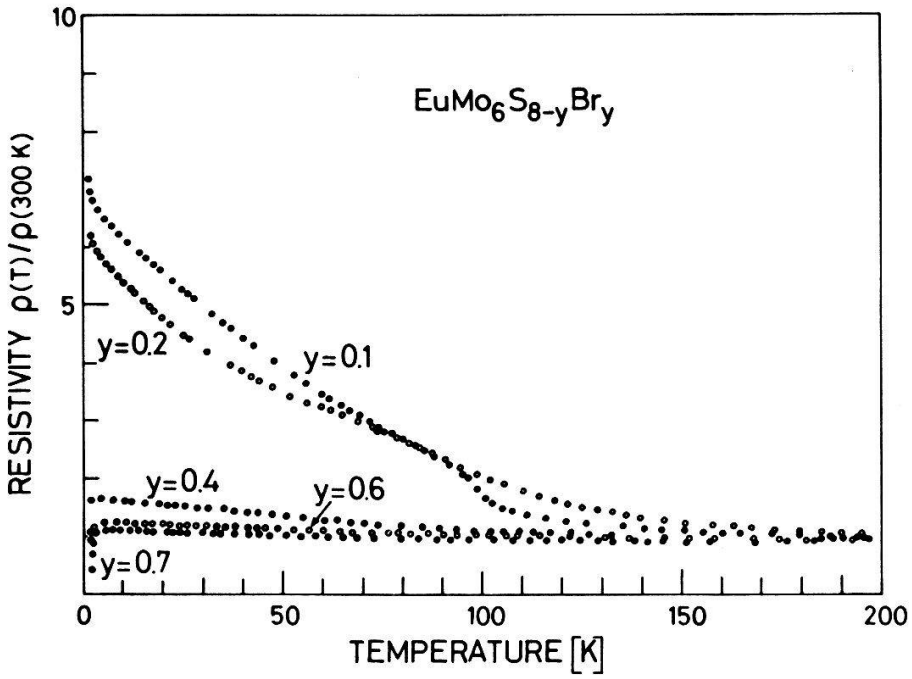

Figure 5.8
Resistivity of the series $EuMo_6S_{8-y}Br_y$ versus temperature for various Br concentrations.

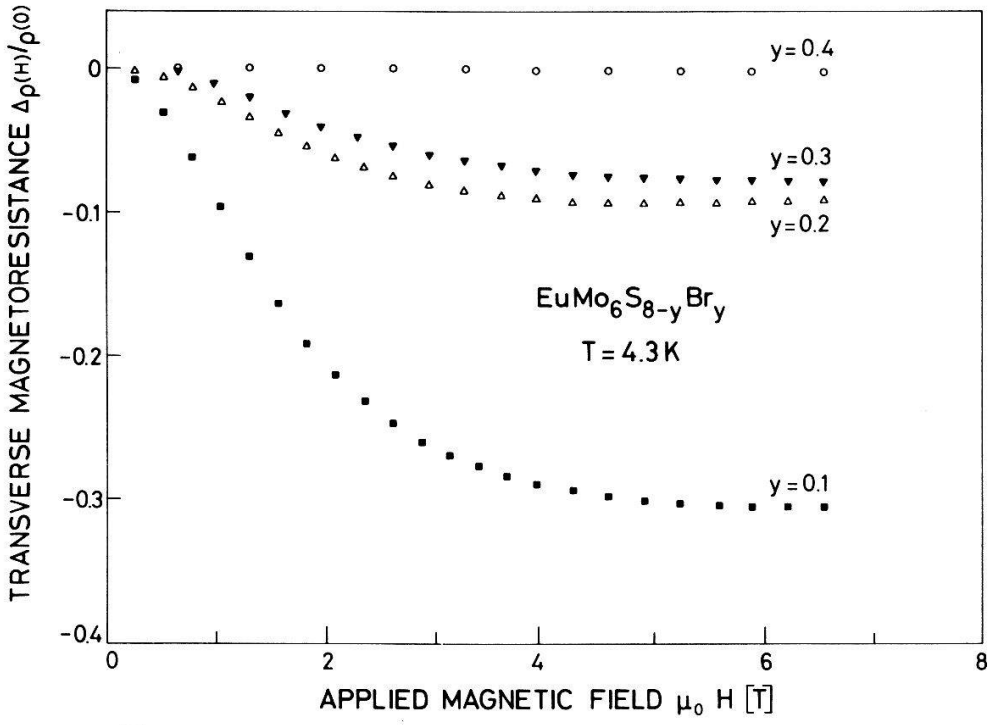

Figure 5.9
Transverse magnetoresistance of the series $EuMo_6S_{8-y}Br_y$ at 4.3 K.

hexagonal unit cell as a function of the Br concentration indicates a contraction along the hexagonal axis [56]. This is exactly what one would expect when the Br occupies the *S* sites on the ternary axis [57]. Thus partial substitution of *S* by Br in $EuMo_6S_8$ progressively suppresses the occurrence of the lattice transformation.

The Hall resistivity of the series $EuMo_6S_{8-y}Br_y$ at 14.8 K which is presented in Fig. 5.10, shows that the absolute value of the Hall coefficient decreases with

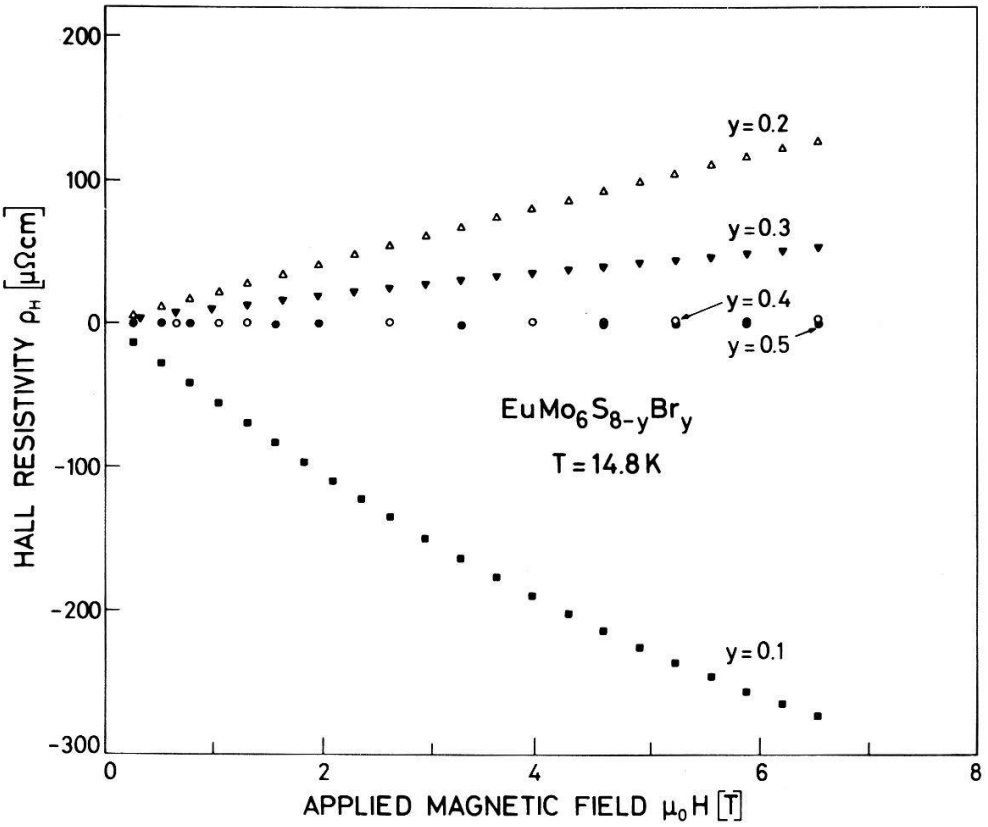

Figure 5.10
Hall resistivity of the series $EuMo_6S_{8-y}Br_y$ at 14.8 K versus magnetic field.

increasing Br concentration at low temperature. However, the observed positive sign in samples with $y \geq 0.2$ is somewhat unexpected. In a rigid band model, the compensation between electrons and holes should be lifted when the conduction band is filled up with additional electrons. Thus, the sign of the Hall constant should stay negative with increasing Br concentration. There are, in principle, three possible explanations for the observation of a positive Hall effect:

(1) The electron mobility is strongly reduced due to additional scattering centers created by the substitution.
(2) The band structure at the Fermi energy is strongly modified.
(3) The Br substitution causes a loss of Eu ions such that the total effect will be a diminution of the number of conduction electrons.

It appeared that the Chevrel phase could not be correctly synthesized when the Br concentration exceeded $y = 0.6$. Furthermore, inductive T_c measurements below 1 K exhibited no diamagnetic signal in any $EuMo_6S_{8-y}Br_y$ samples [58]. This may indicate that the samples become very inhomogeneous when containing larger amounts of Br. The superconducting traces observed in the resistivity measurements for $y = 0.7$, might be due to sample regions consisting mainly of the pseudobinary $Mo_6S_{8-\varepsilon}Br_\varepsilon$ [57]. The suppression of the structural phase transformation may be supported by a significant lattice-defect concentration. In fact, it has been found that the structural transformation temperature T_s of

$Eu_xMo_6S_8$ can be strongly lowered by slight deviations from stoichiometry ($x = 1$) [6, 36].

In conclusion, it is impossible to induce superconductivity in $EuMo_6S_8$ by partial substitution of S by Br, since the crystalline lattice is progressively disturbed as the Br concentration is increased.

6. Magnetic-field-induced superconductivity

6.1. *Introduction*

After the foregoing discussion of the normal-state and superconducting properties of $EuMo_6S_8$ and similar compounds, we are now able to envisage an investigation of the Jaccarino–Peter effect [9] and its possible occurrence in Eu-based molybdenum sulfides. This effect is closely connected with the fascinating question: can a non-superconducting material be made superconducting by applying a high, external magnetic field. This would be just the opposite to the ordinary destructive effect which a magnetic field has on superconductivity. That such an effect could take place in an ordered ferromagnetic metal was considered in 1962 by Jaccarino and Peter. As a mechanism which might allow magnetic-field-induced superconductivity ("MFIS"), they proposed a spin-compensation effect in an applied field. Due to the exchange coupling between localized magnetic moments and conduction electron spins, there will be a polarization of the conduction electrons below the Curie temperature when ferromagnetic ordering of the magnetic moments has set in. If the exchange interaction is negative, the resulting polarization of the electron spins will be opposite to the magnetization and can be compensated by an externally applied magnetic field. Thus, the initial condition of a polarized conduction electron gas which might be the only reason preventing superconductivity to occur, can be removed.

It is clear that a systematic search for MFIS in weak ferromagnets would be hopeless, since *a priori* nothing is known about the superconducting properties of such materials. This phenomenon can only be found in ferromagnets by chance. However, MFIS may equally well occur in the paramagnetic state [10]. Here, a polarization of the conduction electrons can be produced by aligning the localized moments in an external magnetic field. This paramagnetic polarization effect can be described by means of an "exchange field"

$$H_J = \frac{xJ\langle S\rangle}{g\mu_B} \tag{6.1}$$

where J is the exchange constant and x the concentration of magnetic ions with spin S.

If now the exchange field $|H_J|$ is larger than the paramagnetic citical field H_p and if the orbital critical field H_{c2}^* is sufficiently high (not necessarily larger than

H_J), then the field-induced superconducting state should exist. The critical field-temperature phase diagram of such a paramagnetic superconductor will consist of two well separated superconducting domains, one at low fields where the paramagnetic pairbreaking is still weak and one at high fields, where superconductivity is possible due to the compensation effect. Thus a measurement of the resistivity as a function of field at low temperature should consecutively show a transition to the normal state, then to the superconducting state again, and finally to the normal state at very high fields (S–N–S–N behaviour).

6.2. *Search for MFIS in the series* $Eu_xSn_{1-x}Mo_6S_8$

It appeared that Eu-based molybdenum sulfide might be a promising candidate for the observation of MFIS. The finding of an anomalous behaviour of the critical field as a function of both temperature and Eu concentration in the series $Eu_xSn_{1-x}Mo_6S_8$ by Fischer et al. [8] has been interpreted in terms of the Jaccarino–Peter effect. The negative sign of the exchange interaction necessary for the validity of this interpretation, has been confirmed afterwards by NMR and Mössbauer-effect measurements [46], by EPR measurements [45], and is in agreement with band-structure calculations [59]. Therefore, one should expect that the Jaccarino–Peter compensation effect manifests itself not simply in an anomaly of the critical field H_{c2} (Fig. 1.1), but more dramaticaly by the appearance of a new super-conducting state which needs the presence of high magnetic fields in order to exist.

A first indication for the possible existence of such a state has been found by Isino et al. [60] in a sample of nominal composition $Eu_{0.8}Sn_{0.2}Mo_6S_7$ becoming superconducting at about 6 K. After the recovery of resistance in the external field a further field increase led to a reduction of the resistance. A similar behaviour has been reported for $Eu_{1.2}Mo_6S_8$ under pressure [61, 62]. However, in both cases wide superconducting transitions have partially masked the effect and made the interpretation very difficult.

A closer analysis of the critical field data of the series $Eu_xSn_{1-x}Mo_6S_8$ demonstrates that MFIS may indeed appear for $x \simeq 0.8$ [63, 64]. However, due to the strong influence of the structural phase transformation on superconducting and transport properties with the resulting T_c drop at exactly that Eu concentration, it turns out to be extremely difficult to prepare homogeneous samples with sufficiently sharp superconducting transitions, necessary for a clear observation of MFIS.

One way of getting narrower transitions has been discussed in the Section 5, namely doping with small amounts of bromine. However, as can be seen in Fig. 5.6, at $x = 0.8$ where the phenomenon of MFIS is expected to appear, we still have transition width's larger than 1 K which will lead to unsatisfactory results. Thus we have chosen another approach to realize the observation of MFIS. This approach is essentially based on a partial substitution of S by Se at constant Eu concentration $x = 0.75$ and will be discussed in the next subsection. The small amount of Br which the samples still contain will not be explicitly indicated

from now on, in order to avoid too complex chemical formulae, i.e. we will simply write $Eu_{0.75}Sn_{0.25}Mo_6S_{8-y}Se_y$ instead of $Eu_{0.75}Sn_{0.25}Mo_6S_{8-y}Se_y(Br)$. This abbreviation is justified since Br only plays a minor role in the following approach.

6.3. *Observation of magnetic-field-induced superconductivity in the series* $Eu_{0.75}Sn_{0.25}Mo_6S_{8-y}Se_y$ [65, 66]

We have demonstrated in Section 5 that relatively narrow superconducting transitions are obtained with Eu concentrations not higher than $x = 0.75$. However, for those concentrations only an anomalous upturn is observed in the H_{c2}-T phase diagram, but no indication for MFIS. Nevertheless, the observation of MFIS should be possible at any Eu concentration on condition that one finds a method to adjust correctly the various parameters determining the existence of MFIS. Which are the important parameters, and how they must be modified, can be understood with the aid of Fig. 6.1, which presents schematically the free energy density F of a magnetic superconductor with negative exchange interaction versus applied magnetic field at very low temperature $T \ll T_c$. $F_N(H)$ describes the free energy density of the conduction electron gas in the normal state and is given by:

$$F_N(H) = F_N(0) - \tfrac{1}{2}\chi_p \mu_0^2 (H + H_J)^2 \tag{6.2}$$

where χ_p is the Pauli-spin susceptibility. The temperature and field dependence of

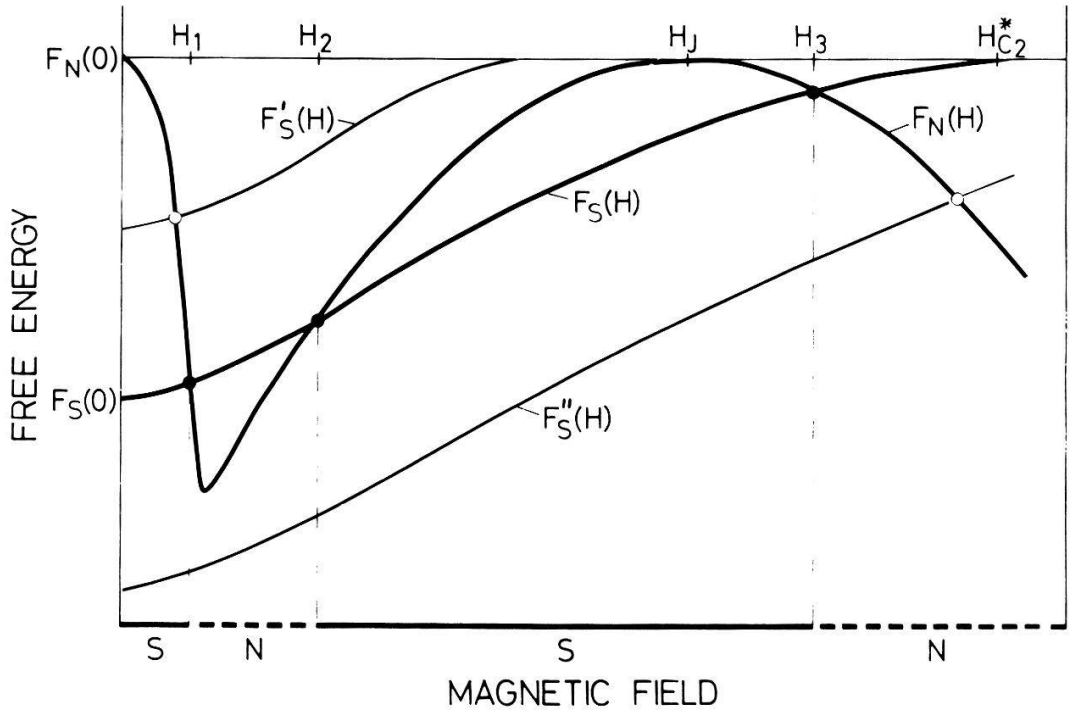

Figure 6.1
Schematic plot of the free energies of the normal and superconducting states vs applied magnetic field for a paramagnetic superconductor with negative exchange constant at $T \ll T_c$. Spin-orbit effects are neglected.

the exchange field is assumed to follow the Brillouin function. For a negative exchange field, strong variations of the free energy $F_N(H)$ due to the interplay of applied field and exchange field are expected. At low fields, F_N is quickly lowered due to the polarization of the electrons in the exchange field. When all magnetic moments are aligned, the exchange field saturates and a further increase of the applied field then causes a weakening of the electron polarization because of the antiparallel direction of the two fields. As a result, the free energy F_N passes through a minimum and increases again up to the compensation point, at which the external field exactly cancels the exchange field. In still higher fields, the ordinary Pauli-spin paramagnetism sets in. $F_N(H)$ describes the essentials of the spin-compensation mechanism in the normal state. How this compensation effect acts on the superconducting properties, depends on the free energy density $F_S(H)$ of the superconducting state. We assume a behaviour with flux penetration, characteristic of a type-II superconductor. $F_S(H)$ is given by:

$$F_S(H) = F_N(0) - \tfrac{1}{2}N(E)\Delta^2 \tag{6.3}$$

where $N(E)$ is the density of states at the Fermi energy and Δ the temperature and field dependent energy gap, proportional to T_c at zero temperature for BCS superconductors. If the condensation energy of the superconducting state, or equivalently T_c, and the exchange field H_J at saturation are correctly adjusted to each other, three intersection points H_1, H_2, H_3 between F_N and F_S appear, indicating the various superconducting-normal transitions which take place when the external field increases. Obviously, there will be only one solution, if the critical temperature T_c is too low (curve F'_S in Fig. 6.1) or too high (curve F''_S).

This qualitative discussion demonstrates that the behaviour of the critical field in the series $Eu_xSn_{1-x}Mo_6S_8$ for Eu concentrations up to $x = 0.8$ (see Fig. 1.1) is typical of a situation where the critical temperature T_c is too high compared with the value necessary for the occurrence of MFIS. This means that we have to find a mechanism which lowers T_c without changing very much the other parameters of the superconductor.

Partial substitution of S by Se fulfills that condition, since it is known to reduce the superconducting transition temperature [64] while leaving unaltered, to a first approximation, the density of states at the Fermi energy [67]. Although this approach should work at any given Eu concentration, our choice of x is restricted by two practical considerations: 1) low Eu concentrations favour relatively narrow superconducting transitions and 2) the lower the Eu concentration, the lower the T_c values required for the occurrence of MFIS (see Fig. 6.1), i.e. the dimensions of the field-induced superconducting domain will shrink with decreasing Eu concentration, demanding progressively lower temperatures for its observation. Therefore, we have chosen $x = 0.75$, the highest possible Eu concentration with a narrow transition width.

Figure 6.2 shows the critical temperature of the series $Eu_{0.75}Sn_{0.25}Mo_6S_{8-y}Se_y$ as a function of the Se concentration. T_c decreases with increasing Se concentration and passes through a narrow interval consistent with field-induced superconductivity (shaded region in Fig. 6.2). The boundaries of this region have been

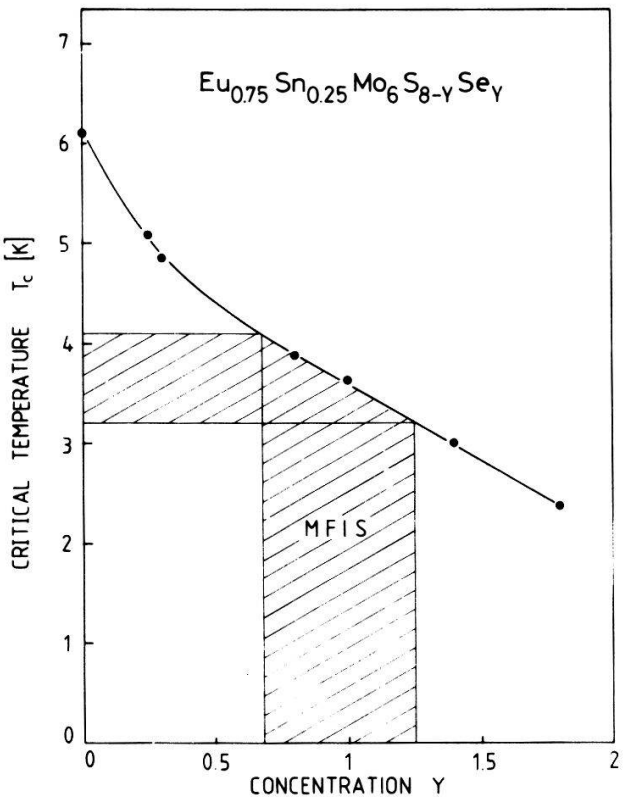

Figure 6.2
Critical temperature T_c versus Se concentration in $Eu_{0.75}Sn_{0.25}Mo_6S_{8-y}Se_y$. The shaded region is consistent with MFIS.

determined experimentally by defining MFIS as the simultaneous appearance of two separated superconducting domains in the $H_{c2} - T$ phase diagram. Note that the variation of the critical temperature with y is much smaller than the variation of T_c in the series $Eu_xSn_{1-x}Mo_6S_8$ close to $x = 0.8$ (see Fig. 5.3).

Figure 6.3 shows the resistance of $Eu_{0.75}Sn_{0.25}Mo_6S_{7.2}Se_{0.8}$ versus applied magnetic field. The critical temperature of that sample in zero field was 3.89 K with a transition width of 0.6 K. R_N is the resistance in the normal state. At $T = 3.55$ K, the $R(H)$ curve is ordinary. The phenomenon of MFIS sets in below 1 K: Superconductivity is first destroyed by a weak magnetic field and the recovery of resistance amounts to more than 70%. At higher fields, the resistance starts to decrease again and disappears at about 10 tesla. The high-field state exists up to fields of the order of 20 tesla, which can be seen from Fig. 6.4. At $T = 0.37$ K the multiple transition S–N–S–N is clearly displayed. It should be emphasized that the field and temperature dependence of the resistance observed here cannot be explained by the well-known "peak effect" near H_{c2} [68]. The position of the resistance maximum at magnetic fields $H \ll H_{c2}$, the crucial composition dependence of the induced superconducting state, and the experimental conditions (field parallel to the measuring current, low current density of about 10 mA/cm^2) exclude an interpretation in terms of the peak effect. Note also, that in the low-field region (Fig. 6.3) a typical reentrant phenomenon is observed: When lowering the temperature in a constant magnetic field of 0.95 tesla, one finds a transition into the superconducting state which is complete at

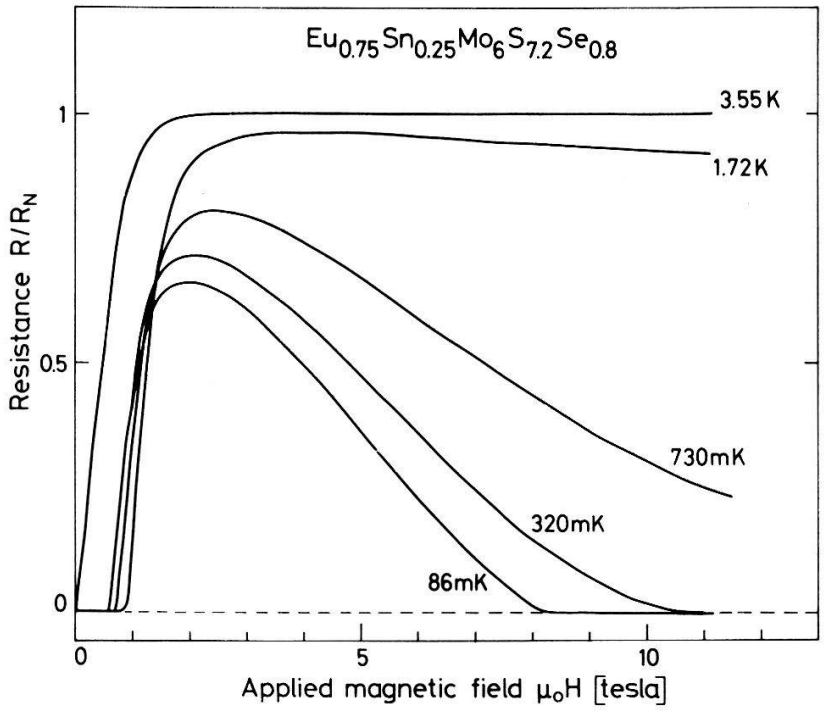

Figure 6.3
Normalized resistance of $Eu_{0.75}Sn_{0.25}Mo_6S_{7.2}Se_{0.8}$ up to 12 tesla.

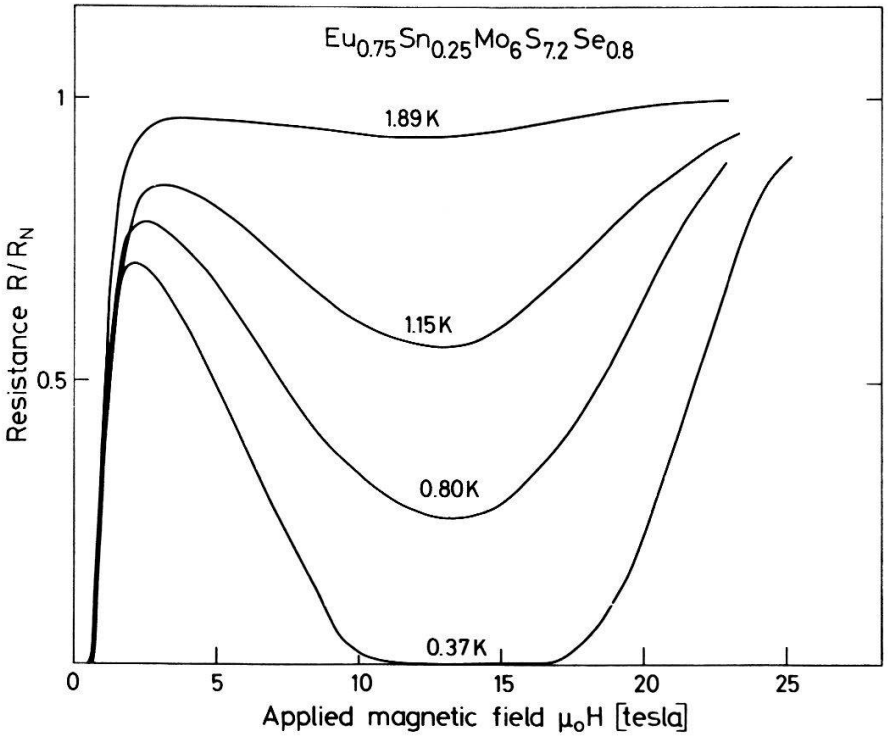

Figure 6.4
Normalized resistance of $Eu_{0.75}Sn_{0.25}Mo_6S_{7.2}Se_{0.8}$ up to 25 tesla.

2 K, but below 1 K the sample becomes again resistive, i.e. reenters the normal state.

The upper critical field $H_{c2}(T)$, which is defined at the midpoint of the resistive transitions in the external field, is presented in Fig. 6.5. We find two separated superconducting domains, an ordinary one at low fields and a new field-induced one, which extends from 4 tesla to 23 tesla at $T = 0$ and from $T = 0$ to $T = 1$ K at $H = 12$ tesla. The solid line in Fig. 6.5 represents the critical field which was calculated by use of a multiple pairbreaking theory. An analysis of the experimental data in terms of this theory will be carried out in the next subsection.

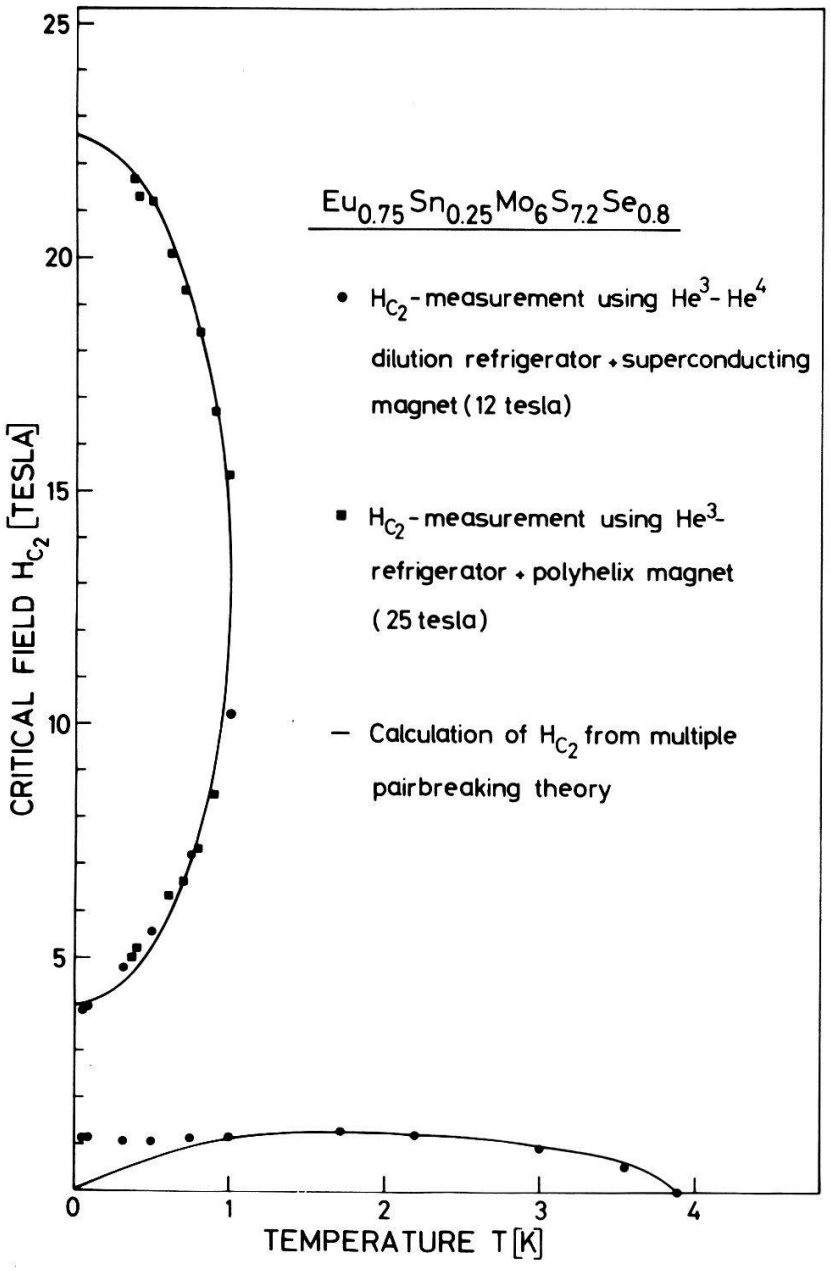

Figure 6.5
Critical field-temperature phase diagram.

Here, we will only comment on the slight disagreement between experiment and theory appearing in the low-field and low-temperature regime. In the calculation, a free ion behaviour has been assumed. Therefore, at zero temperature an infinitesimal field is sufficient to build up the full exchange field which immediately destroys the superconducting state. As a result, the critical field goes to zero with decreasing temperature in the low-field regime. As discussed in Section 4, there is, however, a magnetic ordering which appears in $EuMo_6S_8$ below 0.5 K.

The ordering type is probably some kind of antiferromagnetism which is known to be compatible with superconductivity [69, 70]. The observed departure below 1 K is therefore not surprising. In order to produce the destructive, ferromagnetic exchange field, one first has to break up the antiferromagnetic spin coupling of the Eu ions ($\mu_0 H > k_B T_n$). Somewhat unexpected is however, that the deviation starts to appear at about 1 K, i.e. above the ordering temperature of 0.5 K found in $EuMo_6S_8$. It is worth noting that a drastic Mössbauer-line broadening above the magnetic transition temperature has been observed in $EuMo_6S_8$ [43], which may be interpreted by crystal field effects. The crystal-field-ground state of Eu^{2+} is probably not a pure $S = 7/2$ state, but may be mixed largely with other states of lower S. This might lead to a reduction of the magnetization compared with the free ions case, when the temperature becomes of the order of the overall crystal-field level splitting. Note also, that the density of states at the Fermi energy which is very different in non-superconducting $EuMo_6S_8$ and in superconducting $Eu_{0.75}Sn_{0.25}Mo_6S_{7.2}Se_{0.8}$, may influence the magnetic interaction between the Eu ions. Further susceptibility and magnetization measurements are certainly needed to get a complete understanding of the magnetic ordering and its influence on the critical-field behaviour.

In the following, it will be shown how the compensation mechanism manifests itself in the critical field $H_{c2}(T)$, when the superconducting transition temperature does not lie inside the critical interval consistent with MFIS. Figure 6.6 shows the critical fields of two samples with T_c values above the critical region. The temperature dependence of H_{c2} is still very anomalous with a characteristic upturn and an infinite slope at 2.7 K for the sample with $y = 0.25$, but the phase diagram is only simply connected and MFIS not possible any more. The anomaly becomes increasingly insignificant, the more T_c is removed from the critical region. A similar behaviour of the critical field with positive curvature has been reported in other Eu-based Chevrel compounds $Eu_xM_{1-x}Mo_6S_8$ with M = Pb, La, Tb [8, 71, 72]. If on the other hand the superconducting transition temperature is below the critical interval, one finds a re-entrant behaviour with relatively low critical fields, as can be seen in Fig. 6.7. There is no indication of superconductivity in magnetic fields higher than 1 tesla. Again the critical field remains finite at $T = 0$ due to the anitferromagnetic ordering.

The compositional dependence of the critical field described above, can easily be understood by means of the free-energy diagram, shown in Fig. 6.1. For a quantitative analysis of the critical field data, however, the use of microscopic theories containing all important pairbreaking effects is indispensable.

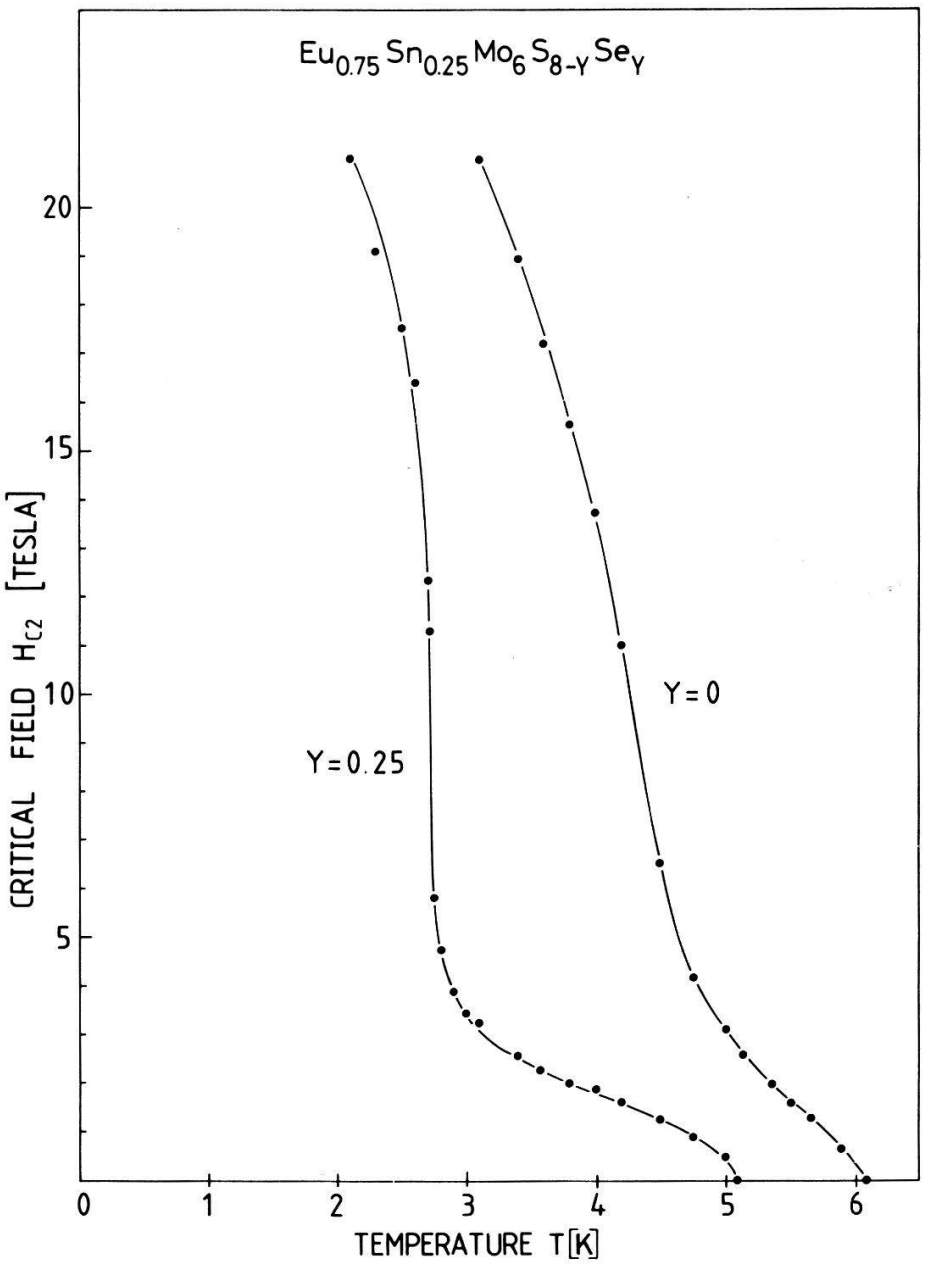

Figure 6.6
Critical field vs temperature for two samples of the series $Eu_{0.75}Sn_{0.25}Mo_6S_{8-y}Se_y$ with T_c values above the critical interval.

6.4. *Analysis of the critical field measurements with the use of a multiple pairbreaking theory*

The well-known microscopic theory of the superconducting critical field by Werthamer, Helfand, and Hohenberg [73], which contains spin-orbit as well as paramagnetic effects, has been extended by Fischer [74] to the case of magnetic superconductors with inclusion of the compensation effect. This multiple pairbreaking picture leads, in the dirty limit, to the following implicit equation for the

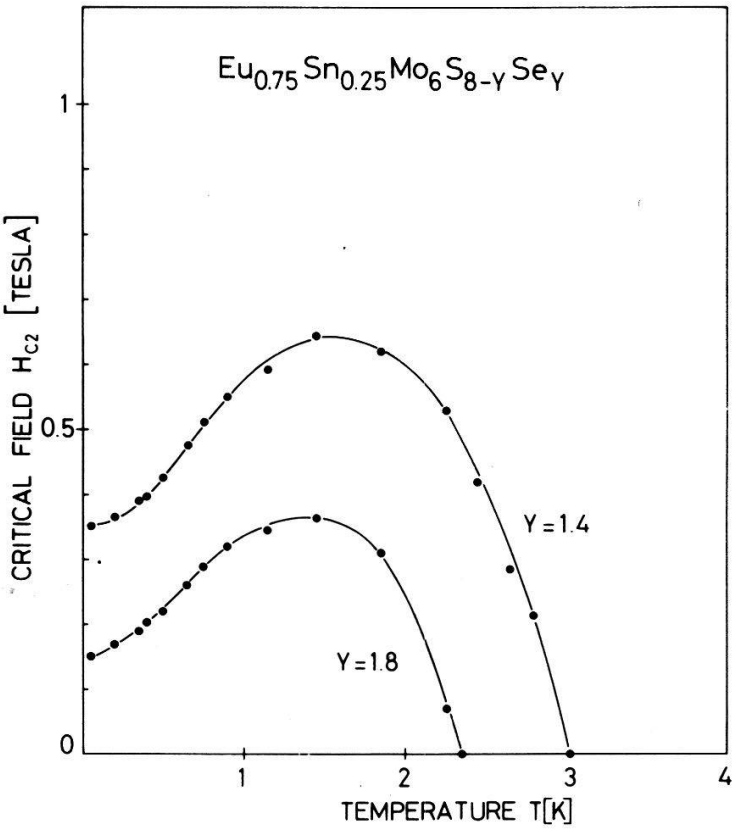

Figure 6.7
Critical field vs temperature for two samples of the series $Eu_{0.75}Sn_{0.25}Mo_6S_{8-y}Se_y$ with T_c values below the critical interval.

critical field:

$$\ln\frac{1}{t}=\left(\frac{1}{2}+\frac{i(\lambda_{s0}-\lambda_m)}{4\gamma}\right)\psi\left(\frac{1}{2}+\frac{h+\lambda_m+\frac{1}{2}(\lambda_{s0}-\lambda_m)+i\gamma}{2t}\right)+\left(\frac{1}{2}-\frac{i(\lambda_{s0}-\lambda_m)}{4\gamma}\right)\left(\frac{1}{2}+\frac{h+\lambda_m+\frac{1}{2}(\lambda_{s0}-\lambda_m)-i\gamma}{2t}\right)-\psi(\tfrac{1}{2}), \tag{6.4}$$

where

$$\gamma=(\alpha^2(h+h_J)^2-\tfrac{1}{4}(\lambda_{s0}-\lambda_m)^2)^{1/2}.$$

The independent variables temperature and magnetic field are expressed in reduced units $t=T/T_{c0}$ and $h=0.281H/H^*_{c2}(0)$. The reduced exchange field h_J is equivalently defined. Ψ is the digamma function. Solutions of this equation as a function of temperature determine the critical field $H_{c2}(T)$. Equation 6.4 contains 5 different parameters: the critical temperature T_{c0} the superconductor would have if there were no magnetic impurity, the spin-orbit scattering parameter $\lambda_{SO}=2/3\pi\tau_{SO}T_{c0}$, the exchange scattering parameter $\lambda_m=1/\pi\tau_m T_{c0}$, the Maki parameter $\alpha=\sqrt{2}\,H^*_{c2}(0)/H_{p0}=-0.533(dH_{c2}/dT)_{Tc}$ with H_{p0} being the paramagnetic critical field in the absence of spin-orbit scattering, and the exchange field

H_{J0} at saturation. Note that the exchange field itself is a function of temperature and applied field. In our calculations we assume a free ion behaviour, i.e. $H_J(T, H) = H_{J0}B_{7/2}(T, H)$ where $B_{7/2}$ is the Brillouin function for Eu spins.

The dependence of the critical temperature on the Eu concentration in the series $Eu_xSn_{1-x}Mo_6S_8$ (Fig. 5.1) suggests that magnetic scattering effects are negligible in the present case. We therefore take $\lambda_m = 0$. This is a very important point, since it demonstrates that exchange scattering processes which may have very interesting effects on superconductivity [75, 76], have nothing to do with the phenomenon discussed here. The pairbreaking effect coming from the exchange scattering is only a second-order effect in J (exchange constant), whereas the exchange field H_J acts in first order as pairbreaker thus dominating the spin scattering effects. The contribution of the magnetization to the magnetic induction B is also negligible in the present case. From the remaining parameters, only $T_{c0} = T_c$ can be determined by experiment, so that there remain three fitting parameters. Because of the strong paramagnetic limitation an accurate measurement of the initial slope $(dH_{c2}/dT)_{T_c}$ was not possible.

Figure 6.8 summarizes the three characteristic types of H_{c2} behaviour, obtained by only varying the critical temperature T_c. This experimental result puts the theory to a crucial test in describing the different $H_{c2}(T)$ curves with solely one set of parameters. As can be seen from Fig. 6.8, the agreement between theory and experiment is remarkably good. The best fit has been obtained with very reasonable values of the parameters. In particular, the value for the exchange field $H_{J0} = -30$ tesla, which is equivalent to an exchange interaction $J = -20$ meV, agrees well with EPR measurements [45]. In the compound $PbMo_6S_7Se_1$ a Maki parameter of 4.26 has been obtained [64], so that our result for the Maki parameter (Fig. 6.8) does not seem unreasonable. Finally the spin-orbit parameters given in the figure are in good agreement with the values reported for the pseudobinary system $Mo_6Se_{8-y}S_y$ [64]. In order to get an optimum fit, a slight variation of the spin-orbit scattering parameter with varying Se concentration has been admitted.

The multiple pairbreaking theory predicts that the shape and size of the field-induced domain depend critically on T_c. It can be shown [77], that a superconducting transition width of only 0.3 K provokes a large transition in field into the second superconducting domain $\Delta H = 6$ tesla at $T = 0$ in agreement with our observation (Fig. 6.3). One needs high-quality specimens with transitions much smaller than 0.1 K (!) in zero field, when sharp transitions into the field-induced state are desired. This may be of interest for an investigation of the order of the MFIS transition.

Finally, we note that the third transition at H_3 (see Fig. 6.1) from the field-induced superconducting state into the normal state is caused by orbital effects in our sample with $y = 0.8$. By taking the weak-coupling formula to calculate $H^*_{c2}(0)$, we find:

$$H^*_{c2}(0) = -0.693 T_c (dH_{c2}/dT)_{T_c}$$
$$= 24 \text{ tesla}$$

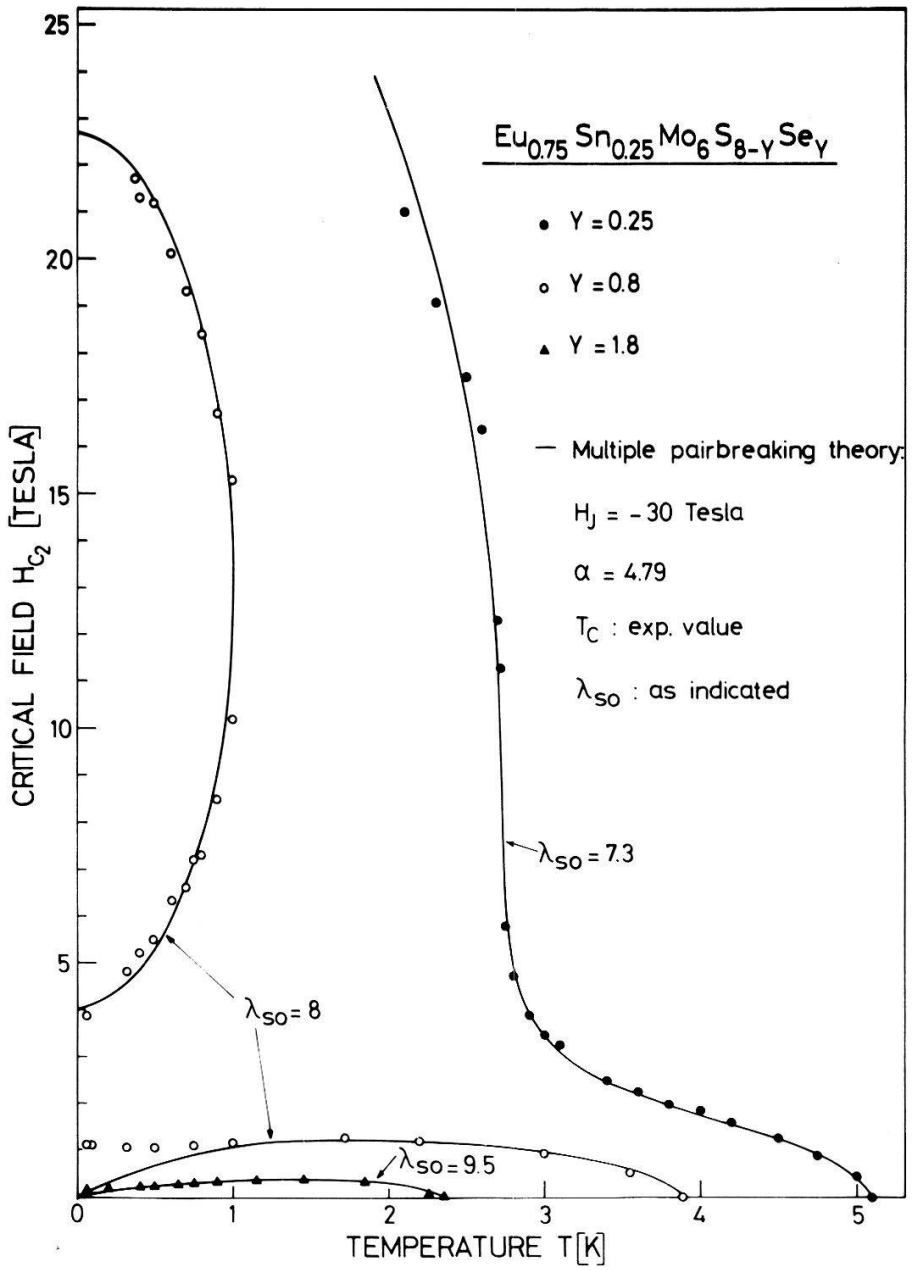

Figure 6.8
Critical fields vs temperature of three different samples of the series $Eu_{0.75}Sn_{0.25}Mo_6S_{8-y}Se_y$, compared with calculations (solid lines) based on a multiple pairbreaking theory [74].

in good accord with the measured value of 23 tesla (Fig. 6.5). This means that the compensation point at $H = -H_J = 30$ tesla has not exactly been reached. One needs a higher initial slope in order to increase $H^*_{c2}(0)$ above the compensation point without destroying the adjusted balance between T_c and H_J.

6.5. *Comments on the novel superconducting state*

The excellent accord between experiment and theory in view of the shape and size as well as the compositional dependence of the $H_{c2}(T)$-phase diagram gives strong evidence that our interpretation of the observed phenomenon in terms of the Jaccarino–Peter effect is correct. This means that the novel

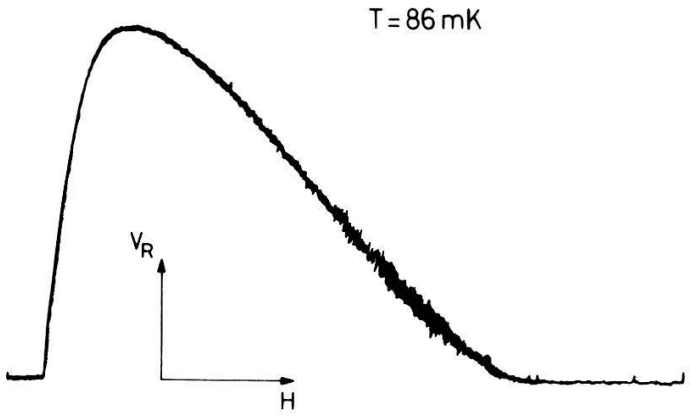

Figure 6.9
Resistive voltage signal vs applied magnetic field.

superconducting state does probably not result from "exotic" electron interactions such as p-wave pairing; superconductivity in both domains seems to be due to ordinary electron–phonon coupling (Cooper pairing). On the other hand, the critical field of "exotic" superconductors must not necessarily be very different from that of a classical superconductor. Thus the final judgement on the exact nature of the superconducting ground state at high magnetic fields is not yet formed. Besides the question about the pairing mechanism, other exciting properties may be attributed to this field-induced state. It is expected [78], that the behaviour of the flux-line lattice and the spatial field variation become particularly interesting, when entering the second superconducting domain.

Figure 6.9 shows a typical example of voltage vs magnetic field curves, as obtained in the resistance measurements by recording the lock-in output signal as a function of the magnetic field produced by a superconducting coil. The voltage signal suddenly becomes very noisy during the transition into the induced superconducting state. This points to a current instability probably due to flux-line motion. Note that there must be magnetic flux expulsion in increasing external fields. When the transition is complete, the noise disappears.

An even more interesting feature of the novel state is shown in Fig. 6.10. It is well known that the mixed state of type-II superconductors is characterized by partial flux penetration, since it is energetically favourable for those superconductors to have a large effective surface between superconducting and normal-state domains. A superconductor with conventional critical field behaviour achieves such a situation by locally increasing its internal magnetic field B above the critical field. As a result, the magnetic field inside the superconductor reveals spatial oscillations and has maximum values in regions where the Cooper-pair density is zero (vortex state). The same picture holds for the upper part of the field-induced superconducting domain, whereas in its lower part, it should be more favourable for the superconductor to reduce locally its magnetic field in order to become normal. This leads to a spatial field variation with minimum values in the non-superconducting regions ("antivortex state"). We expect that there should exist a certain region in the middle of the domain (infinite slope of

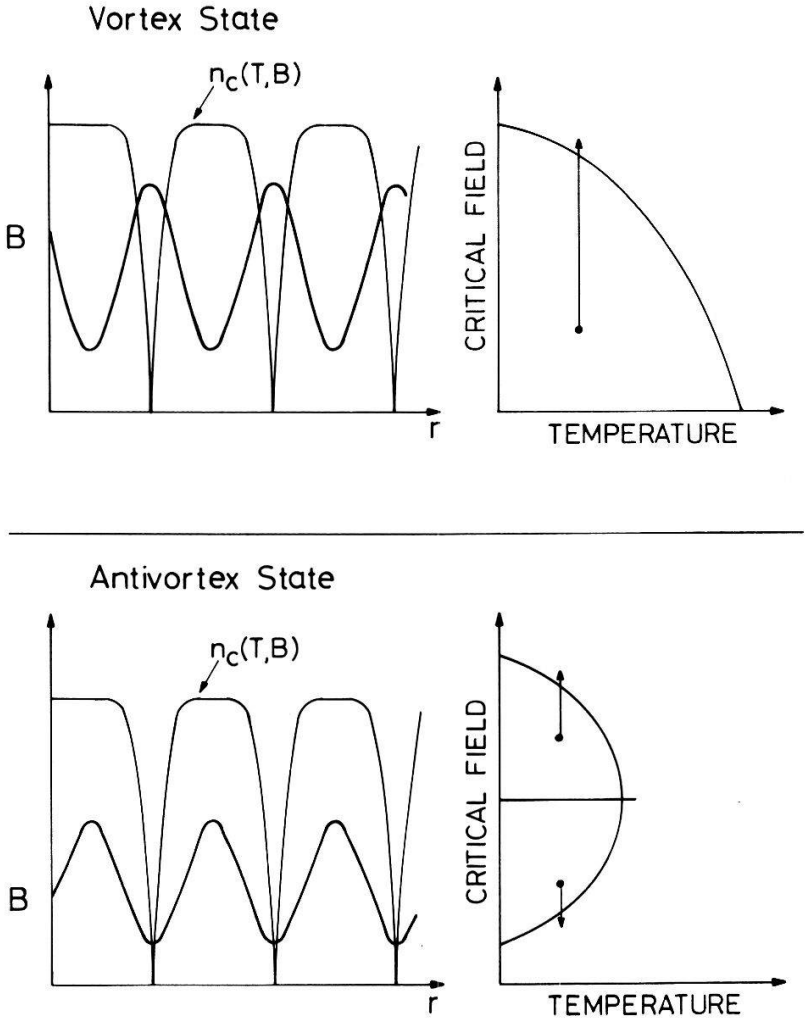

Figure 6.10
Spatial oscillation of Cooper-pair density $n_C(T, B)$ and internal magnetic field B in the vortex and antivortex state. The right part of the figure explains, how the internal field is locally modified to produce normal-state regions.

the critical field), where the transition from the antivortex to the vortex state produces a uniform field distribution without spatial oscillations. In the antivortex state, we expect a paramagnetic behaviour of the flux-line lattice with a magnetic-field enhancement.

In conclusion, the present work answers a long standing question concerning the possibility of the MFIS effect, but it also raises several questions about the exact nature of the novel state and its properties. Particularly interesting will be an investigation of the magnetic properties.

7. Conclusion and perspectives

In this work, some of the unusual physical properties of Eu-based Chevrel phases and related compounds have been investigated. The following results have been obtained:

1) Ternary molybdenum chalcogenides with divalent cations, which undergo

a low-temperature structural phase transformation, already reveal an anomalous behaviour in the high-temperature phase well above this transition temperature. This is characterized by a slight resistance increase with decreasing temperature and a simultaneously appearing variation of the Hall constant suggesting a small reduction of the number of charge carriers. We believe that this anomaly of the transport properties is due to a still undiscovered tiny lattice distortion similar to the one observed just recently in $PbMo_6S_8$ below 100 K. This lattice distortion, which might be some supercell ordering, must be distinguished from the transformation into a triclinic structure occurring at much lower temperature. This triclinic transformation is not observed in superconducting Chevrel compounds like $PbMo_6S_8$. Since the transport anomalies related to the expected first lattice deformation are most pronounced in $BaMo_6S_8$, a closer investigation of the lattice parameters of high-quality $BaMo_6S_8$ would certainly be of great interest for a better understanding of the rhombohedral phase of Chevrel compounds in general.

2) In the low-temperature triclinic phase of $M^{2+}Mo_6S_8$ compounds with M = Eu, Sr, Ba, we have found low conduction electron concentrations of the order of $10^{17}/cm^3$ and carrier mobilities of the order of $1000\,cm^2/Vs$. We have interpreted these results in terms of two weakly overlapping bands with a low density of states at the Fermi energy, i.e. a semimetallic situation. The large, negative magnetoresistance observed in $EuMo_6S_8$ has been interpreted in this picture by exchange splitting effects. However, it cannot be excluded that the low conduction electron density is not an intrinsic feature of the triclinc phase, but rather the result of weak electron localization due to spatial disorder.

3) The triclinc lattice deformation can be suppressed by applying pressure (hydrostatic pressure or chemical pressure) with the result, that superconductivity appears. The suppression of the structural transformation and the occurrence of superconductivity are gradual and lead to a small coexistence region of both superconductivity and the triclinic phase.

4) We have observed the novel phenomenon of magnetic-field-induced superconductivity in the series $Eu_xSn_{1-x}Mo_6S_{8-y}Se_y$ below 1 K. For certain values of the parameters of this series (e.g. $x = 0.75$ and $y = 0.8$) the critical field-temperature phase diagram contains two distinct superconducting domains; one of them exists only in the presence of high external magnetic fields. The shape and size of this phase diagram as well as its compositional dependence are correctly described by the microscopic theory of the Jaccarino–Peter effect. We therefore believe that the pairing mechanism of this novel superconducting state is probably the ordinary electron–phonon coupling. However, more experimental work is needed to establish unambiguously the exact nature of this state. Specific heat and susceptibility measurements would be of immense interest, since they may be sensitive to spin fluctuations of the molybdenun 4d electrons which should be enhanced in the case of p-wave pairing.

Careful dc-magnetization measurements are also very important, because unusual magnetic properties ("antivortices") should be correlated with this fascinating superconducting state. Furthermore, one should look for other

materials which reveal this phenomenon. After the termination of this work the observation of MFIS in the compound $CePb_3$ has been reported [79]. Thus we can expect that the group of superconductors whose superconductivity is induced by an external magnetic field starts to grow now. But for the moment the properties of Eu-based Chevrel phases are still very unusual.

Acknowledgements

This work was supported by Prof. Ø. Fischer, whom I want to thank for continuous interest and invaluable guidance.

I am very grateful to Prof. M. Peter for his interest in this work.

I have appreciated very much a close collaboration with Dr. M. Decroux, whom I wish to thank for many fruitful discussions and valuable advice.

I have benefitted from collaborating with Dr. C. Rossel. Some of the resistivity measurements have been performed by him.

It is a pleasure to thank Dr. G. Remenyi and Dr. A. Briggs for their kind hospitality during my stay at Grenoble. They have much contributed to the realization of the low-temperature and high-field measurements.

I greatly acknowledge Dr. M. G. Karkut for critically reading this manuscript and J. M. Triscone for revising the "resume".

I would like to thank Dr. B. Seeber, Dr. R. Baillif, and all my colleagues at the "Département de physique de la matière condensée" for support and stimulating help. I must thank A. Stettler for technical assistance and for drawing most of the figures.

Last, but by no means least, I would like to thank my wife Ulrike for her unfailing support and her patience on many a week-end, when I was engaged in this work.

REFERENCES

[1] See for example: *Superconductivity in Ternary Compounds, Vol. 1 and 2*, eds. M. B. Maple and Ø. Fischer (Springer, Berlin Heidelberg New York, 1982).
[2] Ø. FISCHER, A. TREYVAUD, R. CHEVREL, and M. SERGENT, Solid State Commun. *17*, 721 (1975).
[3] D. W. HARRISON, K. C. LIM, J. D. THOMPSON, and C. Y. HUANG, Phys. Rev. Lett., *46*, 280 (1981).
[4] C. W. CHU, S. Z. HUANG, C. H. LIM, R. L. MENG, M. K. WU, and P. H. SCHMIDT, Phys. Rev. Lett. *46*, 276 (1981).
[5] R. BAILLIF, A. DUNAND, J. MULLER, and K. YVON, Phys. Rev. Lett. *47*, 672 (1981).
[6] B. LACHAL, R. BAILLIF, A. JUNOD, and J. MULLER, Solid State Commun. *45*, 849 (1983).
[7] R. C. LACOE, S. A. WOLF, P. M. CHAIKIN, C. Y. HUANG, and H. L. LUO, Phys. Rev. Lett. *48*, 1212 (1982).
[8] Ø. FISCHER, M. DECROUX, S. ROTH, R. CHEVREL, and M. SERGENT, J. Phys. *C8*, L474 (1975).
[9] V. JACCARINO and M. PETER, Phys. Rev. Lett *9*, 290 (1962).
[10] B. B. SCHWARTZ and L. W. GRUENBERG, Phys. Rev. *177*, 747 (1969).
[11] R. BAILLIF, Thesis, University of Geneva, 1981.
[12] Rapport Scientifique 1981, University of Geneva, p. 5.
[13] J. VOLGER, Phys. Rev. *79*, 1023 (1950).

[14] E. H. PUTLEY, *The Hall Effect and Related Phenomena* (Butterworths, London, 1960) pp. 23.
[15] C. M. HURD, J. Sci. Instrum. *42*, 465 (1965).
[16] J. D. JORGENSEN and D. G. HINKS, Solid State Commun. *53*, 289 (1985).
[17] H. NOHL, W. KLOSE, and O. K. ANDERSEN, in: *Superconductivity in Ternary Compounds,* Vol. 1, eds. M. B. Maple and Ø. Fischer (Springer, Berlin Heidelberg New York, 1982) pp. 165.
[18] F. A. COTTON and T. E. HAAS, Inorg. Chem. *3*, 10 (1963).
[19] O. K. ANDERSON, W. KLOSE, and H. NOHL, Phys. Rev. *B17*, 1209 (1978).
[20] R. FLÜCKIGER, R. BAILLIF, and E. WALKER, Mat. Res. Bull. *13*, 743 (1978).
[21] Ø. FISCHER, Appl. Phys. *16*, 1 (1978).
[22] C. ROSSEL, H. W. MEUL, A. JUNOD, R. BAILLIF, Ø. FISCHER, and M. DECROUX, Solid State Commun. *48*, 431 (1983).
[23] R. BAILLIF, A. JUNOD, B. LACHAL, and J. MULLER, Solid State Commun. *40*, 603 (1981).
[24] J. S. DUGDALE and L. D. FIRTH, Phys. kondens. Materie *9*, 54 (1969).
[25] C. A. KUKKONEN and P. F. MALDAGUE, Phys. Rev. *B19*, 2394 (1979).
[26] C. M. HURD, *The Hall Effect in Metals and Alloys,* (Plenum Press, New York London, 1972) p. 54.
[27] Z. FISK and G. W. WEBB, Phys. Rev. Lett. *36*, 1084 (1976).
[28] See for example: *Valence Fluctuations in Solids,* eds. L. M. Falicov, W. Hanke, and M. B. Maple (North Holland, Amsterdam, 1981).
[29] J. H. MOOIJ, Phys. Status Solidi (a) *17*, 521 (1973).
[30] A. F. IOFFE and A. R. REGEL, Prog. Semicond. *4*, 237 (1960).
[31] P. D. HAMBURGER, J. C. HO, C. Y. HUANG and H. L. LUO, Phys. Rev. *B26*, 1446 (1982) and Ref. [3].
[32] M. DECROUX, H. W. MEUL, C. ROSSEL, Ø. FISCHER, and R. BAILLIF, in *Superconductivity in d- and f-Band Metals,* eds. W. Buckel and W. Weber (KFK GmbH, Karlsruhe, 1982) p. 167.
[33] H. ADRIAN, G. HOLTER, L. SÖLDNER, and G. SAEMANN-ISCHENKO, Proc. Int. Conf. Low Temp. Phys. *LT17,* Karlsruhe, Vol. I, p. 349 (1984).
[34] W. A. KALSBACH, C. FREIBURG, U. POPPE, T. TAKABATAKE, and F. POBELL, Phys. Lett. *98A*, 364 (1983).
[35] J. D. THOMPSON, M. P. MALEY, C. Y. HUANG, J. O. WILLIS, J. L. SMITH, and H. L. LUO, J. Low Temp. Phys. *43*. 243 (1981).
[36] H. W. MEUL, M. DECROUX, R. ODERMATT, R. NOER, and Ø. FISCHER, Phys. Rev. *B26*, 6431 (1982).
[37] O. LABORDE, R. LEPETIT, R. CHEVREL, O. PENA, and M. SERGENT, J. Physique *46*, 95 (1985).
[38] M. DECROUX, private communication.
[39] J. M. ZIMAN, *Principles of the Theory of Solids* (Cambridge University Press, Cambridge, 1972) p. 250.
[40] M. T. BEAL-MONOD and R. A. WEINER, Phys. Rev. *170*, 552 (1968).
[41] M. PELIZZONE, A. TREYVAUD, P. SPITZLI, and Ø. FISCHER, J. Low Temp. Phys. *29*, 453 (1977).
[42] J. BOLTZ, G. CRECELIUS, H. MALETTA, and F. POBELL, J. Low Temp. Phys. *28*, 61 (1977).
[43] T. TAKABATAKE, R. W. MCCALLUM, M. KUBOTA, and F. POBELL, J. Low Temp. Phys. *55*, 111 (1984).
[44] M. B. MAPLE, L. E. DELONG, W. A. FERTIG, D. C. JOHNSTON, R. W. MCCALLUM, and R. N. SHELTON, in *Valence Instabilities and Related Narrow Band Phenomena,* ed. R. D. Parks (Plenum, New York, 1977) p. 17.
[45] R. ODERMATT, Helv. Phys. Acta *54*, 1 (1981).
[46] F. Y. FRADIN, G. K. SHENOY, B. D. DUNLAP, A. T. ALDRED, and C. W. KIMBALL, Phys. Rev. Lett *38*, 719 (1977).
[47] For a review see: J. K. FURDYNA, J. Appl. Phys. *53*, 7637 (1982).
[48] T. PENNEY, F. HOLTZBERG, L. J. TAO, and S. v. MOLNAR, AIP Conf. Proc. *18*, 908 (1974).
[49] K. YVON and A. PAOLI, Solid State Commun. *24*, 41 (1977).
[50] N. P. ONG and P. MONCEAU, Solid State Commun. *26*, 487 (1978).
[51] K. TSUTSUMI, T. TAKAGAKI, M. YAMAMOTO, Y. SHIOZAKI, M. IDO, T. SAMBONGI, K. YAMAYA, and Y. ABE, Phys. Rev. Lett. *39*, 1675 (1977); R. M. FLEMING, D. E. MONCTON, and D. B. MCWHAN, Phys. Rev. *B18*, 5560 (1978).
[52] I. M. CHAPNIK, Phys. Lett. *72A*, 255 (1979).
[53] M. DECROUX, S. E. LAMBERT, M. S. TORIKACHVILI, M. B. MAPLE, R. P. GUERTIN, L. D. WOOLF, and R. BAILLIF, Phys. Rev. Lett. *52*, 1563 (1984).
[54] M. DECROUX, M. S. TORIKACHVILI, M. B. MAPLE, R. BAILLIF, Ø. FISCHER, and J. MULLER, Phys. Rev. *B28*, 6270 (1983).

[55] M. DECROUX, S. E. LAMBERT, M. B. MAPLE, R. P. GUERTIN, R. BAILLIF, and Ø. FISCHER, Proc. Int. Conf. Low Temp. Phys. *LT17*, Karlsruhe, Vol. I, 333 (1984).
[56] C. ROSSEL, H. W. MEUL, M. DECROUX, and Ø. FISCHER, in: *Europhysics Conference Abstracts 7A*, edited by H. Thomas and W. Czaja (EPS, Lausanne, 1983), p. 325.
[57] M. SERGENT, Ø. FISCHER, M. DECROUX, C. PERRIN, and R. CHEVREL, J. Solid State Chem. *22*, 87 (1977).
[58] C. ROSSEL, private communication.
[59] A. J. FREEMAN and T. JARLBORG, in *Superconductivity in Ternary Compounds, Vol 2,* eds. M. B. Maple and Ø. Fischer (Springer, Berlin Heidelberg New York, 1982) pp. 167–200.
[60] M. ISINO, N. KOBAYASHI, and Y. MUTO, in *Ternary Superconductors,* eds. G. K. Shenoy, B. D. Dunlap, and F. Y. Fradin (North Holland, Amsterdam, 1981) p. 95.
[61] S. A. WOLF, W. W. FULLER, C. Y. HUANG, D. W. HARRISON, H. L. LUO, and S. MAEKAWA, Phys. Rev. *B25*, 1990 (1982).
[62] W. W. FULLER, S. A. WOLF, C. Y. HUANG, D. W. HARRISON, H. L. LUO, and S. MAEKAWA, J. Appl. Phys. *53*, 2622 (1982).
[63] M. DECROUX, Diploma thesis, University of Geneva, 1975 (unpublished).
[64] M. DECROUX and Ø. FISCHER, in *Superconductivity in Ternary Compounds, Vol. 2,* eds. M. B. Maple and Ø. Fischer (Springer, Berlin Heidelberg New York, 1982) pp. 57.
[65] H. W. MEUL, C. ROSSEL, M. DECROUX, Ø. FISCHER, G. REMENYI, and A. BRIGGS, Phys. Rev. Lett. *53*, 497 (1984).
[66] H. W. MEUL, C. ROSSEL, M. DECROUX, Ø. FISCHER, G. REMENYI, and A. BRIGGS, Physica *126B,* 44 (1984).
[67] B. LACHAL, A. JUNOD, and J. MULLER, J. Low Temp. Phys. *55*, 195 (1984).
[68] Y. B. KIM and M. J. STEPHEN, in *Superconductivity, Vol. 2,* ed. R. D. Parks (Marcel Dekker, New York, 1969) Chap. 19.
[69] W. BALTENSPERGER and S. STRÄSSLER, Phys. Condens. Mat. *1*, 20 (1963).
[70] G. ZWICKNAGL and P. FULDE, Z. Phys. *B43*, 23 (1981).
[71] M. S. TORIKACHVILI, M. B. MAPLE, R. P. GUERTIN, and F. FONER, J. Low Temp. Phys. *49*, 573 (1982).
[72] M. S. TORIKACHVILI, J. BEILLE, S. E. LAMBERT, and M. B. MAPLE, in *Superconductivity in d- and f-Band Metals,* eds. W. Buckel and W. Weber (KFK GmbH, Karlsruhe, 1982) p. 241.
[73] H. R. WERTHAMER, E. HELFAND, and P. C. HOHENBERG, Phys. Rev. *147*, 295 (1966).
[74] Ø. FISCHER, Helv. Phys. Acta *45*, 329 (1972).
[75] E. MÜLLER-HARTMANN and J. ZITTARTZ, Phys. Rev. Lett. *26*, 428 (1971).
[76] S. MAEKAWA and M. TACHIKI, Phys. Rev. *B18*, 4688 (1978).
[77] C. ROSSEL, H. W. MEUL, M. DECROUX, Ø. FISCHER, G. REMENYI, and A. BRIGGS, J. Appl. Phys. *57*, 3099 (1985).
[78] Ø. FISCHER, H. W. MEUL, M. G. KARKUT, G. REMENYI, U. WELP, J. C. PICCOCHE, and K. MAKI, Phys. Rev. Lett. *55,* 2972 (1985).
[79] C. L. LIN, J. TETER, J. E. CROW, T. MIHALISIN, J. BROOKS, J. BROOKS, A. I. ABOU-ALY and G. R. STEWART, Phys. Rev. Lett. *54*, 2541 (1985).